

R-Parity Violation at the LHC

Daniel Dercks,^{1,2,*} Herbi Dreiner,^{1,†} Manuel E. Krauss,^{1,‡} Toby Opferkuch,^{1,§} and Annika Reinert^{1,¶}

¹*Bethe Center for Theoretical Physics & Physikalisches Institut der Universität Bonn, Nußallee 12, 53115 Bonn, Germany*

²*II. Institut für Theoretische Physik, Universität Hamburg, Luruper Chaussee 149, 22761 Hamburg, Germany*

We investigate the phenomenology of the MSSM extended by a single R -parity violating coupling at the unification scale. For all R -parity violating couplings, we discuss the evolution of the particle spectra through the renormalization group equations and the nature of the lightest supersymmetric particle (LSP) within the CMSSM, as an example of a specific complete supersymmetric model. We use the nature of the LSP to classify the possible signatures. For each possible scenario we present in detail the current LHC bounds on the supersymmetric particle masses, typically obtained using simplified models. From this we determine the present coverage of R -parity violating models at the LHC. We find several gaps, in particular for a stau-LSP, which is easily obtained in R -parity violating models. Using the program **CheckMATE** we recast existing LHC searches to set limits on the parameters of all R -parity violating CMSSMs. We find that virtually all of them are either more strongly constrained or similarly constrained in comparison to the R -parity conserving CMSSM, including the $\tilde{U}\tilde{D}\tilde{D}$ models. For each R -parity violating CMSSM we then give the explicit lower mass bounds on all relevant supersymmetric particles.

I. INTRODUCTION

Supersymmetry (SUSY) [1–4] is a unique extension of the external symmetries of the Standard Model of particle physics (SM) [5, 6].¹ As a solution to the hierarchy problem [8, 9], the supersymmetry-breaking scale should be $\mathcal{O}(\text{TeV})$ and thus testable at the LHC. To-date no experimental sign of supersymmetry has been found [10], pushing the lower mass limits for some supersymmetric particles into the TeV range, however with some clear model dependence, see for example Ref. [11] on discussing the impact of the $\sqrt{s} = 8 \text{ TeV}$ data.

Requiring supersymmetric invariance of the SM and imposing R -parity conservation yields the minimal supersymmetric SM (MSSM). Its superpotential is given by

$$W_{\text{MSSM}} = \epsilon_{ab} [(Y_u)_{ij} Q_i^a H_u^b \bar{U}_j + (Y_d)_{ij} Q_i^a H_d^b \bar{D}_j + (Y_e)_{ij} L_i^a H_d^b \bar{E}_j - \mu H_d^a H_u^b] , \quad (1)$$

where we have explicitly included the $SU(2)$ indices, while otherwise using standard notation [12], for example $i, j = 1, 2, 3$ are the generation indices. The above superpotential by construction conserves the discrete symmetry R -parity

$$\mathbf{R}_p = (-1)^{3B+L+2S} , \quad (2)$$

where B denotes baryon number, L lepton number and S spin. This requires supersymmetric pair production

in colliders, and often leads to missing transverse momentum signatures. These signatures arise as the lightest supersymmetric particle (LSP) is necessarily stable, guaranteed by conserved \mathbf{R}_p , and in most cases electrically neutral thus evading experimental detection. For many years the constrained minimal supersymmetric SM (CMSSM) [13–17] has been a benchmark for experimental supersymmetry searches. It is defined by five parameters,

$$M_0, M_{1/2}, A_0, \tan\beta, \text{sgn}(\mu) , \quad (3)$$

at the unification scale, $M_X \simeq 10^{16} \text{ GeV}$, in comparison to the $\mathcal{O}(100)$ parameters present in the generic MSSM. Here $M_0, M_{1/2}$ are the universal scalar and gaugino masses, A_0 is the universal trilinear scalar interaction and $\tan\beta$ is the ratio of the two Higgs vacuum expectation values. $\text{sgn}(\mu)$ is the sign of the supersymmetric Higgsino mass term μ .

The lack of a supersymmetric signal at the LHC puts increasing pressure on the CMSSM in particular with respect to fine-tuning [18, 19]. Several groups have performed combined frequentist fits of the CMSSM to all the relevant data, see for example [20, 21]. In Ref. [22] it was shown that the CMSSM is experimentally excluded due to tension between the $(g-2)_\mu$ measurements and the LHC lower bounds on M_0 . Several groups now instead investigate the phenomenological MSSM (pMSSM), which has a more extensive parameter set [23–27]. In particular the slepton and squark masses at the unification scale are now given by separate parameters, decoupling the $(g-2)_\mu$ measurement and the LHC lower mass bound on the squarks [26].

Rather than relaxing the high-scale boundary conditions, we instead consider R -parity violating (RPV) supersymmetry [28–30]. Restricting ourselves to the minimal set of fields as in the MSSM, the superpotential is

*Electronic address: dercks@desy.de

†Electronic address: dreiner@uni-bonn.de

‡Electronic address: mkrauss@th.physik.uni-bonn.de

§Electronic address: toby@th.physik.uni-bonn.de

¶Electronic address: areinert@th.physik.uni-bonn.de

¹ See also Ref. [7] on the early history of supersymmetry, 1967–1976, and references therein.

Couplings	λ_{ijk}	λ'_{ijk}	λ''_{ijk}	λ'''_{ijk}	λ''''_{ijk}
Bound	0.49 ^a	0.09 ^a	0.59	1.1	0.5 ^b

TABLE I: The bounds on the most constrained coupling for each class of RPV operators at M_W . The bounds are given for sfermion masses \tilde{m} of 1 TeV and typically scale as \tilde{m}^{-1} . A complete list with the specific sfermion mass dependence is given in Appendix A. ^a We disregarded the stringent bound on λ_{133} and λ'_{133} arising from upper bounds on neutrino masses [35]. ^b λ''_{112} and λ''_{113} can be more strongly constrained under the assumption of a large hadronic scale for double nucleon decay [36].

extended to include the 48 terms [31]

$$W = \epsilon_{ab} \left[\frac{1}{2} \lambda_{ijk} L_i^a L_j^b \bar{E}_k + \lambda'_{ijk} L_i^a Q_j^b \bar{D}_j - \kappa_i L_i^a H_u^b \right] + \frac{1}{2} \epsilon_{xyz} \lambda''_{ijk} \bar{U}_i^x \bar{D}_j^y \bar{D}_k^z. \quad (4)$$

Here x, y and z are $SU(3)$ color indices and the $\lambda_{ijk}, \lambda'_{ijk}, \lambda''_{ijk}$ are dimensionless Yukawa couplings. As an orientation we present the most strictly bound Yukawas in each class of operators in Tab. I. A complete list is given in Appendix A. The κ_i are mass dimension-one mixing parameters. At a fixed energy scale they can be rotated away. This also holds for complex κ_i and λ 's [32, 33]. Through the renormalization group equations RGEs they are in general, however, regenerated at other scales. As discussed in [34], supergravity models with universal breaking have alignment at the unification scale, and thus only radiatively generated κ_i at the weak scale. The κ_i are then very small and have no impact on the LHC phenomenology. We therefore discard them in the remainder of this paper.

R -parity was originally introduced to stabilize the proton. However, this is not a unique choice, with many viable alternatives [37–43]. There are also a number of simple models which predict a subset of RPV couplings through other discrete gauge symmetries, see for example [33, 44, 45]. In addition phenomenologically RPV supersymmetry models naturally accommodate light massive neutrinos, requiring neither right-handed neutrinos nor an additional heavy Majorana mass scale [32, 46, 47]. As a consequence of R -parity violation, the LSP can decay and is no longer a good dark matter candidate. However, others such as an axion, a sufficiently long-lived axino [48–51] or even the gravitino [52, 53] can account for the measured dark matter relic density [54]. Furthermore, RPV can alleviate part of the light Higgs problem in supersymmetry [55], as it can lead to weaker lower mass bounds on the squark and gluino, see e.g. [56–58] and the discussion below. We conclude that RPV models are just as well motivated as R -parity conserving (RPC) models.

Throughout most of this paper we focus on the RPV–CMSSM, which we shall also denote $\Lambda_{\mathcal{R}_p}$ –CMSSM, as defined in Ref. [34]. A given such model has *one* additional

non-zero trilinear RPV coupling $\Lambda_{\mathcal{R}_p}$ at the unification scale. We have the following parameters at M_X

$$M_0, M_{1/2}, A_0, \tan \beta, \text{sgn}(\mu), \Lambda_{\mathcal{R}_p}, \quad (5)$$

$$\text{with } \Lambda_{\mathcal{R}_p} \in \{\lambda_{ijk}, \lambda'_{ijk}, \lambda''_{ijk}\}.$$

Through the RGEs, several non-zero RPV couplings will be generated at the weak scale [59]. As we see below, this can have an effect on the LHC phenomenology, in particular for $\tilde{\tau}$ -LSPs.

It is the purpose of this paper to investigate the impact of the LHC on the allowed parameter ranges of the $\Lambda_{\mathcal{R}_p}$ –CMSSM. At the LHC supersymmetric production is dominated by the squarks and gluinos, but electroweak gaugino production can also have an impact. For not too large RPV-couplings, the produced sparticles will cascade to the LSP via standard MSSM operators. As the cosmological constraint no longer applies for an unstable LSP, it need not be the lightest neutralino. The LSP then decays in the detector via R -parity violating couplings, usually through the dominant coupling given at the unification scale. It is thus the nature of the LSP, as well as its decay which mainly determines the resulting signatures. We summarize the possibilities as follows:

$$\text{sig.} = \begin{pmatrix} \tilde{q}\tilde{q} \\ \tilde{q}\tilde{g} \\ \tilde{g}\tilde{g} \\ \tilde{\ell}^+\tilde{\ell}^- \\ \tilde{\nu}\tilde{\nu} \\ \tilde{\chi}^0\tilde{\chi}^\pm \end{pmatrix}_{\text{prod}} \otimes \begin{pmatrix} \tilde{\chi}_1^0 \\ \tilde{\chi}_1^\pm \\ \tilde{\nu}_i \\ \tilde{\ell}_i^\pm \\ \tilde{\tau} \\ \tilde{q} \\ \tilde{b} \\ \tilde{t} \\ \tilde{g} \end{pmatrix}_{\text{possible LSP}} \otimes \begin{pmatrix} L_1 L_2 \bar{E}_1 \\ \vdots \\ L_1 \bar{Q}_1 \bar{D}_1 \\ \vdots \\ \bar{U}_3 \bar{D}_2 \bar{D}_3 \end{pmatrix}_{\text{LSP decay}} \quad (6)$$

Here \tilde{q} refers to any squark and the last array represents all forty-five new trilinear RPV operators, as given in Eq. (4). A first systematic analysis of these bewildering possibilities for a neutralino LSP was presented in [60]. A more general classification was presented in [61], allowing for all possible LSPs and also all supersymmetric mass orderings. This is presently beyond a systematic comparison with LHC data. Here we instead address the case of the $\Lambda_{\mathcal{R}_p}$ –CMSSM, Eq. (5). With the smaller number of parameters this is feasible. In particular in this paper we investigate the following points:

- (1) In Sec. II, we analyze the possible LSPs in the $\Lambda_{\mathcal{R}_p}$ –CMSSM. This depends on the type and size of the dominant RPV coupling, as well as the CMSSM parameters. We employ the supersymmetric RGEs [59] and go beyond previous work [62], to take into account the recent Higgs boson discovery.
- (2) In Secs. III to V, we review in detail the RPV LHC signatures, summarize the experimental lower mass bounds and thus determine the current LHC coverage of the $\Lambda_{\mathcal{R}_p}$ –MSSM. The experiments typically

set limits on the parameters of simplified models, with no interpretation in the $\Lambda_{\mathcal{R}_p}$ -CMSSM. These searches can however be applied to a wide range of RPV models.

- (3) In Sec. VI we investigate the $\Lambda_{\mathcal{R}_p}$ -CMSSM as a complete supersymmetric model. We use the program **CheckMATE** [63–65] to determine the LHC bounds on the various versions of this model and compare it to the **CheckMATE** constraints in the RPC-CMSSM.
- (4) In Sec. VIII we use the results from Sec. VI to determine absolute lower mass bounds on the supersymmetric particles for a $\tilde{\chi}_1^0$ -LSP and for a $\tilde{\tau}_1$ -LSP scenario in the $\Lambda_{\mathcal{R}_p}$ -CMSSM, respectively. We compare our bounds to the simplified models experimental bounds in Secs. III to V.

In Sec. IX we summarize and conclude. In Appendix A we collate the current weak-scale bounds on the R -parity violating trilinear couplings. Most bounds are proportional to the mass of a supersymmetric scalar fermion (sfermion). For heavy sfermion masses above a TeV many bounds are weak to non-existent.

II. THE RENORMALIZATION GROUP EVOLUTION OF THE RPV-CMSSM

The renormalization group equations (RGEs) of supersymmetric R -parity violation have previously been studied in Refs. [36, 66–70]. The full two-loop equations are given in Ref. [59]. Through the interface with **SARAH** [71–76], they have been implemented in the numerical program **SPheno** [77, 78], which we employ here.

A. General Considerations

As we saw in Eq. (6), the nature of the LSP plays an important role in determining all possible LHC signatures. Within the $\Lambda_{\mathcal{R}_p}$ -CMSSM, the LSP is determined dynamically as a function of the input parameters given in Eq. (5). The universal gaugino masses at M_X of the CMSSM imply that the lightest *gaugino* is always the neutralino at the weak scale. Regions with the chargino as the LSP are only possible for very small chargino masses and are hence excluded by LEP searches, while the gluino is always heavier. Whether or not a given *sfermion* could be the LSP depends on the corresponding soft SUSY-breaking scalar and gaugino masses at the weak scale. Therefore, apart from the initial choice of M_0 , their RGE evolution from M_X to the TeV scale is crucial. To a good approximation, it is sufficient to consider the one-loop RGEs and neglect the contributions from the 1st and 2nd generation Yukawa couplings of the R -parity conserving MSSM (RPC-MSSM). Given these

assumptions the RGEs for the scalar masses squared can be parametrized as [34, 62]

$$16\pi^2 \frac{d(\tilde{m}_Y^2)}{dt} = -a_i g_i |M_i|^2 - b g_1 \mathcal{S} + \Lambda_{\mathcal{R}_p}^2 \mathcal{F} + c T_\Lambda^2, \quad (7)$$

where $t = \log(Q/M)$, Q is the renormalization scale and M is the reference scale. M_i , $i = 1, 2, 3$, are the soft breaking gaugino masses, and g_i the corresponding gauge couplings for $U(1)_Y$, $SU(2)_L$ and $SU(3)_c$, respectively. $\Lambda_{\mathcal{R}_p}$ denotes the non-zero RPV coupling and T_Λ are the corresponding RPV trilinear soft supersymmetry breaking sfermion interactions, namely $T_\Lambda = \Lambda_{\mathcal{R}_p} A_0$ at M_X . In the $LL\bar{E}$ case we have: $(T_\Lambda^k)_{ij} \equiv (T_\lambda)_{ijk} \equiv \lambda_{ijk} A_0$. The coefficients a_i , b , and c depend on $Y = \{E, L, Q, D, U\}$. \mathcal{F} is a linear function of the soft SUSY-breaking squared scalar masses and is positive if the latter are all positive, and \mathcal{S} is given by

$$\mathcal{S} = m_{H_u}^2 + m_{H_d}^2 + \text{Tr}(\tilde{m}_Q^2 - \tilde{m}_L^2 - 2\tilde{m}_U^2 + \tilde{m}_D^2 + \tilde{m}_E^2). \quad (8)$$

For the sleptons and sneutrinos, the RGEs for the diagonal \tilde{m}_Y^2 entries read

$$16\pi^2 \frac{d(\tilde{m}_E^2)_{ii}}{dt} = -\frac{24}{5} g_1^2 |M_1|^2 + \frac{6}{5} g_1^2 \mathcal{S} + 2\text{Tr}(\lambda^{i\dagger} \lambda^i) (\tilde{m}_E^2)_{ii} + 4\text{Tr}(\tilde{m}_L^2 \lambda^{i\dagger} \lambda^i) + 2\text{Tr}(T_\lambda^{i\dagger} T_\lambda^i), \quad (9)$$

and

$$16\pi^2 \frac{d(\tilde{m}_L^2)_{ii}}{dt} = -\frac{6}{5} g_1^2 |M_1|^2 - 6g_2^2 |M_2|^2 - \frac{3}{5} g_1^2 \mathcal{S} + \sum_r [2(\tilde{m}_L^2)_{ii} (\lambda^r \lambda^{r\dagger})_{ii} + 2(\lambda^r (\tilde{m}_L^2)^T \lambda^{r\dagger})_{ii} + 2(\tilde{m}_E^2)_{rq} (\lambda^r \lambda^{q\dagger})_{ii} + 6(\tilde{m}_L^2 \lambda^{r\dagger} \lambda^r)_{ii} + 6(\tilde{m}_D^2)_{rq} (\lambda^{r\dagger} \lambda^q)_{ii} + 6(\lambda^{r\dagger} (\tilde{m}_Q^2)^T \lambda^{k\dagger})_{ii} + 2(T_\lambda^r T_\lambda^{r\dagger})_{ii} + 6(T_\lambda^r T_\lambda^{r\dagger})_{ii}]. \quad (10)$$

Here we have used the notation $\lambda_{ijk} = (\lambda^k)_{ij}$, $\lambda'_{ijk} = (\lambda^k)_{ij}$ so that, e.g., $\text{Tr}(\lambda^{i\dagger} \lambda^i) = \sum_{k,l} \lambda_{kli}^* \lambda_{kli}$ and $\sum_r (T_\lambda^r T_\lambda^{r\dagger})_{ii} \equiv \sum_{k,r} (T_\lambda)_{ikr} (T_\lambda^*)_{ikr}$. The complete contributions to all soft-masses including all Yukawa couplings can be found in Ref. [34].

As is known from the RPC case, large gaugino masses contribute with a negative slope to the RGEs, thus raising the sfermion masses when running from the high to the low scale. This gaugino mass effect typically dominates over the reverse effect due to the soft-mass contribution $\Lambda_{\mathcal{R}_p}^2 \mathcal{F}$ to the RGEs, even for large values of $M_0(M_X)$. Thus small M_0 is in general favorable for obtaining light sfermions. The most important effect in the RGEs comes from the A -terms, *i.e.* T_Λ , which always decrease the soft-masses at the low scale. As is well-known for the RPC-CMSSM, large A_0 values of several TeV are needed in order to explain the Higgs mass, if at the same time the stops are at the TeV scale. See, e.g., Ref. [22]

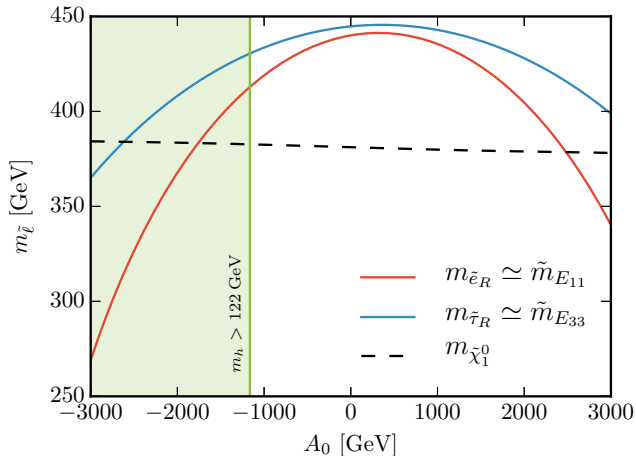


FIG. 1: Dependence at one-loop of the stau, selectron and lightest neutralino mass on the initial choice of A_0 at M_X for $\lambda_{231}|_{M_X} = 0.1$, as well as $M_0 = 300$ GeV, $M_{1/2} = 900$ GeV and $\tan \beta = 10$. The green shaded area indicates the region where the Higgs mass is sufficiently heavy, $m_h > 122$ GeV, see text.

for a recent global fit to the RPC–CMSSM. Therefore, in a constrained SUSY model, it is natural to have large trilinear SUSY-breaking terms, leading to sizable effects in the weak-scale sfermion masses.

Therefore sfermion LSPs are most easily obtained for small M_0 and large $|A_0|$. For illustration purposes we show in Fig. 1 the dependence of the right-handed selectron mass on A_0 for an RPV coupling $\lambda_{231} = 0.1$ at M_X .² Here we show as a solid red line the mass of the right-handed selectron, as a solid blue line the mass of the right-handed stau and as a black dashed line the mass of the lightest neutralino. We see that the lightest neutralino mass is largely unaffected by the initial value of A_0 . Due to the strong T_λ dependence of the soft mass $(\tilde{m}_E^2)_{11}$, the right-handed selectron becomes the LSP for $A_0 \lesssim -1.8$ TeV or $A_0 \gtrsim 2.4$ TeV in this scenario. The dominantly right-handed stau is also strongly affected by the choice of A_0 and becomes the next-to-lightest sparticle (NLSP) for even larger $|A_0|$. The A_0 dependence of $m_{\tilde{\tau}_R}$ is due to the terms in the RGEs proportional to the (RPC) τ Yukawa, which are not included in Eqs. (7)–(10), but have been used in the full numerical evaluation. For $A_0 \lesssim -1.1$ TeV, corresponding to the green shaded region, the mass of the SM-like Higgs is in the correct range, $122 \text{ GeV} < m_h < 128 \text{ GeV}$ [79, 80], in accordance with the ± 3 GeV uncertainties in the numerical programs we employ. Whereas it is too small in the rest of the plot.

We note that large trilinear sfermion interactions tend to make the electroweak vacuum unstable, *i.e.* the scalar

potential can develop additional minima, which for large $|T_i|$ can be deeper than the electroweak minimum [81, 82]. The latter can then tunnel to the energetically preferred configuration at possibly unacceptably large rates. However, using the numerical program **Vevacious** [83], we have verified that possible new minima induced by the RPV operators T_Λ are, for the scenarios we consider here, never deeper than the vacua we already find in the RPC–CMSSM. Therefore, the findings of Ref. [84] concerning the vacuum stability of the RPC–CMSSM also apply here. All scenarios we present in the following feature an electroweak vacuum which is either stable or metastable long-lived, meaning that the tunnelling time to the global minimum is longer than the age of the Universe.

B. Determining the LSP

The different possible LSP scenarios in the RPV–CMSSM have been first explored in Ref. [62]. This analysis was centered around comparatively small values of $M_0, M_{1/2}$ and A_0 . With the recent measurement of the Higgs mass, these small values of the input parameters lead to an unacceptably light Higgs and are hence excluded. Here we reevaluate the possible LSPs in the RPV–CMSSM, taking into account the new Higgs measurements [79]. Due to the necessity of quite heavy universal soft-breaking parameters, the supersymmetric contributions to the muon anomalous magnetic moment can only alleviate but not solve the well-known discrepancy [85–87]. We first consider the case of small couplings and then large couplings which can strongly affect the RGEs.

1. Small $\Lambda_{\tilde{R}_p}$

For small values of the RPV couplings, $\Lambda_{\tilde{R}_p} \lesssim 0.05$, the RGE running of the soft supersymmetry breaking masses is largely unaffected by the R -parity violating interactions. As in the RPC–CMSSM, we thus obtain wide ranges of parameter space with a neutralino LSP. However, for small values of M_0 and larger values of $M_{1/2}$, A_0 and $\tan \beta$, the lightest stau, $\tilde{\tau}_1$, is the LSP. For conserved R -parity the LSP is stable and these regions of parameter space are excluded on astrophysical and cosmological grounds [88]. However, for RPV these regions are viable as the LSP decays. An example of such a parameter region for $A_0 = -3$ TeV and $\tan \beta = 30$ is given in Fig. 2 to the left of the black contour. The Higgs mass measurement restricts the larger $M_{1/2}$ regions compared to Refs. [34, 62].

2. Large λ_{ijk}

For a large $\Lambda_{\tilde{R}_p}$ the RGEs are significantly modified and the low-energy mass spectrum must be re-evaluated

² This large value of the RPV coupling is consistent with the low-energy bounds, *cf.* Tab. I and Appendix A.

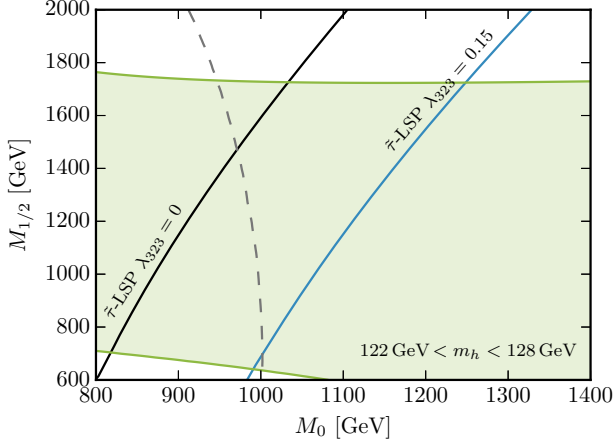


FIG. 2: LSP Plot for both $\lambda_{ijk} = 0$ (black) and $\lambda_{323}|_{M_X} = 0.15$ (blue). The parameter space left of the respective contours features a $\tilde{\tau}$ LSP whereas on the right the $\tilde{\chi}_1^0$ is the LSP. The parameter space on the left of the dashed gray line is excluded in the case of $\lambda_{323}|_{M_X} = 0.15$ from the bounds on the RPV coupling, see Tab. XIII. We see how the stau-LSP region expands as we turn on, in this case, the λ_{323} coupling. The green shaded region corresponds to parameter space where the Higgs mass lies in the range $122 \text{ GeV} < m_h < 128 \text{ GeV}$ [79, 80].

[59]. Specifically for $\Lambda_{\mathcal{R}_p} = \lambda_{ijk}$ and large, the running of the soft-breaking masses results in $(\tilde{m}_E)_{kk} < (\tilde{m}_L)_{ii}, (\tilde{m}_L)_{jj}$ at the weak scale, where \tilde{m}_L includes both $\tilde{m}_{\tilde{L}}$ and \tilde{m}_{ν_L} . As already known from the RPC case, the gaugino contribution is larger for the doublet than for the singlet sleptons. Furthermore from Eqs. (9) and (10) we see that $(\tilde{m}_E)_{kk}$ receives twice the contribution from the A -term compared to $(\tilde{m}_L)_{ii}, (\tilde{m}_L)_{jj}$. Explicitly, consider $\Lambda_{\mathcal{R}_p} = \lambda_{ijk} = -\lambda_{jik} \neq 0, \lambda_{mnl} = 0$ otherwise. Defining $T_\Lambda = A \Lambda_{\mathcal{R}_p}$, we have $2 \text{Tr}(T_\Lambda^{k\dagger} T_\Lambda^k) = 4 A^2 \Lambda_{\mathcal{R}_p}^2$, due to the antisymmetry in the indices, while $\sum_r 2 (T_\Lambda^r T_\Lambda^{r\dagger})_{ii,jj} = 2 A^2 \Lambda_{\mathcal{R}_p}^2$. Therefore, in general, large λ_{ijk} can lead to a right-handed slepton LSP of flavor k . Using a 1-step integration a very rough estimate for the soft-breaking mass squared is:

$$(\tilde{m}_E)_{kk} \simeq (\tilde{m}_E)_{kk}^{\text{RPC}} - 0.76 |\lambda_{ijk}|^2 (A_0^2 + 3M_0^2), \quad (11)$$

where $(\tilde{m}_E)_{kk}^{\text{RPC}} \simeq M_0^2 + 0.15 M_{1/2}^2 - \frac{2}{3} X_k \delta_{k3}$ [89–91] and X_k includes the effects from the third-generation RPC soft-breaking trilinear interactions. Neglecting the D -term contributions, for the stau, it reads

$$X_3 \simeq \frac{(1 + \tan^2 \beta)}{10^4} \left(M_0^2 + 0.15 M_{1/2}^2 + 0.33 A_0^2 \right). \quad (12)$$

For various λ_{ijk} choices, one can obtain the analogue of Fig. 1 for both a $\tilde{\mu}$ and a $\tilde{\tau}$. The latter case is qualitatively different because of the large RPC τ Yukawa coupling, which is $\tan \beta$ -enhanced, *cf.* Eq. (12). In Fig. 2 we show the $\tilde{\tau}$ LSP regions in the $M_0 - M_{1/2}$ plane for both $\lambda_{ijk} =$

0 (solid black curve) and $\lambda_{323} = 0.15$ (solid blue curve) at M_X . The $\tilde{\tau}$ region is to the left of the respective curves and is significantly enlarged for a non-zero λ_{ij3} . The green region represents the allowed Higgs mass and the region to the left of the gray dashed line is excluded by the bounds on the RPV coupling for the case $\lambda_{323}|_{M_X} = 0.15$.

3. Large λ'_{ijk}

For large λ'_{ijk} , the only possible non-neutralino LSP candidate is a slepton or sneutrino of flavor i , as the squarks are always heavier due to the large RGE contribution from the gluino. The RPC contribution to the approximately integrated RGEs for the squarks are [89–92]

$$(\tilde{m}_Q^2)_{kk} \simeq M_0^2 + 5.2 M_{1/2}^2 - \frac{1}{3} (X_b + X_t) \delta_{k3}, \quad (13)$$

$$(\tilde{m}_D^2)_{kk} \simeq M_0^2 + 4.8 M_{1/2}^2 - \frac{2}{3} X_b \delta_{k3}, \quad (14)$$

whereas for the SU(2) doublet sleptons we have

$$(\tilde{m}_L^2)_{kk} \simeq M_0^2 + 0.52 M_{1/2}^2 - \frac{1}{3} X_\tau \delta_{k3}. \quad (15)$$

In the latter case the $M_{1/2}$ coefficient is about an order of magnitude smaller. When including the RPV effects, a one-step integration for the slepton soft-breaking masses is not sensible. This is because the λ' coupling increases by a factor of ~ 3 when running from the high to the low scale, see, *e.g.*, Ref. [93], thus requiring a numerical treatment.³

As the D -term contributions to the sparticle masses slightly suppress $m_{\tilde{\nu}}$ w.r.t. $m_{\tilde{L}}$, only the sneutrino can become the LSP for large λ'_{ijk} and $i = 1, 2$. For $i = 3$ the effect of the left-right-mixing in the stau sector reduces the lightest stau mass below $m_{\tilde{\nu}_\tau}$. The non-neutralino LSP candidates for the large- λ' scenario are thus $\tilde{\nu}_e, \tilde{\nu}_\mu$ and $\tilde{\tau}_1$, where the latter is mainly a $\tilde{\tau}_L$, unlike $\tilde{\tau}_R$ within RPC models. However, the parameter space for a λ' -induced non-neutralino and non-stau LSP is small because of (i) the already comparably large \tilde{m}_L^2 from the RPC RGEs alone and (ii) the smaller effect of a large A_0 when compared with the $\lambda_{ijk} \neq 0$ case.

In Fig. 3, as an example we show the nature of the LSP in the $M_0 - M_{1/2}$ plane for the case $\lambda'_{233}|_{M_X} = 0.08$, where $\tan \beta = 10$ and $A_0 = -2.8 \text{ TeV}$. The gray contours denote the LSP iso-mass curves. In the gray shaded region at the bottom the Higgs mass is too small [79, 80]. Here and in the following figures, all shown regions satisfy the bounds on single RPV couplings as given in Appendix A.

³ We found large discrepancies between the full treatment and the approximate one-step integration. This is also the case using the approximations in Refs. [69, 94].

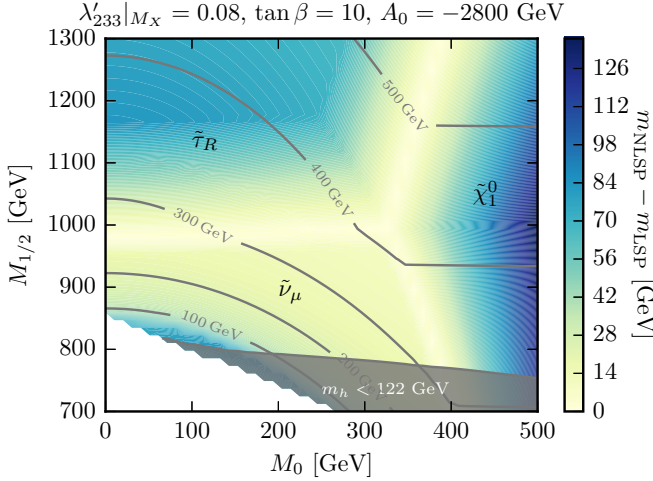


FIG. 3: Regions in the M_0 – $M_{1/2}$ plane with different LSPs for $\lambda'_{233}|_{M_X} = 0.08$. The other parameters are $\tan\beta = 10$ and $A_0 = -2.8$ TeV. The gray contours are LSP iso-mass curves, which are labeled in black for the different LSP regions. In most of the $\tilde{\nu}_\mu$ LSP region, the NLSP is the smuon. The gray shaded region corresponds to a too small Higgs mass below 122 GeV. Using the scale on the right, the color regions show the mass difference $m_{\text{NLSP}} - m_{\text{LSP}}$ in GeV.

The color scale on the right is given in GeV and denotes the mass difference $m_{\text{NLSP}} - m_{\text{LSP}}$. The LSP name is given in black and the boundary of the mass cross over is shown in beige. For large M_0 the lightest neutralino is the LSP. For $M_0 \lesssim 350$ GeV and $M_{1/2} \gtrsim 980$ GeV, $\tilde{\tau}_1$ is the LSP. Only in the small remaining region is a $\tilde{\nu}_\tau$ -LSP obtained. The white region in the lower left corner results in tachyons.

4. Large λ''_{ijk}

The constraints on the λ'' couplings, *cf.* Tab. XIII, are typically rather loose, leaving more room to have strong RPV effects on the RGE squark running. An exception are the strong bounds on $\lambda''_{112,113}$, *cf.* Appendix A. Therefore the only possibility with an operator solely coupled to the 1st and/or 2nd generation squarks is λ''_{212} . In Fig. 4 we show as an example the LSP nature for the case $\lambda''_{212}|_{M_X} = 0.5$ in the M_0 – $\tan\beta$ plane. This is to also show the $\tan\beta$ dependence of the LSP nature for the case of two particle species ($\tilde{\chi}_1^0$ and \tilde{s}_R, \tilde{d}_R) whose mass is largely independent of $\tan\beta$, and the lightest stau, whose mass depends strongly on $\tan\beta$. The other parameters are $M_{1/2} = 1$ TeV and $A_0 = -3.3$ TeV. Here, for large $M_{1/2}$, the \tilde{d}_R and \tilde{s}_R are almost degenerate and can be the joint LSPs. In the figure we have disregarded the \tilde{s}_R – \tilde{d}_R mass-splitting, as it is below 1 GeV. Throughout the figure the neutralino and gluino masses do not vary significantly as $M_{1/2}$ is fixed. Their masses are $m_{\tilde{\chi}_1^0} \simeq 430$ GeV and $m_{\tilde{g}} \simeq 2.2$ TeV. The remaining labels are as in Fig. 3.

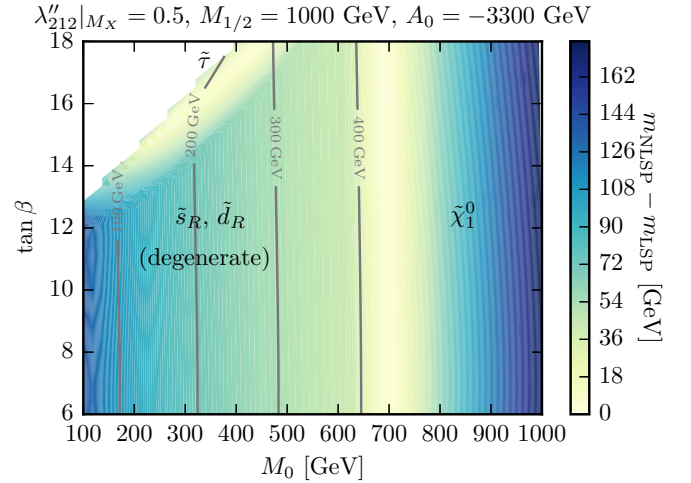


FIG. 4: Different LSPs in the M_0 – $\tan\beta$ plane for $\lambda''_{212}|_{M_X} = 0.5$. The other parameters are $M_{1/2} = 1$ TeV and $A_0 = -3.3$ TeV. The white region in the upper left corner corresponds to a tachyonic stau and/or squarks. The other labels are as in Fig. 3.

In the center of the figure we have a large \tilde{s}_R/\tilde{d}_R -LSP region. To the right, for large values of M_0 , we again have a $\tilde{\chi}_1^0$ -LSP. In the far upper left corner the white area indicates a tachyonic stau and/or squarks. Just below that is a small region with a $\tilde{\tau}$ -LSP. In the λ''_{212} -scenario the charm-squarks, in turn, cannot become the LSP because of their slightly heavier soft-breaking masses at the low scale, $\tilde{m}_U^2 - \tilde{m}_D^2 \simeq 0.05 M_{1/2}^2$ [89, 90, 92].

For λ''_{ij3} , $i \neq 3$ the \tilde{b}_R couples directly to the leading RPV operator, allowing for a sbottom LSP. We always have $m_{\tilde{b}_R} < m_{\tilde{u}_{i=1,2}}, m_{\tilde{d}_{i=1,2}}$ due to the larger RPC bottom Yukawa coupling.

Similarly for λ''_{3jk} , we can only get a stop LSP as a novel scenario, even for $k = 3$, as the RPC top-Yukawa dominates. To demonstrate this, we show in Fig. 5 the LSP nature in the A_0 – $\tan\beta$ plane, for the case $\lambda''_{323}|_{M_X} = 0.5$. The other parameters are fixed as $M_0 = 600$ GeV and $M_{1/2} = 1200$ GeV. This results in a gluino mass fixed around $m_{\tilde{g}} \simeq 2.6$ TeV and a lightest neutralino mass of about $m_{\tilde{\chi}_1^0} \simeq 520$ GeV. The labelling is otherwise as in Fig. 3. Note the scaling of the x -axis is fairly fine. Besides the usual $\tilde{\chi}_1^0$ - and $\tilde{\tau}$ -LSP regions we have an extended \tilde{t}_R -LSP region for $A_0 \lesssim -2.65$ TeV. No \tilde{b} -LSP region is obtained.

C. Summarizing the LSP Scenarios

In Tab. II we summarize all possible LSP scenarios we have found, stating the required (large) RPV coupling, as appropriate. This is the first main result of this paper. For small values of $\Lambda_{\tilde{R}_p} \ll 1$ we reproduce the results of the RPC–CMSSM, *i.e.* large regions of pa-

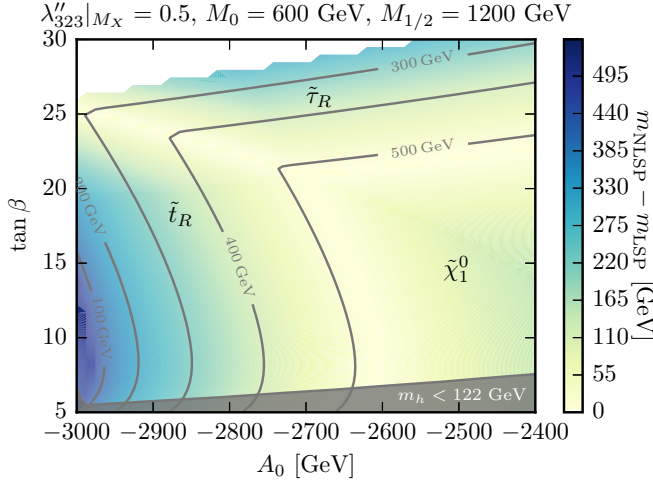


FIG. 5: Regions in the A_0 - $\tan \beta$ plane with different LSPs for $\lambda_{323}^{''}|_{M_X} = 0.5$. The other parameters are $M_0 = 0.6$ TeV and $M_{1/2} = 1.2$ TeV. In the top left white region the staus become tachyonic. As in Fig. 4, the neutralino and gluino masses do not vary significantly as $M_{1/2}$ is fixed. Their masses are $m_{\tilde{\chi}_1^0} \simeq 520$ GeV and $m_{\tilde{g}} \simeq 2.6$ TeV. The other labels are as in Fig. 3.

parameter space give a neutralino LSP. However significant regions of parameter space result in a stau LSP, which is predominantly a right-handed stau. This occurs for small values of M_0 and moderate to large values of $M_{1/2}$. In Fig. 2 we show as an example regions of parameter space with a stau LSP. Both the neutralino and the stau LSP scenarios are special, in the sense that any R -parity violating operator can be dominant. When discussing the phenomenology at the LHC, we thus in principle have to consider all 45 different possibilities for a dominant RPV operator. We do this for the neutralino in Sec. III, and for the stau in Sec. IV. The other LSP cases for large couplings are discussed in Sec. V.

D. RGE-Induced Operators

Once lepton (baryon) number is violated by a non-zero $\Lambda_{\tilde{R}p}|_{M_X}$, other lepton (baryon) number-violating operators $\Lambda_{\tilde{R}p}^{\text{ind}} \neq 0$ are induced at M_W via RGE effects. This occurs via diagrams of the type shown in Fig. 6. The explicit RGEs for λ and λ' are, for instance, given in Ref. [93]. These RGE-generated operators are typically phenomenologically irrelevant as they are loop suppressed and $\Lambda_{\tilde{R}p}^{\text{ind}} \ll \Lambda_{\tilde{R}p}$. However, they become relevant once new decay channels open which would otherwise be absent [34, 95, 96].

Consider a stau LSP and a single non-zero RPV coupling λ'_{ijk} with $i \neq 3$. Then at tree-level the $\tilde{\tau}_1$ cannot decay directly to an R -parity even two-body final state

LSP	Required Couplings
$\tilde{\chi}_1^0$	$\Lambda_{\tilde{R}p} \ll 1$ or large M_0
$\tilde{\tau}_1$	$\Lambda_{\tilde{R}p} \ll 1$, small M_0 and large $M_{1/2}$
$\tilde{\tau}_1$	λ_{ij3} (dominantly $\tilde{\tau}_R$), λ'_{3jk} ($\tilde{\tau}_L$)
\tilde{e}_R	λ_{ij1}
$\tilde{\mu}_R$	λ_{ij2}
$\tilde{\nu}_e$	λ'_{1jk} , $\{j, k\} \neq \{1, 1\}^\dagger$
$\tilde{\nu}_\mu$	λ'_{2jk}
\tilde{s}_R, \tilde{d}_R	λ''_{212} (degenerate LSPs)
\tilde{b}_1	$\lambda''_{123}, \lambda''_{213}, \lambda''_{223}^\dagger$ (dominantly \tilde{b}_R)
\tilde{t}_1	λ''_{3jk} (dominantly \tilde{t}_R)

TABLE II: Summary of the various LSP scenarios in the $\Lambda_{\tilde{R}p}$ -CMSSM as a function of the dominant necessary RPV coupling at M_X .[†] Note that the couplings on the right column are required but their presence is not necessarily sufficient to get the corresponding LSP. The couplings λ'_{111} , λ''_{112} and λ''_{113} are too constrained to produce an LSP of that kind, see Tab. XIII.

but rather decays via the chain

$$\tilde{\tau}_1 \rightarrow \begin{cases} \tau + \tilde{\chi}^{0(*)} & \rightarrow \tau + (\ell_i u_j d_k, \nu_i d_j d_k), \\ \nu_\tau + \tilde{\chi}^{\pm(*)} & \rightarrow \nu_\tau + (\ell_i d_j d_k, \nu_i u_j d_k), \end{cases} \quad (16)$$

to a four-body final state. Here we have neglected charge-conjugations and assumed the chargino to be dominantly wino. $X^{(*)}$ indicates that the respective particle X need not necessarily be on-shell. There is also a similar scenario for λ_{ijk} with $\{i, j, k\} \neq 3$.

However, through RGE running, in both cases the couplings $\lambda_{ijk}^{(r)}|_{M_X}$ generate a non-zero $\lambda_{i33}|_{M_W}$, enabling the two-body decays $\tilde{\tau} \rightarrow \ell_i \nu_\tau / \tau \nu_i$. The RGEs for this case read

$$16\pi^2 \frac{d}{dt} \lambda_{i33} = \lambda_{i33} \left[-\frac{9}{5} g_1^2 - 3g_2^2 + 4(Y_e)_{33}^2 \right] + 3\lambda'_{ijk}(Y_e)_{33}(Y_d)_{jk} + \lambda_{ijk}(Y_e)_{33}(Y_e)_{jk}. \quad (17)$$

The RGE-induced RPV operators scale as a function of the down-type Yukawas, which are themselves a function of $\tan \beta$. This means that the size of $\tan \beta$ has a strong effect on the relative magnitude of the initial and the induced coupling and thus on the branching ratio of a stau LSP into four- and two-body final states. This is depicted in Fig. 7 where we show various stau LSP decay branching ratios as a function of $\tan \beta$, assuming a non-zero $\Lambda_{\tilde{R}p} = \lambda'_{211} = 0.07$ at M_X . In solid black and blue we show the two four-body decays via the neutralino, corresponding to the top line in Eq. (16), respectively. Note that the two actually differ, unlike the assumptions in many experimental analyses, *cf.* Sec. III. The solid lavender curve shows the negligible decay via the chargino, corresponding to the second line in Eq. (16).

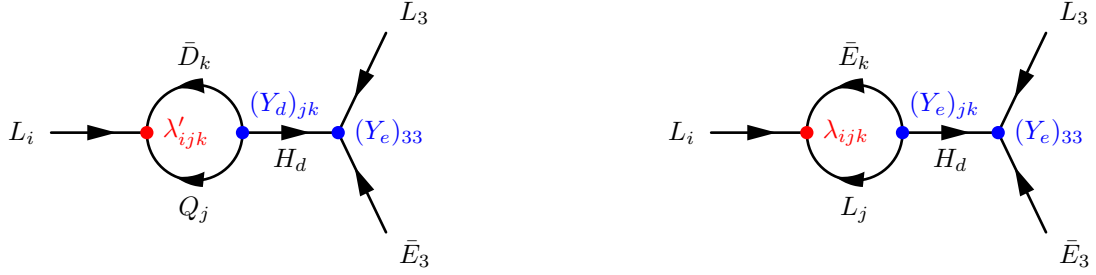


FIG. 6: Superfield Feynman diagrams corresponding to the one-loop RGE-induced λ_{i33} operators. The diagrams assuming non-zero λ'_{ijk} and λ_{ijk} are shown on the left- and right-hand side respectively.

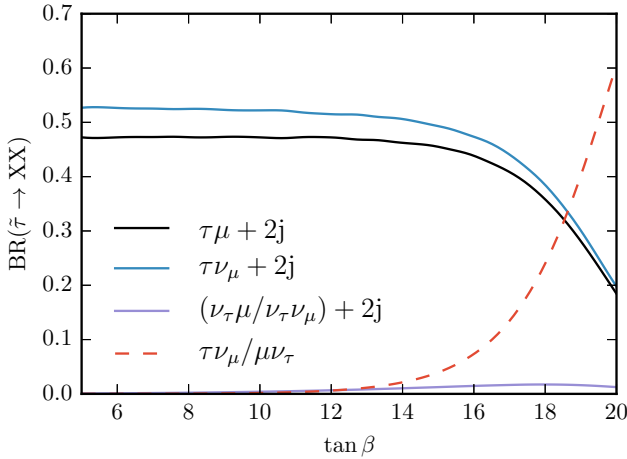


FIG. 7: Branching ratios of the decaying $\tilde{\tau}$ LSP as a function of $\tan\beta$ using $\lambda'_{211}|_{\text{GUT}} = 0.07$ as well as $M_0 = 0.2$ TeV, $M_{1/2} = 1$ TeV and $A_0 = -1.75$ TeV. The solid black and blue curves indicate the four-body decay via the neutralino. In solid lavender we show the branching ratio for the four-body decay via the chargino. The dashed red curve denotes the branching ratio for the two-body decay via the RGE-induced coupling λ_{233} .

The dashed red curve shows the branching ratio for the RGE-generated two-body decay via the operator λ_{233} . This becomes significant for $\tan\beta > 16$ and dominant for $\tan\beta \gtrsim 18$.

The four-body decay branching ratio $\tilde{\tau} \rightarrow \tau\mu + 2\text{jets}$ for $\lambda'_{211}|_{M_X} = 0.07$ is shown in the left plot of Fig. 8 as a function of $\tan\beta$ and A_0 . For $A_0 \simeq -2300$ GeV, at the finger shaped region, there is a small resonance in the partial width $\tilde{\tau} \rightarrow \tau\mu + 2\text{j}$. This occurs due to a level-crossing in the mixing between the left- and right-handed gauge eigenstates of the staus as $|A_0|$ increases. Subsequently, the largest branching ratio occurs where the stau left-right mixing is maximal as the RPV operator $L\bar{Q}\bar{D}$ involves only left-handed sleptons. One should note that this level crossing only appears as a result of the large RPV coupling. For smaller RPV couplings, the right smuon is always the lighter one. However, for the rela-

tively large RPV value used in Fig. 8, the RGE effects of this coupling in conjunction with A_0 drive the left-handed slepton soft-mass towards smaller values, leading to a level-crossing at a particular value of A_0 . Once again, the gray parameter region is excluded as the Higgs mass is too small.

If we consider the analogous scenario for $\lambda'_{222}|_{M_X} = 0.07$ instead of λ'_{211} , shown in the left plot of Fig. 8, the partial widths of the four-body decays do not change. On the other hand the RGE-induced coupling λ_{233} is larger because of the significantly larger strange-quark Yukawa coupling $(Y_d)_{22} \gg (Y_d)_{11}$. Therefore the corresponding two-body partial width is much larger. For a more detailed discussion of the effect of the RGE-induced operators and the impact of four-body decays, we refer to Ref. [93].

III. LHC COVERAGE OF RPV-INDUCED NEUTRALINO LSP DECAY SCENARIOS

As we saw in the previous section, throughout wide ranges of the RPV-CMSSM parameter space, and in particular for $\Lambda_{\tilde{R}_p} \ll 1$, the LSP is given by the lightest neutralino. We first discuss in this section the decay lifetime of the neutralino, to see what ranges of parameter space we probe when restricting ourselves to prompt decays. We then discuss in detail the LHC final state signatures, depending on the dominant RPV operator at M_X , and their coverage by existing LHC searches.

A. Neutralino Lifetime

For a given dominant RPV operator, if kinematically allowed, the neutralino LSP will decay via a three-body mode to the R -parity even particles of the operator, *e.g.*

$$L_i L_j \bar{E}_k : \quad \tilde{\chi}_1^0 \rightarrow \{\ell_i^- \nu_j \ell_k^+, \nu_i \ell_j^- \ell_k^+\} + c.c. \quad (18)$$

Note that in R -parity violating models the neutralino LSP can in principle be very light or even massless [97–100]. A very light neutralino would decay for example as $\tilde{\chi}_1^0 \rightarrow \gamma \nu_{i,j}$ via $L_i L_j \bar{E}_i$ or $L_i Q_j \bar{D}_j$ operators. However,

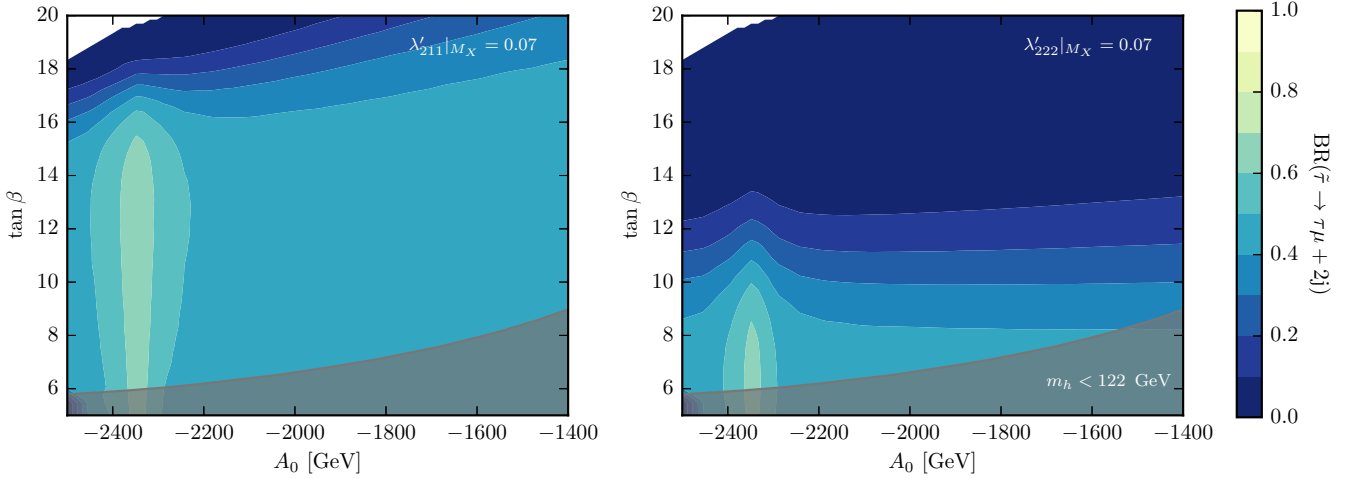


FIG. 8: Branching ratios of the stau four-body decay $\tilde{\tau} \rightarrow \tau \mu j j$ as a function of A_0 and $\tan \beta$ using $\lambda'_{211}|_{M_X} = 0.07$ (left) and $\lambda'_{222}|_{M_X} = 0.07$ (right). The other parameter values are $M_0 = 0.2$ TeV and $M_{1/2} = 1$ TeV. The gray parameter space is excluded due to a too light Higgs mass, whereas the white upper-left corner features a tachyonic stau.

neutralino masses below ~ 50 GeV [101] only arise with non-universal gaugino masses at the unification scale, which is outside of the RPV-CMSSM which we investigate here. Thus we shall only consider the three-body neutralino decay modes for the $\tilde{\chi}_1^0$ -LSP.

Here we are interested in the effects of the R -parity violating neutralino decay on LHC physics. In this paper we restrict ourselves to neutralinos decaying promptly in the detector, *i.e.*

$$c\tau_{\tilde{\chi}_1^0} \lesssim 10^{-4} \text{ m}. \quad (19)$$

We shall consider the long-lived case with detached vertices

$$10^{-4} \text{ m} < c\tau_{\tilde{\chi}_1^0} < 5 \text{ m}, \quad (20)$$

elsewhere.

As an example, for a pure photino the partial neutralino decay width via $L_1 Q_2 \bar{D}_1$ is given by [102]

$$\Gamma(\tilde{\gamma} \rightarrow \nu_e s \bar{d}) = \frac{3\alpha e_d^2 \lambda_{121}^{\prime 2}}{128\pi^2} \frac{M_{\tilde{\chi}_1^0}^5}{M_{\tilde{f}}^4}, \quad M_{\tilde{\chi}_1^0} \ll M_{\tilde{f}}, \quad (21)$$

assuming the final state fermion masses are negligible. \tilde{f} represents the virtual squarks/sleptons in the propagator of the decay, all assumed to be degenerate. The neutralino lifetime is thus inversely proportional to the R -parity violating coupling squared and depends sensitively on the neutralino and the sfermion masses. In the general case it depends on the neutralino admixture [103].

In Fig. 9 we show in the $\Lambda_{\tilde{R}_p}$ -CMSSM, for fixed $\Lambda_{\tilde{R}_p} = 5 \cdot 10^{-5}$ at the unification scale, how the neutralino decay length $c\tau$ (color scale on the right) depends on M_0 and $M_{1/2}$ for the cases $\Lambda_{\tilde{R}_p} = \lambda_{123}$ (upper-left panel), λ'_{112} (lower-left panel) and λ'_{323} (lower-right panel), respectively. We also show the A_0 , $\tan \beta$ dependence of

the decay length for λ_{123} in the upper-right panel. In the upper-left panel, we see that we get decay lengths ranging from 10 cm, which is readily observable as a detached vertex, down to $1 \mu\text{m}$.

Besides being proportional to the R -parity violating coupling squared, as we see in Eq. (21), the decay width scales as the fifth power of the neutralino mass, which is strongly connected to $M_{1/2}$, and the fourth inverse power of the scalar fermion propagator mass, which is not only strongly correlated with M_0 , but also depends on $M_{1/2}$ via the RGEs. When comparing the top left with the lower panels in Fig. 9, we see that the lifetime can be quite different for equally sized $\Lambda_{\tilde{R}_p}$ at the unification scale. λ'' is almost a factor three larger than λ at the low-scale, due to the RGEs. However for λ the slepton masses in the propagator are much lighter than the squark masses for λ'' . The propagator effect dominates, as $\Gamma \propto (\lambda''')^2 M_{\tilde{f}}^{-4}$. Furthermore, when comparing the $M_{1/2}$ dependence for $\Lambda_{\tilde{R}_p} = \lambda$ versus $\Lambda_{\tilde{R}_p} = \lambda''$, there is a much slower decrease of $c\tau$ with increasing $M_{1/2}$ for the λ'' scenarios, since the squark masses also increase with $M_{1/2}$. In the lower panels we also see a marked difference in the decay lengths for the two couplings, λ'_{323} and λ'_{122} . For λ'_{323} the final state top quark leads to a phase space suppression if $M_{1/2}$ and therefore $m_{\tilde{\chi}_1^0}$ is small. For larger $M_{1/2}$ as well as large M_0 (corresponding to large $|A_0|$ in the setup at hand), a lighter virtual top squark, in comparison to the first-/second-generation squarks, is more important. This lighter top squark leads to smaller decay lengths for λ'_{323} compared to λ'_{121} in these regions.

When $m_{\tilde{\chi}_1^0} < m_t + m_b$ (not shown in the figure), the three body decay $\tilde{\chi}_1^0 \rightarrow tbs$ is kinematically forbidden. We found that the corresponding four-body decay $\tilde{\chi}_1^0 \rightarrow t^{(*)}bs \rightarrow (bW^+)bs$ can be prompt for $\lambda'_{323} \sim \mathcal{O}(0.1)$ and $m_t + m_b - m_{\tilde{\chi}_1^0} \lesssim 10$ GeV. In addition, CKM-effects

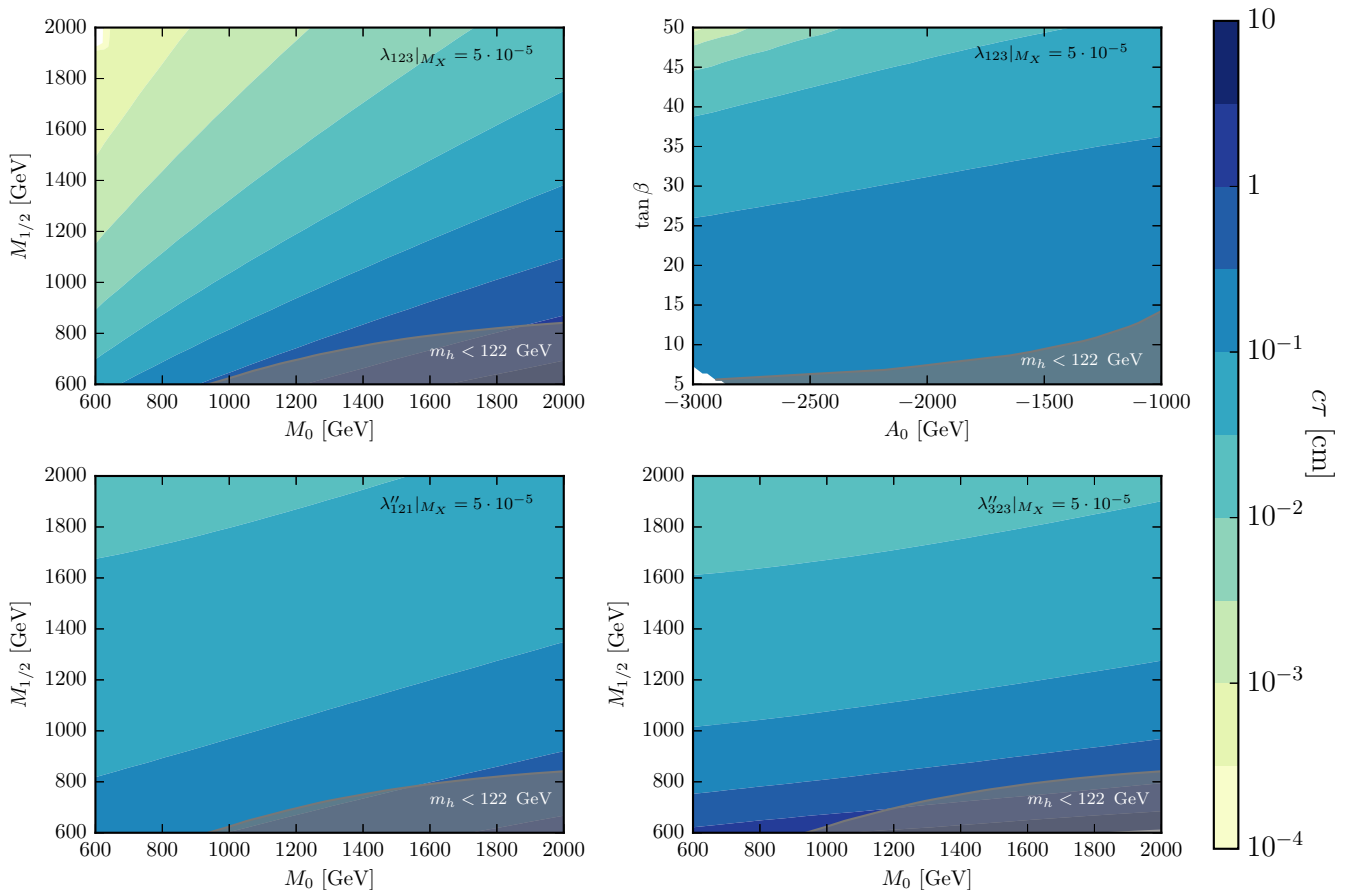


FIG. 9: Decay length $c\tau$ of the lightest neutralino for $\Lambda_{\mathcal{R}_p} = 5 \cdot 10^{-5}$ at the GUT-scale as a function of $\{M_0, M_{1/2}\}$ using $\tan\beta = 10$ and $A_0 = -2$ TeV (left upper panel) or $\{A_0, \tan\beta\}$ using $M_0 = 1.5$ TeV and $M_{1/2} = 1$ TeV (right upper panel). For both upper panels: $\Lambda_{\mathcal{R}_p} = \lambda_{123} = -\lambda_{213}$. The parameter space in the gray shaded region is excluded due to a too small Higgs mass. In the upper left corner of the figure, the $\tilde{\tau}$ is the LSP, so that the two-body decay $\tilde{\chi}_1^0 \rightarrow \tau\tilde{\tau}_1$ is possible, therefore drastically increasing the neutralino width. For the lower figures, we have used $\Lambda_{\mathcal{R}_p} = \lambda''_{112} = -\lambda''_{121}$ (left) and $\Lambda_{\mathcal{R}_p} = \lambda''_{323} = -\lambda''_{332}$ (right).

in the RGE evolution of the λ'' coupling lead to a nonzero λ''_{223} at the scale of the decaying particle and therefore open the alternate three-body decay $\tilde{\chi}_1^0 \rightarrow cbs$. However, we found the 4-body decay remains the dominant channel.⁴ The RGE-generated coupling is loop suppressed and thus if only the decay $\tilde{\chi}_1^0 \rightarrow cbs$ is kinematically accessible, the lightest neutralino is stable on detector scales. Note, however, that a neutralino as light as a top quark or lighter requires $M_{1/2} \lesssim 410$ GeV, resulting in $m_{\tilde{g}} \lesssim 1$ TeV, and can therefore be safely regarded as excluded, as we see below.

B. Neutralino LSP Decay via an $LL\bar{E}$ Operator

In the case of $LL\bar{E}$ operators, the neutralino decays to two charged leptons and a neutrino, *cf.* Eq. (18). At the LHC with the pair or associated production of squarks and/or gluinos, we expect cascade decays to two neutralinos. Such a process would therefore contain at least four charged leptons and some jets in the final state. The possible flavor and charged combinations depend on the dominant operator.⁵ We have summarized the charged lepton part of the leading order final state signatures in Table III. These are always accompanied by (at least) two neutrinos, resulting in additional missing transverse

⁴ The numerical details depend on assumptions where the CKM mixing takes place [104, 105].

⁵ As discussed above, for example an operator $L_1 L_2 \bar{E}_1$ can generate at 1-loop $L_2 Q_j \bar{D}_k$ operators. The corresponding neutralino decay branching ratios are however suppressed, as there is no kinematic or other suppression of the leading operators.

Scenario	Charged Lepton Signatures	RPV Operators
Ia	$e^+e^-e^+e^-$	$\lambda_{121,131}$
Ib	$\mu^+\mu^-\mu^+\mu^-$	$\lambda_{122,232}$
Ic	$\tau^+\tau^-\tau^+\tau^-$	$\lambda_{133,233}$
Id	$e^+e^-e^\pm\mu^\mp$	λ_{121}
Ie	$e^+e^-e^\pm\tau^\mp$	λ_{131}
If	$\mu^+\mu^-\mu^\pm e^\mp$	λ_{122}
Ig	$\mu^+\mu^-\mu^\pm\tau^\mp$	λ_{232}
Ih	$\tau^+\tau^-\tau^\pm e^\mp$	λ_{133}
Ii	$\tau^+\tau^-\tau^\pm\mu^\mp$	λ_{233}
Ij	$e^+\mu^-e^\pm\mu^\mp$	$\lambda_{121,231,122,132}$
Ik	$e^+\tau^-e^\pm\tau^\mp$	$\lambda_{131,231,123,133}$
Il	$\mu^+\tau^-\mu^\pm\tau^\mp$	$\lambda_{132,232,123,233}$
Im	$e^-\tau^+\mu^\pm\tau^\mp$	λ_{123}
In	$e^-\mu^+\tau^\pm\mu^\mp$	λ_{132}
Io	$e^-\mu^+e^\pm\tau^\mp$	λ_{231}

TABLE III: Possible charged lepton final states in the $LL\bar{E}$ case for a pair of LSP neutralinos resulting from the cascade decays of pair/associated produced SUSY particles. In each case, if distinct, the charged conjugate final state is also possible. The various charge combinations have equal branching ratios, due to the Majorana nature of the $\tilde{\chi}_1^0$ -LSP. All final states are accompanied by (at least) two neutrinos typically leading to some missing transverse momentum.

momentum in the signature.

As can be seen, for each dominant RPV operator, we can get SFOS (same flavor, opposite sign) lepton pairs. In all cases we can also get SFSS (same flavor, same sign) lepton pairs. This includes the somewhat exotic signatures (Im) $\tau^-\tau^+e^+\mu^+$, (In) $\mu^-\mu^+e^+\tau^+$, and (Io) $e^-e^+\mu^+\tau^+$. For each dominant operator one should check which final state leads to the optimal experimental sensitivity. In the case of a discovery, we see that each operator has two alternate channels, with definitive branching ratios, which should give a good experimental cross check.

Both ATLAS [106–108] and CMS [109–111] have searched for supersymmetry with RPV in four lepton events. Typically they have investigated simplified models where the supersymmetric particles are pair-produced and then directly decay to the neutralino LSP. The latter decays to a 3-body final state via the dominant RPV operator. We thus have the simplest cascades for the various produced

supersymmetric particles

$$\left. \begin{aligned} \tilde{\chi}_1^\pm &\rightarrow W^\pm \tilde{\chi}_1^0 \\ \tilde{\ell}^\pm &\rightarrow \ell^\pm \tilde{\chi}_1^0 \\ \tilde{\nu} &\rightarrow \nu \tilde{\chi}_1^0 \\ \tilde{q} &\rightarrow q \tilde{\chi}_1^0 \\ \tilde{g} &\rightarrow q\bar{q} \tilde{\chi}_1^0 \end{aligned} \right\} \text{ and } \tilde{\chi}_1^0 \rightarrow \ell^\pm \ell^\mp \nu. \quad (22)$$

The best resulting bounds with the appropriate reference are given in Tab. IV together with the couplings probed by the given experiments. We see that for each type of supersymmetric particle only a small subset of couplings has explicitly been probed. We note however, that the analysis considering the chargino limit, which looks for $N_{e,\mu} \geq 4$ (here $N_{e,\mu}$ refers to the number of first two generation charged leptons), can easily be extended to the operators $\lambda_{131,132,231,232}$ by computing the appropriate branching ratios of the neutralino decays and adjusting the signal rate accordingly. This holds for all searches focusing on (e^\pm, μ^\pm) .

Similarly in the case of the squark and gluino limits from Ref. [112], CMS searched for separate signatures with: a) $N_{e,\mu} = 4$, b) $N_{e,\mu} = 2$, $N_\tau = 2$, and c) $N_\tau = 4$. As we can see from Tab. III, this also covers the six operators not explicitly listed in the analysis. Thus again, adjusting the neutralino decay branching ratios allows, in this case, for complete coverage of all possible scenarios, when employing this existing search.

In Ref. [107], ATLAS designed three signal regions specifically for $LL\bar{E}$ RPV searches

$$(N_{e,\mu}, N_\tau, \cancel{E}_T [\text{GeV}]) = \begin{cases} (i) & (\geq 4, \geq 0, \geq 75), \\ (ii) & (= 3, \geq 1, \geq 100), \\ (iii) & (= 2, \geq 2, \geq 100). \end{cases} \quad (23)$$

Here, \cancel{E}_T [GeV] gives the missing transverse energy in GeV. ATLAS always employed SFOS signatures. They also considered several simplified models with chargino, slepton, sneutrino or gluino pair production, respectively, followed by the decays as in Eq. (22). This resulted in several of the bounds listed in Tab. IV. Comparing Eq. (23) with Tab. III we see that these searches cover all possible scenarios. Thus, again possibly adjusting for the decay branching ratios of the neutralinos, these searches can be employed to constrain all RPV $LL\bar{E}$ models.

Employing Refs. [107, 112] we see that at least at the level of simplified models the neutralino LSP model with a dominant $L_i L_j \bar{E}_k$ operator has been tested at the LHC, setting lower mass bounds. When going to the full Λ_{R_p} -CMSSM we expect these bounds to be weaker, as the rates will be degraded through additional decay modes. However, several distinct decay chains will contribute to a signal rate, possibly compensating the above degradation. In Sec. VI we set bounds on the Λ_{R_p} -CMSSM parameter space using the LHC searches which have been implemented in the program CheckMATE [63, 64],

Particle	Lower Bound [GeV]	$LL\bar{E}$ Coupling	Simplified Model	Comment	Reference
$\tilde{\chi}_1^0$	900 (740)	λ_{122} ($\lambda_{123,233}$)	$m_{\tilde{\chi}_1^\pm} = m_{\tilde{\chi}_1^0} + 1 \text{ GeV}$	Wino production	[110]
$\tilde{\chi}_1^0$	900 (560) [260]	λ_{122} (λ_{123}) [λ_{233}]	$m_{\tilde{\chi}_1^\pm} = m_{\tilde{\chi}_1^0} + 1 \text{ GeV}$	Higgsino production	[110]
$\tilde{\chi}_1^\pm$	up to 750 (470)	λ_{121} (λ_{133})	$\tilde{\chi}_1^\pm \rightarrow W^\pm \tilde{\chi}_1^0$	$\tilde{W}^- \tilde{W}^+$ production	[56]
$\tilde{\chi}_1^\pm$	up to 1100	$\lambda_{121,122}$	$\tilde{\chi}_1^\pm \rightarrow W^\pm \tilde{\chi}_1^0$	13 TeV update of [56]	[113]
$\tilde{\ell}_L^\pm$	500 (425)	$\lambda_{121,122}$ ($\lambda_{133,233}$)	$\tilde{\ell}^\pm \rightarrow \ell^\pm \tilde{\chi}_1^0$	$N_\ell \geq 4$, 8 TeV	[107]
$\tilde{\ell}_R^\pm$	425 (325)	$\lambda_{121,122}$ ($\lambda_{133,233}$)	$\tilde{\ell}^\pm \rightarrow \ell^\pm \tilde{\chi}_1^0$	$N_\ell \geq 4$, 8 TeV	[107]
$\tilde{\nu}_L$	450	$\lambda_{121,122}$	$\tilde{\nu} \rightarrow \nu \tilde{\chi}_1^0$	$N_\ell \geq 4$, 8 TeV	[107]
\tilde{q}	1850 (1750) [1600]	λ_{122} (λ_{123}) [λ_{233}]	$\tilde{q} \rightarrow q \tilde{\chi}_1^0$	$N_\ell \geq 3$, 8 TeV	[112]
\tilde{t}_R	950 (900) [900]	λ_{122} (λ_{123}) [λ_{233}]	$\tilde{t}_R \rightarrow t \tilde{\chi}_1^0$	$m_{\tilde{\chi}_1^0} = 300 \text{ GeV}$ in [112] [110, 112, 114]	[110, 112, 114]
\tilde{g}	1450 (1270) [1200] {1050}	$\lambda_{121,122}$ (λ_{123}) [λ_{233}] { λ_{133} }	$\tilde{g} \rightarrow q \bar{q} \tilde{\chi}_1^0$	$N_\ell \geq 3$, 8 TeV	[107, 112]

TABLE IV: Best limits in RPV searches using simplified models and $LL\bar{E}$ operators. The pair-produced SUSY particles are assumed to decay down to the neutralino LSP which itself always decays as $\tilde{\chi}_1^0 \rightarrow \ell_i^\pm \ell_k^\mp \nu_j$, $\ell_j^\pm \ell_k^\mp \nu_i$, for $L_i L_j \bar{E}_k$. The bounds are only estimates, as they have been read off the relevant plots. The first column shows the particle on which a bound is set. The second and third columns show the lower mass bounds and the $LL\bar{E}$ operator which has been assumed for the respective scenario.

but which have not necessarily been designed for RPV searches. We note that a fit similar to [22] could possibly exclude these models, even though the dark matter constraint does not apply. In Sec. VIII we give the explicit resulting lower mass bounds for the individual supersymmetric particles.

ATLAS has performed an RPV-mSUGRA/CMSSM search [107] for the fixed parameters $M_0 = A_0 = 0$ excluding $M_{1/2} < 800 \text{ GeV}$. This corresponds roughly to a gluino mass of 1.8 TeV. CMS has also performed an RPV-CMSSM analysis using 9.2 fb^{-1} of data at $\sqrt{s} = 8 \text{ TeV}$ for the specific coupling λ_{122} [112]. They obtain a lower bound of $M_{1/2} \gtrsim 1200 \text{ GeV}$ for $M_0 = 1000 \text{ GeV}$, $\tan\beta = 40$ and $A_0 = 0$. This corresponds roughly to a lower gluino mass bound of 2.6 TeV, and a lower squark mass bound of 1.9 TeV, at this benchmark point.

We also note that in scenarios Ij-Il, we have with equal rates the special signatures SFSS-SF'SS, *i.e.* for two distinct lepton flavors they have same flavor, same sign. These should have an even lower background and in particular for the τ scenarios could lead to improved bounds.

The special case of stop pair production followed by the cascade decay to neutralinos which then decay via $LL\bar{E}$ operators was also investigated in Ref. [112]. In Ref. [110, 115], simplified models of squark, gluino and stop pair production have been considered. For not too light neutralino masses they obtain lower mass bounds of about 1750 GeV for the squarks, 1500 GeV for the gluinos and 950 GeV for the top squark, when considering λ_{122} . Similar results are obtained for λ_{121} .

In addition to colored production, the electroweak production of wino- or higgsino-like neutralinos has been considered [110]. In Ref. [56], the pair-production of wino-like charginos is considered. It is assumed that

the charginos are the NLSPs which decay to $W\tilde{\chi}_1^0$. The results are then interpreted in terms of $\lambda_{121} \neq 0$ and $\lambda_{133} \neq 0$, with the chargino mass bound depending on the mass difference $m_{\tilde{\chi}_1^\pm} - m_{\tilde{\chi}_1^0}$. The respective lower mass bounds range up to 750 GeV for λ_{121} and 470 GeV for λ_{133} . The analysis has been updated using 13 TeV data [113], yielding bounds which range up to 1140 GeV, when considering $\lambda_{12a} \neq 0$, $a = 1, 2$.

However, in a realistic model, a wino-like chargino is accompanied by a wino-like neutralino. The relevant associated production $pp \rightarrow \tilde{\chi}^0 \tilde{\chi}^\pm$ has a larger cross-section than both the neutralino or chargino pair-production alone. This has been taken into account in Ref. [110] where wino- and higgsino-LSPs are treated separately in a simplified model setup, always assuming the associated chargino state to be $\sim 1 \text{ GeV}$ heavier. However, it is further assumed that the bino is sufficiently heavy to play no role in either the production or decay. The resulting bounds for winos are about 900 GeV for λ_{122} and 740 GeV for both λ_{123} and λ_{233} . For a higgsino-like neutralino LSP the range of the bounds is much larger, constraining the mass below 260 – 900 GeV, where the strongest bound is obtained for λ_{122} and the weakest one for λ_{233} .

In Sec. VIB2, we will compare this simplified model approach directly with the bounds we obtain for a more realistic scenario with CMSSM boundary conditions. In that case, the bino is always the LSP whose production cross section is, however, negligible compared to the wino and higgsino production. This results in a decay of the produced wino/higgsino state down to a bino first which then itself decays via the $LL\bar{E}$ -operator-induced three-body decay. We will see that, using the search strategy of Ref. [56] and also taking into account electroweak

Scenario	Signature	$LQ\bar{D}$ Operator
IIa	$[\ell_a^+ \ell_a^\pm, \ell_a^+ \cancel{E}_T] 4j$	λ'_{abc}
IIb	$[\ell_a^+ \ell_a^\pm, \ell_a^+ \cancel{E}_T] 2b 2j$	λ'_{ab3}
IIc	$[\ell_a^+ \ell_a^\pm \bar{t}^{(-)}, \ell_a^+ \bar{t} b \cancel{E}_T] 2j$	λ'_{a3c}
IId	$[\ell_a^+ \ell_a^\pm \bar{t}^{(-)}, \ell_a^+ \bar{t} b \cancel{E}_T] 2b$	λ'_{a33}
IIe	$[\tau^+ \tau^\pm, \tau^+ \cancel{E}_T] 4j$	λ'_{3bc}
IIIf	$[\tau^+ \tau^\pm, \tau^+ \cancel{E}_T] 2b 2j$	λ'_{3b3}
IIg	$[\tau^+ \tau^\pm \bar{t}^{(-)}, \tau^+ \bar{t} b \cancel{E}_T] 2j$	λ'_{33c}
IIh	$[\tau^+ \tau^\pm \bar{t}^{(-)}, \tau^+ \bar{t} b \cancel{E}_T] 2b$	λ'_{333}
IIi	$4j \cancel{E}_T$	$\lambda'_{abc}, \lambda'_{3bc}$
IIj	$2b 2j \cancel{E}_T$	$\lambda'_{ab3}, \lambda'_{3b3}, \lambda'_{a3c}, \lambda'_{33c}$
IIk	$4b \cancel{E}_T$	$\lambda'_{a33}, \lambda'_{333}$

TABLE V: Possible final states in the $LQ\bar{D}$ case for a pair of neutralino LSPs decaying via the same operator. There will be further accompanying particles from the cascade decay of the originally produced particles, e.g. for squark pair-production $\tilde{q}\tilde{q}^* \rightarrow q\bar{q}\tilde{\chi}_1^0$, giving two extra jets. ℓ denotes a charged lepton and the indices $a, b, c = 1, 2$ denote leptons or quarks from the first or second generation. We have separated out the signatures with no charged lepton. For each listed signature there is a corresponding charge-conjugate signature due to the Majorana nature of the neutralino.

neutralino-chargino production, we can improve upon the bounds which have been obtained in Ref. [56].

C. Neutralino LSP Decay via an $LQ\bar{D}$ Operator

At leading order a neutralino decays via an $LQ\bar{D}$ operator to one lepton and two jets:

$$L_i Q_j \bar{D}_k : \quad \tilde{\chi}_1^0 \rightarrow \{\ell_i^- u_j \bar{d}_k, \nu_i d_j \bar{d}_k\} + c.c. \quad (24)$$

When discussing the decay signatures in the following ‘ j ’ shall denote a first- or second-generation quark jet, and ‘ ℓ ’ a first or second generation charged lepton. Top, bottom and tau are treated separately, as they can be identified by tagging-algorithms. The neutrino in the final state leads to missing transverse energy, \cancel{E}_T . When collectively describing states: $a, b, c = 1, 2$ denote the first two generations and $i, j, k = 1, 2, 3$ refer to all three generations.

The possible signatures arising from the decay of a pair of neutralinos together with the couplings they probe are summarized in Tab. V. Here we assume that squarks or gluinos are pair-produced at the collider and cascade-decay to two neutralino LSPs. We see that we obtain at most two charged leptons, as well as various combinations of jets, b -, t -quarks, τ -leptons and \cancel{E}_T , depending on the dominant coupling.

In the simplified models considered by the experimental collaborations, the gluinos or squarks cascade-decay

as in Eq. (22), however with the neutralino decay replaced by that in Eq. (24). Thus in order to obtain the total signature, those in Tab. V should be supplemented by 4 (2) jets in the case of gluino (squark) pair production. For example, for the dominant coupling λ'_{123} , cases IIb and IIj, assuming squark pair production we obtain the signatures:

$$\tilde{q}\tilde{q}^* + \text{IIb} : \quad [\ell_a^+ \ell_a^\pm, \ell_a^+ \cancel{E}_T] 2b 4j, \quad (25)$$

$$\tilde{q}\tilde{q}^* + \text{IIj} : \quad 2b 4j \cancel{E}_T. \quad (26)$$

A promising signature would then be two same-sign charged leptons, and two b -jets. This has been searched for in Ref. [116] yielding

$$m_{\tilde{q}} \geq 1160 (1360) \text{ GeV}, \quad m_{\tilde{\chi}_1^0} = 0.5 (0.9) m_{\tilde{q}}. \quad (27)$$

Note that Ref. [116] assumed $\text{BR}(\tilde{\chi}_1^0 \rightarrow \tau^\pm + 2j) = 0.5$, with the remaining 50% being decays to neutrinos and two jets. Even in these simplified models this is not true in general, as we saw in Fig. 7. The exact number depends on the admixture of the neutralino LSP [103], as well as on the masses of the involved off-shell stau and sneutrino propagators.

In Tab. V we see that each coupling leads to three distinct signatures, modulo lepton charge assignments. In the case of a discovery these should be cross-checked against each other. Presently, the most sensitive mode should be chosen, most likely same-sign di-leptons, together with possible b -quarks for λ'_{ij3} .

A summary of the experimental lower mass bounds on the supersymmetric particles for a given dominant coupling is given in Tab. VI. For squarks we have lower mass bounds ranging from about 1 to 1.4 TeV. In one special case for light gluino masses there is a bound of 2 TeV. The lower gluino mass bounds are similar, ranging from about 1 to 1.3 TeV, with some stricter bounds achieved in special scenarios with light squarks or heavy neutralino LSPs. The pair-production cross section of neutralino LSPs is typically much smaller than for squarks and gluinos resulting in the correspondingly weaker lower limits ranging from 500 to 720 GeV. Unlike the $LL\bar{E}$ case there are no RPV searches for charginos or sleptons here. In the last three lines of the table we have included lower limits on the top squark, which in the case at hand decays via a chargino instead of a neutralino while the chargino decays to a charged lepton and two jets. The lower mass bounds range from 580 GeV to 1100 GeV depending on the flavor of the charged lepton and the jets. This decay is not in the spirit of this section, but we considered it similar enough to include, as the neutralino decay could be blocked by the heavy top quark.

Regarding the coverage of the $LQ\bar{D}$ R -parity violating signatures by explicit R -parity violating searches, we see that Ref. [116] focused on leptons plus jets signatures. They consider τ leptons and b quarks, but explicitly omit top quarks, and also do not consider the neutrino \cancel{E}_T cases. They thus cover the signatures IIa, IIb, IIe, and IIIf. Comparing with Tab. VI we see that [116] covers a

Particle	Lower Bound [GeV]	$LQ\bar{D}$ Coupling	Simplified Model	Comment	Reference
$\tilde{\chi}_1^0$	720 (620) [660] {500}	λ'_{131} (λ'_{131}) [λ'_{233}] { λ'_{233} }		$\tan \beta = 2$ (40) [2] {40}	[110]
$\tilde{\mu}$	440 (825) [1290]	$\lambda'_{211} = 0.003$ (0.01) [0.04]	$\tilde{\mu} \rightarrow \mu \tilde{\chi}_1^0$	res. $\tilde{\mu}$ prod, $m_{\tilde{\chi}_1^0} = 200$ GeV	[117]
\tilde{q}	1160 (1090) [1065]	$\lambda'_{abc,ab3}$ (λ'_{3bc}) [λ'_{3b3}]	$\tilde{q} \rightarrow q \tilde{\chi}_1^0$	$m_{\tilde{\chi}_1^0} = 0.5 m_{\tilde{q}}$	[116]
	1315 (1360) [1225] {1215}	λ'_{abc} (λ'_{ab3}) [λ'_{3bc}] { λ'_{3b3} }		$m_{\tilde{\chi}_1^0} = 0.9 m_{\tilde{q}}$	[116]
	1310 (1400) [2000]	$\lambda'_{23c,233}$		$m_{\tilde{g}} \lesssim 2000$ (1500) [1000] GeV	[112]
\tilde{g}	1010 (970) [1070] {1050}	λ'_{abc} (λ'_{ab3}) [λ'_{3bc}] { λ'_{3b3} }	$\tilde{g} \rightarrow q \tilde{q} \tilde{\chi}_1^0$	$m_{\tilde{\chi}_1^0} = 0.1 m_{\tilde{g}}$	[116]
	1135 (1085) [1220]	λ'_{abc} (λ'_{ab3}) [$\lambda'_{3bc,3b3}$]		$m_{\tilde{\chi}_1^0} = 0.5 m_{\tilde{g}}$	[116]
	1285 (1260) [1200]	λ'_{abc} (λ'_{ab3}) [$\lambda'_{3bc,3b3}$]		$m_{\tilde{\chi}_1^0} = 0.9 m_{\tilde{g}}$	[116]
	2000 (1500) [1000]	$\lambda'_{23c,233}$		$m_{\tilde{q}} \lesssim 1310$ (1400) [2000] GeV	[112]
	1520 (1770) [1820]	λ'_{abc}		$m_{\tilde{\chi}_1^0} = 100$ (500) [890] GeV	[118] [119]
\tilde{t}	890 (1000)	λ'_{1bc} (λ'_{2bc})	$\tilde{t} \rightarrow b(\ell^+ 2j)_{\tilde{\chi}_1^+}$	$m_{\tilde{\chi}_1^+} = 100$ GeV	[120]
	580	λ'_{3bc}	$\tilde{t} \rightarrow b(\tau^+ 2j)_{\tilde{\chi}_1^+}$	$m_{\tilde{\chi}_1^+} = 100$ GeV	[121]
	710 (860)	λ'_{132} (λ'_{232})	$\tilde{t} \rightarrow 2b(\ell^+ j)_{\tilde{\chi}_1^+}$	$m_{\tilde{\chi}_1^+} = m_{\tilde{t}} - (100 \text{ GeV})$	[122]

TABLE VI: Best limits in RPV searches using simplified models and $LQ\bar{D}$ operators. Here $a, b, c \in \{1, 2\}$. The pair-produced supersymmetric particles are assumed to decay directly to the neutralino LSP. The bounds are only estimates, as they have been read off the relevant plots. The neutralino LSP always decays as $\tilde{\chi}_1^0 \rightarrow (\ell_i^- u_j \bar{d}_k, \nu_i d_j \bar{d}_k) + c.c.$ for $L_i Q_j \bar{D}_k$. We have included the analysis of a scalar top decaying via a chargino and not the neutralino LSP in the last line, since it is similar. The neutralino decay can be blocked due to the heavy top quark. The search in Ref. [112] allows for simultaneously non-decoupled squarks and gluinos. In Ref. [114] CMS was able for a given $m_{\tilde{\chi}_1^0} \in [200, 800]$ GeV to exclude a range of scalar top squark masses, without a fixed lower bound. We have included the bound on the smuon mass, which is from a search for resonant production, since it also decays via the neutralino LSP. Each mass bound is for a fixed value of the RPV coupling.

wide range of possible $LQ\bar{D}$ couplings, however it omits the couplings λ'_{i3k} , since in that case the charged leptons are accompanied by a heavy top quark. Ref. [112] explicitly looked for the cases λ'_{23k} , partially covering the signatures IIc and IId. The signatures IIg-IIk either involve charged leptons with top quarks, or have \cancel{E}_T signatures instead of the charged leptons. None of these have been covered by explicit RPV searches at the LHC. In particular the couplings λ'_{33k} have not been looked for. Note that in Ref. [110], CMS did search for electroweak gaugino production decaying via $\lambda'_{331,333}$, however the sensitivity was insufficient to lead to any bound. In Ref. [116] explicitly looked for τ 's and b -quarks, giving specific sensitivity to the cases λ'_{3jk} and λ'_{ij3} . However, they did not look for top quarks together with charged leptons and therefore explicitly omitted λ'_{i3j} .

We make a special mention of Ref. [117], where CMS analyzed resonant smuon production, with the smuon decaying via the neutralino LSP [123, 124]. The production cross section is proportional to the RPV coupling squared and in order to get an appreciable rate requires $\lambda'_{211} \gtrsim 0.003$. The lower mass limit then depends strongly on the assumed coupling value, as can be seen in Tab. VI. We point out that CMS have interpreted this search also in terms of the RPV-CMSSM.

We note that some of the signatures listed in Tab. V are also covered by RPC searches. The first two scenarios,

IIa and IIb, involve only light leptons and jets, possibly b -jets. They always include an option also with \cancel{E}_T . The scenarios IId-IIk involve multijet events with missing transverse momentum, but zero leptons. These correspond to the standard RPC supersymmetry searches, see for instance Refs. [125–127] for isolated leptons and jets, and [128–132] for zero leptons and multijets accompanied by missing energy. The signatures including a τ lepton, *i.e.* IIe-IIh are in principle also covered by these multijet analyses. In this case, a hadronically decaying tau lepton is not explicitly tagged but handled as a hadronic object. Thus the couplings λ'_{i3k} have in principle been probed via the scenarios IId-IIk. The exact sensitivity will only be known once the corresponding experimental searches have been interpreted in terms of these RPV models.

All of the searches listed in Tab. VI, except the smuon search, employ minimal or next-to-minimal simplified models, with an intermediate neutralino LSP state in the decay chain. Thus it is difficult to see how the bounds in Tab. VI are modified in the case of realistic cascade decay branching ratios, as for example in the CMSSM. In Sec. VI, we shall use LHC analyses implemented in the computer program CheckMATE to obtain realistic limits on the parameters of the RPV-CMSSM models. We shall see for example that the search of Ref. [128] which looks for RPC as well as $\bar{U}\bar{D}\bar{D}$ -RPV is very sensitive to the signatures arising from the λ'_{3ij} operators within CMSSM

Scenario	Signature	$\bar{U}\bar{D}\bar{D}$ Operator
IIIa	$6j$	λ''_{a12}
IIIb	$(2b)(4j)$	λ''_{ab3}
IIIc	$(2t)(4j)$	λ''_{312}
IIId	$(2t)(2b)(2j)$	λ''_{3b3}

TABLE VII: Possible final states in the $\bar{U}\bar{D}\bar{D}$ case for a pair of neutralino LSPs decaying via the same operator. There will be further accompanying particles from the cascade decay of the originally produced particles, e.g. for squark pair production $\tilde{q}\tilde{q}^* \rightarrow q\tilde{q}\tilde{\chi}_1^0\tilde{\chi}_1^0$, giving two extra jets. The indices $a, b = 1, 2$ denote quarks from the first or second generation.

boundary conditions. In Ref. [116], a re-interpretation of the RPC searches of Refs. [125, 128, 129, 133] in terms of lepton-number-violating SUSY is presented. The resulting lower bounds on the gluino mass are around 1 TeV, for some cases similar limits are obtained for squark masses. In a CMSSM context, the bounds are even stronger as we see in Sec. VIII.

D. Neutralino LSP Decay via an $\bar{U}\bar{D}\bar{D}$ Operator

If the RPV operator $\bar{U}_i\bar{D}_j\bar{D}_k$ is non-zero, the neutralino LSP decays via an intermediate squark to three jets:

$$\bar{U}_i\bar{D}_j\bar{D}_k : \quad \tilde{\chi}_1^0 \rightarrow u_i d_j d_k + c.c. \quad (28)$$

Thus, for neutralino pair production we get six jets, possibly accompanied by further jets from intermediate cascade decays. The detailed jet flavor listings are given in Tab. VII. As we see, out of the six jets up to two can be bottom quark jets and up to two can be top quarks. Most searches for these scenarios are focused on multi-jet events with different numbers of b-tags [57, 134–142]. Some analyses also account for leptons, which could arise from leptonic top decays [110, 116, 141, 143–145]. The top quarks are not necessarily produced via the RPV operator but can originate from cascade decays, *e.g.* in stop pair production.

In Tab. VIII we have collected the best LHC lower mass bounds on the squark mass (treating the stop separately) and the gluino mass for various dominant couplings. We see that most searches have been performed for the case of gluino pair production. The mass bounds range from 650 GeV up to 2400 GeV depending on the scenario. For the case of a simplified model with only a light gluino and a neutralino mass of $m_{\tilde{\chi}_1^0} = 100$ GeV, ATLAS obtained a lower bound of 840 GeV. The search employed the “total jet mass of large-radius” [135]. Compared to a jet-counting analysis, it was shown that this technique allows for slightly higher sensitivity for light jets, whereas the jet-counting analysis provides the better bounds in the case of *b*-tagging requirements. The

strictest bound of 2400 GeV is achieved in a CMS search for a simplified model which also contains kinematically accessible squarks [112].

For squarks we found only one direct search [112] by CMS. They utilized an extended simplified model involving accessible squarks, gluinos and the second neutralino $\tilde{\chi}_2^0$. The pair production of $SU(2)$ singlet squarks is considered, followed by the cascade decay via

$$\tilde{q}R \rightarrow q\tilde{\chi}_2^0 \rightarrow q[\ell^+\tilde{\ell}^{(*)-}] \rightarrow q[\ell^+(\ell^-\tilde{\chi}_1^0)]. \quad (29)$$

The intermediate sleptons need not be on-shell but cannot be too heavy.

In the case of the stop we have an ATLAS search, which also assumes an intermediate chargino [119], giving rise to an additional decay mode. The resulting lower mass bounds are of the order 1 TeV.

The most pertinent question for us is how well the $\bar{U}\bar{D}\bar{D}$ models with a neutralino LSP are covered by searches at the LHC. Looking at Tab. VIII we see that the search from Ref. [57] in the last line seems to cover all possible λ''_{ijk} . However, ATLAS here explicitly assumed that *all* $\lambda''_{ijk} \neq 0$ simultaneously, with every coupling taking the same value. Thus the sensitivity of the search could rely unduly on bottom quarks from λ''_{ij3} and/or from top quarks from λ''_{3jk} couplings. If we look at explicit searches based on the single coupling dominance assumption, then we have gluino searches for $\lambda''_{112,212,213}$ [112, 118, 119, 138]. All such searches make additional assumptions on the squark and/or neutralino masses. We would expect the search for λ''_{213} to be equally sensitive to λ''_{223} . Similarly we would expect the λ''_{213} search to apply equally to λ''_{113} , provided $m_{\tilde{u},\tilde{d}} < m_{\tilde{g}}$, and to λ''_{123} , provided $m_{\tilde{u},\tilde{s}} < m_{\tilde{g}}$. Thus for the case of gluino production there is no coverage only of the three couplings λ''_{3jk} . This should be performed by the LHC experimental groups. As we see from Tab. VII, the final states involve either two top quarks and four jets or two top quarks, two bottom quarks and two jets, plus of course the accompanying jets from the cascade decay.

In Sec. VI, we also take into account dominant λ''_{3jk} couplings in the context of CMSSM boundary conditions and show that we can set bounds on this scenario using multijet analyses as well as searches for same-sign leptons. We do however expect a boost in discovery potential when designing a dedicated search for the signature outlined above.

As we see in rows two and three of Tab. VIII, the searches for top squarks cover at least two of these missing scenarios, namely λ''_{3b3} . Overall then the case λ''_{312} is missing for the scenarios considered here.

Once again, none of these models have been interpreted in terms of the CMSSM, thus it is difficult to see how realistic these mass bounds are. We shall come back to this question in Sec. VI and with explicit mass bounds in Sec. VIII.

Particle	Lower Bound [GeV]	$\bar{U}\bar{D}\bar{D}$ Coupling	Simpl. Model	Comment	Reference
\tilde{q}	1725 (1900) [2800]	λ''_{112}	$\tilde{q}_R \rightarrow j(\ell\tilde{\chi}_1^0)_{\tilde{\chi}_2^0}$	$m_{\tilde{g}} \leq 2400$ (1500) [1200] GeV	[112]
\tilde{t}	950 (980)	λ''_{3b3}	$\tilde{t} \rightarrow t\tilde{\chi}_{1,2}^0/b\tilde{\chi}_1^+$	$\tilde{\chi}_1^0 = \tilde{H} (\tilde{B})$, $m_{\tilde{\chi}_1^0} = 300$ GeV	[119]
	1090 (1260)	λ''_{3b3}	$\tilde{t} \rightarrow t\tilde{\chi}_{1,2}^0/b\tilde{\chi}_1^+$	$\tilde{\chi}_1^0 = \tilde{H} (\tilde{B})$, $m_{\tilde{\chi}_1^0} = 800$ GeV	[119]
\tilde{g}	1200 (1500) [2400]	λ''_{112}	$\tilde{g} \rightarrow jj(\ell\tilde{\chi}_1^0)_{\tilde{\chi}_2^0}$	$m_{\tilde{q}} \leq 2800$ (1900) [1725] GeV	[112]
	1850 (2100)	λ''_{112}	$\tilde{g} \rightarrow t\tilde{t}\tilde{\chi}_1^0$	$m_{\tilde{\chi}_1^0} = 100$ (800) GeV	[119]
				$m_{\tilde{g}} > 2m_t + m_{\tilde{\chi}_1^0}$	[119]
	650 (950) [1020]	λ''_{212}	$\tilde{g} \rightarrow q\bar{q}\tilde{H}_1^0$	$m_{\tilde{q}} \leq 100$ (500) [900] GeV	[138]
				$m_{\tilde{H}_1^0} = \frac{3}{4}m_{\tilde{q}}, m_{\tilde{c}} < m_{\tilde{g}}$	
	675 (1020) [1075]	λ''_{212}	$\tilde{g} \rightarrow q\bar{q}\tilde{H}_1^0$	$m_{\tilde{q}} \leq 100$ (500) [900] GeV	[138]
				$m_{\tilde{H}_1^0} = \frac{3}{4}m_{\tilde{q}}; m_{\tilde{b}} < m_{\tilde{g}}$	
	650 (1020) [1100]	λ''_{213}	$\tilde{g} \rightarrow q\bar{q}\tilde{H}_1^0$	$m_{\tilde{q}} \leq 100$ (500) [900] GeV	[138]
				$m_{\tilde{H}_1^0} = \frac{3}{4}m_{\tilde{q}}, m_{\tilde{b}} < m_{\tilde{g}}$	
	650 (990) [1075]	λ''_{213}	$\tilde{g} \rightarrow q\bar{q}\tilde{H}_1^0$	$m_{\tilde{q}} \leq 100$ (500) [900] GeV	[138]
	1040 (1555)	λ''_{ijk}	$\tilde{g} \rightarrow q\bar{q}\tilde{\chi}_1^0$	$m_{\tilde{\chi}_1^0} = 100$ (900) GeV	[57]
				all $\lambda''_{ijk} \neq 0$	
	800 (1050)	λ''_{abc}	$\tilde{g} \rightarrow 5q$	$m_{\tilde{\chi}_1^0} = 50$ (600) GeV	[142]

TABLE VIII: Best limits in RPV searches using simplified models and $\bar{U}\bar{D}\bar{D}$ operators. Here $a, b, c \in \{1, 2\}$. The pair-produced supersymmetric particles are assumed to decay directly to the neutralino LSP if not stated otherwise. The bounds are only estimates, as they have been read off the relevant plots. The neutralino LSP always decays as $\tilde{\chi}_1^0 \rightarrow \bar{u}_i \bar{d}_j \bar{d}_k + c.c.$ for $\bar{U}_i \bar{D}_j \bar{D}_k$. Each mass bound is for a fixed value of the RPV coupling.

IV. LHC COVERAGE OF RPV-INDUCED STAU LSP DECAY SCENARIOS

As we saw in Sec. II, even for small RPV couplings, we have substantial regions of CMSSM parameter space, where the LSP is the lightest stau, $\tilde{\tau}_1$. The question is: how does the phenomenology change compared to a neutralino LSP, and what are the experimental constraints? The stau LSP case has been discussed from the theoretical perspective in some detail in the literature [34, 93, 95, 96, 146]. In [95] a set of appropriate LHC benchmarks was defined. Here we are interested in the case of small, but not too small $\Lambda_{\tilde{R}_p}$. Thus the stau is the LSP but it still decays promptly. We shall consider the long-lived case where the stau leads to detached vertices, or is even stable on detector scales, elsewhere.

In order to discuss the LHC coverage for the stau LSP scenario, we distinguish two cases⁶

- (a) $\tilde{\tau}$ LSP with the dominant operator directly coupling to a tau/stau: $\Lambda_{\tilde{R}_p} \in \{\lambda_{aj3, a3c}, \lambda'_{3jk}\}$.

- (b) $\tilde{\tau}$ LSP with the dominant operator *not* coupling to tau/stau $\Lambda_{\tilde{R}_p} \in \{\lambda_{12c}, \lambda'_{ajk}, \lambda''_{ijk}\}$.

In case (a) we do not expect significant changes compared to the neutralino phenomenology. Consider the small $\Lambda_{\tilde{R}_p}$ case in the CMSSM, where we get a $\tilde{\tau}$ LSP for small M_0 and larger $M_{1/2}$, as discussed in Sec. IIB. There the NLSP is typically the lightest neutralino $\tilde{\chi}_1^0$. We then have the usual cascade decays of the strongly produced sparticles down to the neutralino, as shown in the bottom two rows on the left in Eq. (22). This is followed by the decay of the neutralino to the $\tilde{\tau}$. For example for the gluino we could have

$$\tilde{g} \rightarrow q\bar{q}\tilde{\chi}_1^0 \rightarrow q\bar{q}(\tau^\pm \tilde{\tau}^\mp). \quad (30)$$

This is followed by the direct RPV stau decay (plus charge conjugate)

$$\tilde{\tau}^- \rightarrow \begin{cases} \nu_a \ell_c^-, & L_a L_3 \bar{E}_c, \\ (\nu_1 \ell_2^-, \ell_1^- \nu_2), & L_1 L_2 \bar{E}_3, \\ (\nu_a \tau^-, \ell_a^- \nu_\tau), & L_a L_3 \bar{E}_3, \\ \bar{u}_j d_k, & L_3 Q_j \bar{D}_k, \end{cases} \quad (31)$$

depending on the dominant operator. These final states

⁶ Here again: $a, b, c \in \{1, 2\}$ and $i, j, k \in \{1, 2, 3\}$.

with the same couplings were also obtained for the neutralino LSP scenarios. However, there are slight differences here for the stau. If the RPV operator involves an L_3 chiral superfield, the neutralino decay to the tau neutrino is strongly disfavored in comparison to the on-shell decay mode. For example:

$$\tilde{\chi}_1^0\text{-LSP} : \tilde{\chi}_1^0 \rightarrow \{\nu_\tau e^\pm e^\mp, \tau^\pm \nu_e e^\mp\}; \quad L_1 L_3 \bar{E}_1, \quad (32)$$

$$\tilde{\tau}_1\text{-LSP} : \tilde{\chi}_1^0 \rightarrow \tau^\pm \tilde{\tau}^\mp \rightarrow \tau^\pm (\nu_e e^\mp); \quad L_1 L_3 \bar{E}_1. \quad (33)$$

In the $L_1 L_3 \bar{E}_1$ case one thus loses the $e^\pm e^\mp$ signature, instead having a tau lepton with 100% branching ratio. This could dilute the experimental sensitivity. Similarly for $L_3 Q_j \bar{D}_k$ operators, where the branching ratio for the charged tau is enhanced, possibly increasing the sensitivity compared to the neutralino LSP scenario.

In case (b), the stau does not couple to the dominant operator and the phenomenology changes, as the two-body decay channels in Eq. (31) are absent. The leading stau decay is four-body. In the case of a λ''_{ijk} operator, for example, the decay chains would be

$$\begin{aligned} \tilde{\tau} &\rightarrow \tau \tilde{\chi}^{0(*)} & \text{or} & \rightarrow \nu_\tau \chi^{\pm(*)} & (34) \\ &\hookrightarrow \tau u_i \tilde{u}_i^{(*)} / \tau d_{j,k} \tilde{d}_{j,k}^{(*)} & & \hookrightarrow \nu_\tau u_{j,k} \tilde{d}_{j,k}^{(*)} / \nu_\tau d_i \tilde{u}_i^{(*)} \\ &\hookrightarrow \tau u_i d_j d_k & & \hookrightarrow \nu_\tau u_{j,k} u_i d_{k,j} / \nu_\tau d_i d_j d_k \end{aligned}$$

where we have neglected charge-conjugations and denote virtuality by $^{(*)}$. We have allowed for decays via a chargino, as the intermediate states are virtual.

Whether the four-body decay is prompt or not depends heavily on the sparticle mass spectrum. The stau decay length, assuming a four-body decay only, scales roughly as [34]

$$\begin{aligned} c\tau_{\tilde{\tau}_1} &\simeq 6.2 \cdot 10^{-6} \text{ m} \left(\frac{10^{-3}}{\Lambda_{\tilde{R}_p}} \right)^2 & (35) \\ &\times \left(\frac{m_{\tilde{\chi}}}{100 \text{ GeV}} \right)^2 \left(\frac{m_{\tilde{f}}}{100 \text{ GeV}} \right)^4 \left(\frac{100 \text{ GeV}}{m_{\tilde{\tau}_1}} \right)^7, \end{aligned}$$

where $\tilde{\chi}$ refers to the virtual neutralino/chargino and \tilde{f} to the virtual sfermion in the decay.

In the stau LSP parameter regions, the lightest stau is mostly a $\tilde{\tau}_R$, so that the coupling to the wino is reduced w.r.t. the bino. In conjunction with the hierarchy in the CMSSM of $m_{\tilde{B}} < m_{\tilde{W}}$, this means that the decays via charginos, *i.e.* the ones resulting in $\nu_\tau + X$ are suppressed and the final states including a τ^\pm dominate. However, for λ''_{3jk} this is not true. In this case, all neutralino-mediated channels end up in a top quark, which is kinematically suppressed w.r.t. the chargino mediated $\nu_\tau b d_j d_k$ mode, unless the stau is very heavy.

As discussed in Sec. IID, even if the non-zero RPV operators at a given scale only involve couplings to first- and/or second-generation (s)leptons, operators coupling to (s)taus will be induced through the RGE evolution. Thus scenarios (a) and (b) are not strictly separated. This is particularly important in the case of large $\tan\beta$

Operators	LHC Signatures	Couplings
$LL\bar{E}$	$2\tau 4\ell \cancel{E}_T$	λ_{12c}
	$2\ell \cancel{E}_T$	$\lambda_{a3b,ab3,a33}$
	$\tau \ell \cancel{E}_T$	λ_{a33}
	$2\tau \cancel{E}_T$	λ_{a33}
$LQ\bar{D}$	$4j 2\tau 2\ell$	λ'_{aij}
	$4j 2\tau 1\ell \cancel{E}_T$	λ'_{aij}
	$4j 2\tau \cancel{E}_T$	λ'_{aij}
	$4j$	λ'_{3ij}
$\bar{U}\bar{D}\bar{D}$	$6j 2\tau$	λ''_{ijk}
	$6j \cancel{E}_T$	λ''_{3jk}^\ddagger

TABLE IX: LHC signatures for a stau LSP from the decay of two staus. $a, b, c = 1, 2$; $i, j, k = 1, 2, 3$. We did not distinguish between top quarks, bottom quarks and the jets arising from the first two generations. These are analogous to Tabs. V and VII. The special case in the last line denoted with ‡ refers to scenarios where the stau LSP is light so that the decay into a top quark is kinematically disfavoured, leading to the dominance of the chargino-mediated final state $\nu_\tau d_3 d_j d_k$ as in Eq. (34).

for any λ_{ijk} operators where $i, j, k \neq 3$ as well as all λ'_{ijj} operators with $i \neq 3$, see Eq. (17) and the corresponding Figs. 7 and 8 in Sec. IID. Thus in complete models, such as the CMSSM, this must be taken into account.

The complete listings of the stau-LSP LHC signatures for all RPV operators, including both $LL\bar{E}$ and $LQ\bar{D}$ as well as the two- and four-body stau decays, are given in Ref. [96], assuming a cascade originating from a squark. See Tables II-IV, therein. We summarize the signatures of two decaying staus in Tab. IX. Depending on the production mechanism of the two staus at the LHC, the signature will be accompanied by extra taus, missing \cancel{E}_T and jets. We do not distinguish between top quarks, bottom quarks and the jets arising from the first two generations. These are dependent on the generation indices of the couplings and are analogous to Tabs. V and VII. We see that these scenarios always involve multiple τ 's in the final state. For all $LL\bar{E}$ and $LQ\bar{D}$ couplings we can also have \cancel{E}_T arising from neutrinos. In the $LL\bar{E}$ case it is possible to have 1st and 2nd generation charged leptons. Contrastingly, the $\bar{U}\bar{D}\bar{D}$ scenario contains challenging final states with only two taus and jets.

LHC analyses explicitly looking for $\tilde{\tau}$ LSPs are rarely performed. The only one we are aware of with prompt stau decays is Ref. [106], where the CMSSM with $\lambda_{121} = 0.032$ at M_X is considered. It is assumed there that the stau always decays via a four-body decay into $\tau e \mu \nu_e$ and $\tau e \nu_\mu$ with equal probability and the results are interpreted in the $M_{1/2} - \tan\beta$ plane, assuming $M_0 = A_0 = 0$. Values of $M_{1/2} \lesssim 820$ GeV could be excluded for most values of $\tan\beta$. Note however that the RGE-induced operator λ_{233} and the corresponding partial two-body decay widths, Γ_2 , of $\tilde{\tau}_1 \rightarrow (\mu \nu_\tau, \tau \nu_\mu)$ have not been taken

into account. While there is only a mild dependence of the ratio of the total four-body versus two-body decay width, Γ_4/Γ_2 , on $M_{1/2}$ [93], the ratio, however, scales with $1/\tan^2\beta$. Therefore, only taking into account Γ_4 is a well-justified assumption in the low $\tan\beta$ region, but the $\tilde{\tau}$ -LSP results of Ref. [106] for large $\tan\beta$ can, unfortunately, not be trusted. Note also that Ref. [106] uses data from the 7 TeV run of the LHC. Because of the high occurrence of $\tilde{\tau}$ LSPs in RPV models, we want to encourage the LHC collaborations to reanalyze these scenarios with more recent data.

In conclusion these models are basically not covered at all by LHC searches. Individual final states listed in Tab. IX have been searched for in other contexts, however. In particular, we would like to mention a recent analysis looking for multi-lepton final states and including up to two hadronic tau tags, with various signal regions requiring different amounts of E_T [147]. This search is dedicated to RPC models where pair-produced electroweak gauginos decay via an intermediate slepton or sneutrino down to the lightest neutralino. Including the leptonically decaying tau modes, this search is therefore in principle sensitive to the $LL\bar{E}$ and $LQ\bar{D}$ signatures of Tab. IX. Unfortunately, so far no interpretation in terms of RPV models has been performed. Thus the corresponding mass sensitivity is also unknown. In Sec. VI, we discuss the impact of $\tilde{\tau}$ LSPs on the LHC sensitivity, making use of non-dedicated searches and taking into account RGE-generated operators as well as four-body decays. In Sec. VIII we present our best estimate of the LHC mass bounds in these scenarios.

V. LHC COVERAGE OF RPV-INDUCED NON-STANDARD LSP DECAY SCENARIOS

The standard scenario in the $\Lambda_{\mathcal{R}_p}$ -CMSSM with small RPV couplings is the neutralino or stau LSP. Instead, as we saw in Sec. IIB, for various large RPV couplings, we can also have the following LSPs: \tilde{e}_R , $\tilde{\mu}_R$, $\tilde{\nu}_e$, $\tilde{\nu}_\mu$, $(\tilde{s}_R, \tilde{d}_R)$, \tilde{b}_1 , and \tilde{t}_1 , *cf.* Tab. II. Here we discuss the phenomenology of these models and how they are covered by LHC searches. We also briefly summarize other related searches at the LHC with non-standard LSPs, which do not occur in the $\Lambda_{\mathcal{R}_p}$ -CMSSM.

A. Slepton LSPs

1. Selectron or Smuon LSP

For large λ_{ijc} , $c = 1, 2$, we can have either an \tilde{e}_R or $\tilde{\mu}_R$ LSP, respectively. Since by construction the LSP couples to the dominant operators, we have the decays

$$\tilde{e}_R^- \rightarrow \{\ell_i^- \nu_j, \nu_i \ell_j^-\}, L_i L_j \bar{E}_1, \quad (36)$$

$$\tilde{\mu}_R^- \rightarrow \{\ell_i^- \nu_j, \nu_i \ell_j^-\}, L_i L_j \bar{E}_2. \quad (37)$$

At the LHC, where strong production usually dominates,⁷ the cascade decay will proceed as before to the neutralino, and the latter will decay to an on-shell slepton LSP

$$\tilde{g} \rightarrow q\bar{q}^* \rightarrow q[\bar{q}\tilde{\chi}_1^0] \rightarrow q[\bar{q}(\tilde{e}_R^- e^+)], \quad (38)$$

and analogously for the $\tilde{\mu}_R$ case. This model has not been explicitly constrained by existing analyses of LHC searches. However, we see from Eq. (38) that the signature is identical to the case discussed in Sec. IIIB, with a neutralino LSP and a dominant $LL\bar{E}$ coupling. The only difference is that here the intermediate \tilde{e}_R is on-shell. Thus the signatures are covered by the corresponding $L_i L_j \bar{E}_{1,2}$ searches discussed in Sec. IIIB, respectively. The experimental lower mass bounds can differ from Tab. IV, since the on-shell $\tilde{e}_R/\tilde{\mu}_R$ -LSP can lead to differing kinematic distributions.

2. Sneutrino LSP

A $\tilde{\nu}_e$ -LSP is obtained in the $\Lambda_{\mathcal{R}_p}$ -CMSSM for large λ'_{1jk} , $\{j, k\} \neq \{1, 1\}$. A $\tilde{\nu}_\mu$ -LSP is obtained for large λ'_{2jk} . The LSP decays are then given as (plus charge conjugate)

$$\tilde{\nu}_e^* \rightarrow d_j \bar{d}_k, L_1 Q_j \bar{D}_k, \{j, k\} \neq \{1, 1\}, \quad (39)$$

$$\tilde{\nu}_\mu^* \rightarrow d_j \bar{d}_k, L_2 Q_j \bar{D}_k. \quad (40)$$

The cascade decay at the LHC would proceed from for example a gluino down to the on-shell sneutrino, but through a neutralino, as with the charged sleptons above

$$\tilde{g} \rightarrow q\bar{q}^* \rightarrow q[\bar{q}\tilde{\chi}_1^0] \rightarrow q[\bar{q}(\tilde{\nu}_{e,\mu}^* \nu_{e,\mu})] \rightarrow q[\bar{q}(\{d_j \bar{d}_k\} \nu_{e,\mu})]. \quad (41)$$

Again for this specific model there is *no* interpretation of LHC data within or outside of the $\Lambda_{\mathcal{R}_p}$ -CMSSM. However, in principle $L_{1,2} Q_j \bar{D}_k$ models have been searched for, as discussed in Sec. IIIC. There the intermediate neutralino could also decay to a charged lepton: $\tilde{\chi}_1^0 \rightarrow (\tilde{\ell}_i^+)^* \ell_i^- \rightarrow \ell_i^- u_j \bar{d}_k$, with comparable probability. The charged lepton in the final state leads to a higher sensitivity than the diluted E_T from the neutrino in Eq. (41). For the sneutrino LSP scenario one might think the slepton three-body decay is suppressed. However in the $\Lambda_{\mathcal{R}_p}$ -CMSSM the charged slepton and the sneutrino are nearly mass degenerate, as discussed in Sec. IIB. Thus for the sneutrino LSP the associated charged slepton is the NLSP and the neutralino the NNLSP. Thus the decay via the charged slepton is in fact two-body and if at all only marginally suppressed. Therefore, the searches

⁷ In the case of $LL\bar{E}$ operators, however, the most stringent bounds may arise from electroweakino pair-production, as we shall see in Sec. VI.

Particle	Lower Bound [GeV]	$\bar{U}\bar{D}\bar{D}$ Coupling	Simpl. Model	Comment	Reference
\tilde{t}	405	λ''_{312}	$\tilde{t} \rightarrow q\bar{q}$	445-510 GeV also excluded	[148]
	385	λ''_{3b3}	$\tilde{t} \rightarrow \bar{d}_b\bar{b}$		[139]
\tilde{g}	1440	λ''_{312}	$\tilde{g} \rightarrow t\bar{t}$	$m_{\tilde{t}} = 800$ GeV	[118]
	1460	λ''_{3b3}	$\tilde{g} \rightarrow t\bar{t}$	$m_{\tilde{t}} = 700$ GeV	[118]

TABLE X: Lower mass bounds for the case of a stop LSP discussed in Sec. V B. Here $b = 1, 2$.

in Sec. III C are approximately applicable, with the further difference that the on-shell slepton and sneutrino will modify the kinematic distributions. Overall, these scenarios still need to be checked at the LHC, presumably via \cancel{E}_T searches.

Note, that other interesting scenarios can occur if we go beyond the CMSSM boundary conditions or/and consider more than one RPV operator at M_X . We thus mention searches for an s -channel production of tau-sneutrino LSPs, $\tilde{\nu}_\tau$, which decay further into leptons, assuming both λ'_{311} and one of $\{\lambda_{132}, \lambda_{133}, \lambda_{232}\}$ to be sizable [149, 150], see also Sec. V C 1. However, the excluded combination of masses and couplings is not yet competitive with the more stringent bounds from the non-observation of $\mu - e$ conversion in nuclei [151, 152].

3. Stau LSP with large λ_{ij3} or λ'_{3jk}

This scenario directly corresponds to the case (a) in Sec. IV, just with a large coupling constant. The 2-body stau decays will be prompt and the previous discussion holds.

B. Squark LSPs

As we see in Tab. II, there are essentially three cases of squark LSPs in the Λ_{R_p} -CMSSM.

1. A first or second generation right-handed down-like squark with a large coupling λ''_{212} , decaying to first or second generation quark jets. Experimentally this would lead to four jets, arising from the decay of two on-shell strongly interacting particles, *i.e.* these are pair-produced dijet resonances.
2. A right-handed bottom squark decaying via $\lambda''_{123,2b3}$, with the same signature as in the previous case.
3. A right-handed top squark decaying via λ''_{3jk} . For $(j, k) = (1, 2)$ this is again as in case 1. above. The pair-produced stops lead to two di-jet resonances. For $k = 3$ there will be bottom quark jets in the final state.

Of all three, only the third case, namely the top squark LSP, has been directly searched for in the context of RPV, assuming the couplings λ''_{312} [139, 153, 154], and

λ''_{3b3} [136, 139, 148]. We assume this is due to the standard (RPC) lore that only a top squark can be particularly light. In addition, there has been a considerable effort in the theory community to point out interesting signatures, as well as search strategies for the light-stop scenarios, see for example Refs. [155, 156], many of which have been adopted by the experimental collaborations. The corresponding best lower bounds on the top squark mass are given in Tab. X. Included in the table are also two gluino lower mass bounds, obtained in top squark LSP models.

We note that the signature of the other two cases, pair-produced di-jet resonances, is identical to the signature probed in λ''_{312} [139, 153, 154]. For the case of a very heavy gluino, the production cross section should also be identical, so that the bound can be carried over.

C. Non-Neutralino LSP Outside the CMSSM

Experimentally there are quite a few searches for sparticles directly decaying through an RPV operator. These correspond to scenarios where the sparticle at hand is the LSP. For completeness we briefly collect here the cases which are not possible within the CMSSM and which are therefore not listed in Tab. II.

1. Sneutrino LSP

At the LHC it is possible to produce a sneutrino on-resonance via an $L_i Q_j \bar{D}_k$ operator and for it to decay via a separate $L_i L_j \bar{E}_k$ operator. This can lead to spectacular lepton flavor violating signatures [123, 162–167]

$$d_j \bar{d}_k \rightarrow \tilde{\nu}_i \rightarrow \ell_l \ell_m, \quad L_i Q_j \bar{D}_k \wedge L_i L_l \bar{E}_m. \quad (42)$$

Experimentally this has been searched for by both CMS and ATLAS [150, 157, 158]. We list the best lower sneutrino mass bounds in Tab. XI. The production cross section of the sneutrino is proportional to the λ' coupling squared, the bound is correspondingly sensitive. As we see, the bound ranges from 3.3 TeV for a substantial coupling, $\lambda'_{311} = 0.2$, to 1.3 TeV for a modest coupling, $\lambda'_{311} = 0.01$. The bound quickly vanishes when reducing the size of the coupling further [165].

The experimental search results are given for a $\tilde{\nu}_\tau$ [158], but the opposite flavor lepton searches apply equally to

Particle	Lower Bound [GeV]	RPV Coupling	Simpl. Model	Comment	Reference
$\tilde{\nu}_\tau$	1280 (3300)	$\lambda'_{311} \cdot \lambda_{231,132}$	$d_j \bar{d}_k \rightarrow \tilde{\nu}_\tau \rightarrow e^- \mu^+$	$\lambda'_{311} = \lambda_{231,132} = 0.01$ (0.2)	[150, 157]
	2300	$\lambda'_{311} \cdot \lambda_{231,132}$	$d_j \bar{d}_k \rightarrow \tilde{\nu}_\tau \rightarrow e^- \mu^+$	$\lambda'_{311} = \lambda_{231,132} = 0.07$	[158]
	2200	$\lambda'_{311} \cdot \lambda_{133}$	$d_j \bar{d}_k \rightarrow \tilde{\nu}_\tau \rightarrow e^- \tau^+$	$\lambda'_{311} = \lambda_{133} = 0.07$	[158]
	1900	$\lambda'_{311} \cdot \lambda_{233}$	$d_j \bar{d}_k \rightarrow \tilde{\nu}_\tau \rightarrow \mu^- \tau^+$	$\lambda'_{311} = \lambda_{233} = 0.07$	[158]
\tilde{u}_{Lb}	1050* (1080*)	λ'_{1bc} (λ'_{2bc})	$\tilde{u}_b \rightarrow ej$ (μj)	Br = 1, (3, 2, $+\frac{2}{3}$)	[122, 159]
\tilde{d}_{Lb}	625*	λ'_{ib3}	$\tilde{d}_{Lb} \rightarrow b\nu_i$	Br = 1, (3, 2, $-\frac{1}{3}$)	[159]
\tilde{d}_{Rc}	900* (850*)	λ'_{1bc} (λ'_{2bc})	$\tilde{d}_c \rightarrow ej/\nu_e j$ ($\mu j/\nu_\mu j$)	Br = 0.5 each, ($\bar{3}, 1, -\frac{1}{3}$)	[159]
	480*	λ'_{i3c}	$\tilde{d}_c \rightarrow b\nu_i$	Br = 0.5, ($\bar{3}, 1, -\frac{1}{3}$)	[159]
\tilde{d}_R	650 (450)	λ''_{313}	$\tilde{d} \rightarrow \bar{b}\bar{t}$	$m_{\tilde{g}} = 1.4$ TeV ($m_{\tilde{g}} = 2$ TeV)	[118]
	570 (420)	λ''_{321}	$\tilde{d} \rightarrow \bar{s}\bar{t}$	$m_{\tilde{g}} = 1.4$ TeV ($m_{\tilde{g}} = 2$ TeV)	[118]
\tilde{t}_L	1100	λ'_{133} (λ'_{233})	$\tilde{t} \rightarrow e^+ b$ ($\mu^+ b$)		[160]
	740	λ'_{333}	$\tilde{t} \rightarrow \tau^+ b$		[121]
	1010* (1080*)	λ'_{132} (λ'_{232})	$\tilde{t} \rightarrow e^+ j$ ($\mu^+ j$)	Br = 1, (3, 2, $+\frac{2}{3}$)	[122]
\tilde{b}_R	307	λ''_{3b3}	$\tilde{b} \rightarrow \bar{t}\bar{d}_b$		[110]
	560*	λ'_{333}	$\tilde{b} \rightarrow t\tau^-$	Br = 0.5, ($\bar{3}, 1, -\frac{1}{3}$)	[161]
\tilde{g}	650	λ''_{112}	$\tilde{g} \rightarrow uds$		[140]
	835	λ''_{113} (λ''_{113})	$\tilde{g} \rightarrow udb$ (csb)		[140]
	1360	λ''_{323}	$\tilde{g} \rightarrow tsb$	$m_{\tilde{q}} = 5$ TeV	[143]
	917 (929) [874]	$\lambda''_{abc}(\lambda''_{ab3})[\lambda''_{3b3}]$	$\tilde{g} \rightarrow 3q$	$m_{\tilde{q}} = 5$ TeV	[142]

TABLE XI: Lower mass bounds on supersymmetric particles as the LSP decaying directly via an RPV operator. These are all *not* $\Lambda_{\mathcal{R}P}$ -CMSSM scenarios. The bounds marked by an asterisk * are re-interpreted leptoquark scenarios. For the leptoquark searches, we have included the SU(3), SU(2), and U(1)_{EM} quantum numbers in the comment.

the following coupling combinations which involve a $\tilde{\nu}_\mu$ propagator

$$e\mu : (\lambda'_{211} \cdot \lambda_{122}), \quad (43)$$

$$e\tau : (\lambda'_{211} \cdot \lambda_{123}), (\lambda'_{211} \cdot \lambda_{231}), \quad (44)$$

$$\mu\tau : (\lambda'_{211} \cdot \lambda_{322}). \quad (45)$$

We have disregarded the case of an s -channel $\tilde{\nu}_e$ as the required coupling combinations rely on λ'_{111} , on which there are very strict bounds, see Tab. XIII.

2. Squark LSP

There have been many searches for squarks decaying directly via RPV operators [110, 121, 135–137, 141, 143, 144, 160, 161], several focusing on the decay $\tilde{t} \rightarrow bs$ induced by the coupling λ''_{323} , discussed in Sec. VB. There have also been many leptoquark searches which can be directly interpreted as squark production followed by RPV decays via the $L_i Q_j \bar{D}_k$ operators, see for example [121, 122, 159, 161, 168]. In particular there are three

RPV scenarios corresponding directly to leptoquarks:

$$\tilde{u}_{Lj} \rightarrow \ell_i^+ + d_k, \quad \text{Br} = 1, \quad (46)$$

$$\tilde{d}_{Lj} \rightarrow \bar{\nu}_i + d_k, \quad \text{Br} = 1, \quad (47)$$

$$\tilde{d}_{Rk} \rightarrow \ell_i^- + u_j/\nu_i + d_j, \quad \text{Br} = 0.5 \text{ each,} \quad (48)$$

if $j \neq 3$.

If an up-like squark, \tilde{u}_{Lj} , is the LSP, for an $L_i Q_j \bar{D}_k$ operator it can only decay to a charged lepton and a down-like quark with a branching ratio of 1, *cf.* Eq. (46). For a $\bar{U}_i \bar{D}_j \bar{D}_k$ operator it will decay to two jets, possibly including one b -jet. This latter case has only been considered for top quarks, $i = 3$. For the former case the best bounds are given in Tab. XI, with a lower mass bound of about 1 TeV.

On the other hand, a left-handed down-like squark, \tilde{d}_{Lj} , can only decay via a neutrino, leading to \not{E}_T , *cf.* Eq. (47). In the table listings we interpret an ATLAS leptoquark search as the decay of a \tilde{d}_{Lb} , $b = 1, 2$, to a bottom quark resulting in a weaker lower mass bound of 625 GeV [159]. The right-handed down-like squark has two possible decay modes, one involving a charged lepton and one involving a neutrino. Combining the two often leads to stricter bounds. For jets from the first two generations $\lambda'_{1bc,2bc}$, $b, c = 1, 2$, the lower experimental

bound is about 900 GeV. For the case λ'_{i3c} , $c = 1, 2$, the charged lepton mode involves a top quark, which would be a separate search. The neutrino mode alone leads to the much weaker bound of only 480 GeV. These are again all reinterpreted leptoquark searches.

The top squark LSP has been more widely considered in the literature, as it is naturally lighter than the other squarks, even for RPC, see for example [169–171]. The decays via $\bar{U}\bar{D}\bar{D}$ operators are discussed in Sec. V B. The decays via $LQ\bar{D}$ operators are just special cases of the decay of up-like squarks, Eq. (46), and the bounds are similar, around 1100 GeV. The case λ'_{333} leads to a final-state tau and thus weaker bounds, around 750 GeV.

In the $\Lambda_{\mathcal{R}_p}$ -CMSSM, for λ'_{3b3} , the top squark can be the LSP, but not the bottom squark. Nevertheless the direct decay of a bottom squark via λ'_{3b3} with 100% branching ratio was searched for giving a lower mass bound of 307 GeV [110]. A leptoquark search was reinterpreted as the direct decay of a right-handed bottom squark via the operator $L_3 Q_3 \bar{D}_3$ to a top quark and a tau with a branching ratio of 50%. In this case the lower mass bound is 560 GeV [161].

3. Gluino LSP

As we saw in Tab. II, a gluino LSP is not dynamically generated in the $\Lambda_{\mathcal{R}_p}$ -CMSSM. All the same we briefly discuss this scenario here, as there are several LHC searches for such models. Depending on the dominant operator, a gluino LSP decays as

$$\tilde{g} \rightarrow \begin{cases} q\bar{q}\{\ell_i\nu_j\bar{\ell}_k, \nu_i\ell_j\bar{\ell}_k\}, & L_i L_j \bar{E}_k, \\ \{\ell_i u_j \bar{d}_k, \nu_i d_j \bar{d}_k\}, & L_i Q_j \bar{D}_k, \\ u_i d_j \bar{d}_k, & \bar{U}_i \bar{D}_j \bar{D}_k. \end{cases} \quad (49)$$

The first decay proceeds via a virtual squark and a virtual neutralino. In the second and third case, the gluino decays via a virtual squark, which couples directly to the relevant operator. Of these three scenarios only the last one has been investigated at the LHC [57, 110, 134, 135, 140–143].

However the first case, $LL\bar{E}$, leads to identical signatures as in Sec. III B, the only difference is that now the intermediate neutralino is virtual. The second case, $LQ\bar{D}$, is novel, although very similar to the electroweak production in Section 10 of Ref. [110]. There the pair production of neutralinos is investigated, followed by their three-body RPV decay. Here one should consider the pair production of gluinos, which has a significantly higher cross section, which should lead to stricter lower mass bounds.

The best bounds for the third case in Eq. (49) are listed in Tab. XI. The weaker bounds in the first two rows for the gluino were obtained with $\sqrt{s} = 8$ TeV data. Nevertheless the tbs search is the most sensitive channel. ATLAS has several searches for this scenario [57, 134, 135], however, they always allow more than one coupling to be

non-zero, often even all λ'_{ijk} with equal value. It is again not clear how to interpret the resulting bounds.

VI. TESTING THE RPV-CMSSM WITH CHECKMATE

For the remainder of this paper we are interested in the sensitivity of the LHC with respect to the $\Lambda_{\mathcal{R}_p}$ -CMSSM, *i.e.* to a complete supersymmetric model. In particular, we are interested in how the presence of R -parity violating operators affects the well-known results for the R -parity conserving CMSSM [20, 22, 172, 173]. For this we shall use the program **CheckMATE** [63–65]. As we saw in Secs. III to V, the LHC experiments mainly set bounds on simplified supersymmetric R -parity violating models. They set little or no bounds on the complete $\Lambda_{\mathcal{R}_p}$ -CMSSM model. We here use **CheckMATE** to recast ATLAS and CMS searches and thus set bounds on the various $\Lambda_{\mathcal{R}_p}$ -CMSSM models.

A. Method

The program **CheckMATE** automatically determines if a given parameter point of a particular model beyond the Standard Model (BSM) is excluded or not by performing the following chain of tasks. First, the Monte Carlo generator **MadGraph** [174] is used to simulate proton proton collisions. The resulting parton level events are showered and hadronized using **Pythia 8** [175]. The fast detector simulation **Delphes** [176] applies efficiency functions to determine the experimentally accessible final state configuration, including the determination of the jet spectrum using **FastJet** [177, 178]. Afterwards, various implemented analyses from ATLAS and CMS designed to identify different potentially discriminating final state topologies are used.

Events which pass well-defined sets of constraints are binned in signal regions for which the corresponding prediction for the Standard Model and the number of experimentally observed events are known. By comparing the predictions of the Standard Model and the user's BSM model of interest to the experimental result using the CLs prescription [179], **CheckMATE** concludes if the input parameter combination is excluded or not at the 95% confidence level. For more information we refer to Refs. [63–65].

1. Model Setup

For the proper description of the RPV Feynman rules in **MadGraph**, we take the model implementation from **SARAH**, which we already used in Sec. II, and export it via the UFO format [180]. For a given set of $\Lambda_{\mathcal{R}_p}$ -CMSSM parameters, we make use of the respective **SPheno** libraries created from the same **SARAH** model used to de-

termine the low energy particle spectrum, the mixing matrices and the decay tables. We calculate the SUSY and Higgs masses including RPV-specific two-loop corrections [181–183] which are particularly important for light stops [55]. As discussed in Sec. IID, four-body decays of the stau can be dominant and lead to important experimentally accessible final states. In regions where this occurs, see for instance in Sec. VIB 4, the four-body stau decays have been determined using **MadGraph**.

2. Monte Carlo Simulation

In $\Lambda_{\mathcal{R}_p}$ -CMSSM parameter regions where the entire SUSY spectrum is kinematically accessible at the LHC, *i.e.* with masses at or below $\mathcal{O}(1 \text{ TeV})$, there exists a plethora of possible final state configurations. To maintain computational tractability in our study, we applied the following list of simplifying assumptions:

- We include only two-body supersymmetric final state production: $pp \rightarrow AB + X_{\text{soft}}$, and require both supersymmetric particles, A and B , to be produced on-shell. Note that in RPC supersymmetry, additional hard QCD radiation, *i.e.* $pp \rightarrow ABj$, is important in parameter regions with highly degenerate spectra due to the resulting kinematic boost of the decay products, see e.g. Ref. [184]. However, due to the instability of the LSP in the $\Lambda_{\mathcal{R}_p}$ -CMSSM, this additional boost is not needed and therefore this final state is not expected to contribute sizably to the final constraining event numbers.
- We do not consider final state combinations which are strongly suppressed by the relevant parton density distributions and/or which only exist in RPV supersymmetry. Most importantly, this excludes flavor-off-diagonal combinations of “sea”-squarks (we clarify the meaning below) or squark-slepton combinations.
- We include in our simulations production processes, which can only proceed via the electroweak interactions, *i.e.* the production of sleptons, electroweak gauginos and the mixed production of electroweak gauginos and squarks or gluinos. However, in the case of electroweak gauginos we only include the production of the two lightest neutralinos and the lightest chargino, *i.e.* the dominantly bino and wino states in a CMSSM setup. We expect no sizeable contributions from the ignored Higgsinos, since these are typically significantly heavier and therefore have negligible production rates in comparison with the lighter winos. Similarly, we do not include flavor-off-diagonal slepton combinations and mixed electroweak gaugino-squark production with “sea”-squarks.
- With the above considerations, the resulting set of production channels that we consider are listed below:
Strong processes:

- $\tilde{g}\tilde{g}$
- $\tilde{g}\tilde{q}_V^{(*)}$
- $\tilde{q}_V^{(*)}q_V^{(*)}$ (all combinations)
- $\tilde{q}_S\tilde{q}_S^*$ (only flavor-diagonal)

Electroweak processes:

- $\tilde{\chi}\tilde{\chi}$ [all (non-Higgsino) combinations]
- $(\tilde{\ell}_L, \tilde{\ell}_R, \tilde{\nu}_{\ell,L})(\tilde{\ell}_L^*, \tilde{\ell}_R^*, \tilde{\nu}_{\ell,L}^*)$ (only flavor-diagonal)

Mixed processes:

- $\tilde{g}\tilde{\chi}$
- $\tilde{q}_V^{(*)}\tilde{\chi}$ (all combinations)

Here, \tilde{q}_V refers to the superpartners of the light quarks: $\tilde{u}_{L,R}, \tilde{d}_{L,R}$ and $\tilde{s}_{L,R}$, while \tilde{q}_S refers to the remaining squarks $\tilde{c}_{L,R}, \tilde{b}_{1,2}$ and $\tilde{t}_{1,2}$. Furthermore, $\tilde{\chi}$ subsumes the two lightest neutralinos $\tilde{\chi}_{1,2}^0$ and the lightest chargino $\tilde{\chi}_1^\pm$.

- Decays of supersymmetric particles are performed within **Pythia 8**, using the information from the decay table determined in **SPheno**. This ignores any potential spin-dependent information, which could be relevant when performing the proper matrix-element calculation. However, as we do not assume spin-effects to be important here, we take the computationally faster approach of using decay tables.
- To take into account the sizable contributions from higher order QCD effects in the production cross section, we multiply the leading-order production cross-sections taken from **MadGraph** with the next-to-leading-logarithm K-factors determined by **NLLFast** [185–191]. This tool interpolates gluino- and squark-mass-dependent higher-order cross sections for all “strong Processes” listed above. **NLLFast** assumes degenerate first- and second-generation squark sector where we use the median of the squark masses for the calculation. Note that this degeneracy is present in models with small $\Lambda_{\mathcal{R}_p}$ but not necessarily if $\Lambda_{\mathcal{R}_p}$ is large.⁸ Stops and sbottoms are always treated separately and obtain individual K-factors. The consideration of higher order effects for the remaining processes is computationally far more involved as tools like **PROSPINO** [192] need to perform the full NLO calculation. These effects are however expected to be significantly smaller compared to the strong production processes and thus we neglect them here.

⁸ For the only benchmark case with large $\Lambda_{\mathcal{R}_p}$ we consider, the squark sector is not degenerate. However, as in this case stop production dominates, we can still use the **NLLFast** K-factors for rescaling the cross sections.

atlas_conf.2013_036 <i>4ℓ + E_T</i>	cms_1405_7570 <i>various electroweakino searches</i>	atlas_1403_4853 <i>2ℓ + ≥ 1b + E_T</i>	atlas_1403_5294 <i>2ℓ + E_T</i>
atlas_1402.7029 <i>3ℓ + E_T</i>	atlas_1407_0583 <i>1ℓ + 1b + E_T</i>	cms_1504_03198 <i>1ℓ + ≥ 3j incl ≥ 1b + E_T</i>	atlas_1407_0600 <i>0 - 1ℓ + 3b + E_T</i>
atlas_conf.2013_061 <i>0 - 1ℓ + 3b + E_T</i>	atlas_1405_7875 <i>0ℓ + 2 - 6j + E_T</i>	atlas_1308_1841 <i>0ℓ + ≥ 7j + E_T</i>	atlas_conf.2013_062 <i>1 - 2ℓ + 3 - 6j + E_T</i>
atlas_1404.2500 <i>3ℓ or SS 2ℓ + 0 or ≥ 0b + E_T</i>			

FIG. 10: This legend shows the different colors/shadings presented on the right-hand side of the following figures. Each colored box contains a bold label, which corresponds to the name under which the respective reference is listed within **CheckMATE**, furthermore in small type, each box contains a brief description of the analyzed signature.

3. Incorporated Analyses

CheckMATE provides a large set of implemented **ATLAS** and **CMS** results from both the $\sqrt{s} = 8$ and 13 TeV runs of the LHC. These analyses target a large variety of possible final states which typically appear in theories beyond the Standard Model. The vast majority, however, are designed to target RPC supersymmetry. This implies cuts which require significant amounts of missing transverse momentum and/or highly energetic final state objects, namely leptons or jets. As many of the most prominent decay chains in the Λ_{R_p} -CMSSM indeed correspond to these signatures, it is therefore interesting to determine the relative exclusion power of these tailored analyses in comparison to the RPC-CMSSM.

In this study we consider all $\sqrt{s} = 8$ TeV LHC analyses implemented in **CheckMATE** 2.0.1. For a full, detailed list we refer to the documentation in Refs. [63–65] and the tool’s website.⁹ We discuss the target final states of the relevant analyses in more detail below, alongside our results. Some final states have been reanalyzed and the corresponding bounds have been updated with new LHC results taken at $\sqrt{s} = 13$ TeV center-of-mass energy. For our purpose of comparing the relative exclusion power when going from an RPC to an RPV scenario, using the $\sqrt{s} = 8$ TeV analysis set has the advantage of covering a much larger variety of final states.

To set the limit, **CheckMATE** tests all signal regions in all selected analyses, determines the one signal region with the largest expected sensitivity and checks if the corresponding observed result of that signal region is excluded at 95% C.L. or not. In the following, the analysis which contains this limit-setting signal region is referred to as the “most sensitive analysis” for a given Λ_{R_p} -CMSSM parameter point. Due to the lack of information about correlations in systematic uncertainties between different

signal regions, **CheckMATE** is currently incapable of combining information from different signal regions.¹⁰

The list of analyses we employ are shown in Fig. 10. In bold is the name under which the analysis is listed in **CheckMATE**. Underneath in small italics type we briefly denote the physical signature. Here ℓ refers to a charged lepton, E_T refers to missing transverse energy. j refers to a jet in the final state, b specifically a b -jet. The references for the analyses are given in the **CheckMATE** documentation. The boxes of the analyses carry different colors and hatchings. This is employed in the later exclusion plots, to show which analysis within **CheckMATE** is the most sensitive.

4. Scanned Parameter Regions

Even though one of the appealing features of the CMSSM is the small number of free parameters compared to other supersymmetric theories, we still need to fix certain degrees of freedom in order to be able to show results in an understandable 2-dimensional parameter plane. As the masses of the supersymmetric particles will be one of the most important variables when it comes to the observability of a model realization at the LHC, we show results in the M_0 - $M_{1/2}$ plane. To be specific we scan over the parameter range

$$M_0 \in [0, 3000] \text{ GeV}, \quad M_{1/2} \in [200, 1000] \text{ GeV}. \quad (50)$$

For better comparison, we choose the remaining model parameters as in the RPC-CMSSM **ATLAS** analysis in Ref. [172] where $\tan \beta$ is fixed to a relatively large value of 30 while A_0 is set via the standard formula $A_0 = -2M_0$ which ensures a realistically large value of the lightest

⁹ <http://checkmate.hepforge.org>

¹⁰ The statistical combination of signal regions for **CheckMATE** is work in progress [193].

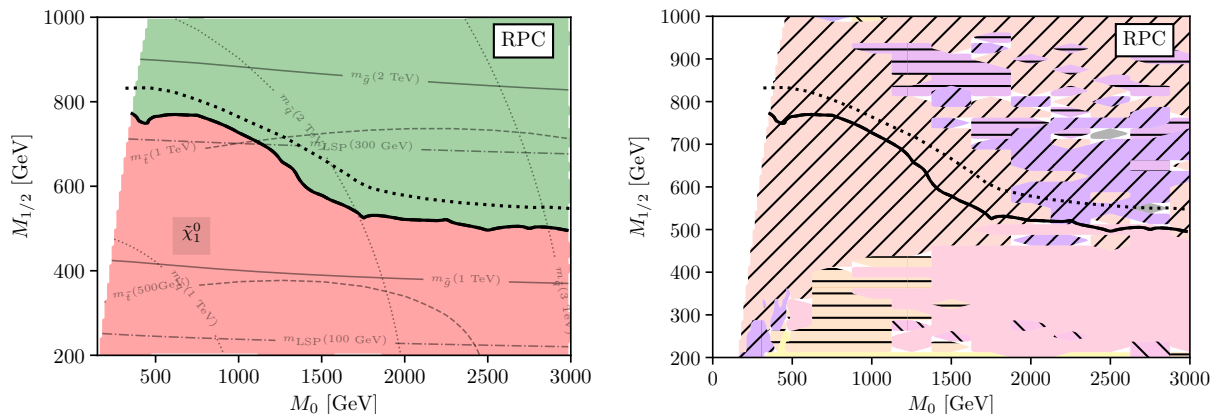


FIG. 11: LHC exclusion limits in the M_0 – $M_{1/2}$ plane determined by **CheckMATE** (black solid line) using the RPC–CMSSM with the remaining model parameters set to $\tan\beta = 30$, $\mu > 0$ and $A_0 = -2M_0$. On the left-hand side, the red region below the solid line is excluded, the green region is allowed by **CheckMATE**. The black dotted line denotes the corresponding **ATLAS** bound from Ref. [172]. The discrepancy is discussed in the text. The left-hand figure further contains in light gray the iso-mass contours of the gluino (solid), the squarks (dotted), the lightest stop (dashed) and the LSP (dot-dashed), respectively. The white area on the left for which no results are shown corresponds to the cosmologically excluded region with a $\tilde{\tau}$ LSP. On the right-hand side, we show for each region the most sensitive LHC analysis, according to the legend in Fig. 10.

neutral CP-even Higgs boson mass. The sign of the μ parameter is fixed to be positive, to avoid further tension with $(g-2)_\mu$ [194]. Allowing any number of RPV-operators to have non-vanishing values would yield an unmanageable set of possible scenarios to study. We therefore restrict ourselves to cases where only one of the many operators has a non-zero value at the unification scale. In order to directly compare our results to the RPC–CMSSM, we use a small RPV coupling at the GUT scale, $\Lambda_{R_p}|_{\text{GUT}} = 0.01$. This essentially mimics the RPC mass spectrum, but allows for the prompt decay of the LSP. We comment on possible effects of increasing the RPV coupling in Sec. VII.

B. Results

In this section we show the results of the scans. Throughout the analysis of these results, the principle questions which we seek to answer are the following:

1. To what extent do the existing **ATLAS** and **CMS** analyses, which largely focus on RPC supersymmetry, exclude the parameter space of the Λ_{R_p} –CMSSM?
2. Does breaking R -parity weaken the bounds of the RPC–CMSSM due to a gap in the coverage of possible final states?
 - (a) If the answer is yes, how could these gaps be closed?
 - (b) Alternatively, if the answer is no, in the cases where the bounds become stronger, which of the effects mentioned in previous sections lead to this result?

When presenting our results, we show in the figures for each parameter point, which **CheckMATE** analysis is the most sensitive. We do this by using the color code of Fig. 10.

1. R -parity Conserving CMSSM

We start with a short discussion of the RPC–CMSSM in Fig. 11. On the left we denote in the M_0 – $M_{1/2}$ plane by the thick, solid black line the 95%-CL exclusion range we obtained using **CheckMATE** for this model. Thus below the curve, in red is the excluded parameter area. Above the curve, in green is the allowed area. The remaining CMSSM parameters have been set to $\tan\beta = 30$, $\mu > 0$ and $A_0 = -2M_0$. In light gray we present supersymmetric mass isocurves for the LSP (dot-dashed), the first two generation squarks (dotted), the gluino (solid), and the lightest stop (dashed). The white region on the far left at low M_0 results in a $\tilde{\tau}$ -LSP, which is not viable phenomenologically if R -parity is conserved: as there is no possible decay channel for the stau, these regions result in stable charged particles which e.g. spoil big bang nucleosynthesis [195]. This is why here and in the following, we do not show any RPC results in the stau-LSP region. We do include them in the RPV cases.

In the right plot, we show in the M_0 – $M_{1/2}$ plane, which analysis implemented in **CheckMATE** is most sensitive at a given parameter point or region. We use the color and hash code of Fig. 10. Thus for example the point ($M_0 = 1000$ GeV, $M_{1/2} = 500$ GeV) is excluded by the analysis denoted `atlas_1405_7875` [129] in **CheckMATE**.

The most sensitive analyses target either a 0-lepton multijet (`atlas_1405_7875`), or a $\geq 3b$ -jet final state (`at-`

las_conf_2013_061, Ref. [196]), both requiring a significant amount of missing transverse momentum. The former final state is especially sensitive when light gluinos decay into jets via on-shell squarks and therefore – as can be seen in our results – covers the low M_0 region where the squarks are relatively light. On the contrary, the latter targets stop and gluino pair production, the dominant modes for large M_0 , which can produce 4 b -jets due to the resulting top quarks in the final decay chain.

In this particular set of plots, see Fig. 11, we also show the nominal ATLAS exclusion limit taken from Ref. [172] as an additional, black dotted line. The discrepancies arise due to the ATLAS result including a statistical combination of the orthogonal sets of 0 and 1ℓ signal regions which CheckMATE cannot perform. Apart from this combination, the detailed, analysis-dependent results given in Ref. [172] match our determination of the respective most sensitive analysis in this model.

2. $LL\bar{E}$, $\Lambda_{\mathcal{R}_p}$ -CMSSM

We now consider the case of a *small* non-zero $LL\bar{E}$ operator as discussed in Secs. IIIB and IV. We determine excluded parameter regions of the corresponding $\Lambda_{\mathcal{R}_p}$ -CMSSM and compare with the LHC exclusion line obtained in the RPC case. Since we consider a small RPV coupling, the particle spectrum remains virtually unchanged with respect to the RPC-CMSSM. However, as emphasized before, such an operator leads to the decay of the LSP. Therefore, a neutralino LSP will decay into two leptons and one neutrino for a generic λ_{ijk} coupling, cf. Eq. (18) and Tab. III. In parameter regions where the lightest stau is the LSP its possible decay modes are: (i) directly into $\ell_i \nu_j$, if either i, j or k equals 3, (ii) via the RGE-generated λ_{i33} coupling if the non-zero RPV coupling at M_X is of form λ_{ijj} and $\{i, j\} \neq 3$ (see Sec. IID) or (iii) via a four-body decay, cf. see Sec. IV, and Tab. IX for the corresponding LHC signatures. However, the four-body decay does not happen here due to the large $\tan\beta$ value employed and the consequential dominance of the two-body decay through the RGE-generated operators.

The generic LHC searches for RPC supersymmetry look for missing energy in combination with jets and/or leptons. They should thus also perform well for the $LL\bar{E}$ models, due to the many extra leptons from the RPV decay. Although the amount of missing energy is in general not as pronounced as for an RPC model, the energy carried away by the neutrino in the final decay can still be sizable enough to produce a striking signature, see Ref. [197, 198].

In the top row of Fig. 12 we show the CheckMATE exclusion in the M_0 - $M_{1/2}$ plane for the $\Lambda_{\mathcal{R}_p}$ -CMSSM with $\lambda_{122} \neq 0$. The remaining CMSSM parameters and the light gray iso-mass curves are as in Fig. 11. The excluded region is shown below the thick solid black curve in red. The allowed region is shown above this curve in

green. The dark red/green colored regions correspond to a $\tilde{\tau}$ -LSP, which must be considered in the RPV case. The light red/green colored regions correspond to a $\tilde{\chi}_1^0$ -LSP, as in the RPC case. The RPC-CMSSM exclusion line of Fig. 11 (thick solid black curve there) is shown here as a thick dashed black curve for comparison. It does not extend into the $\tilde{\tau}$ -LSP region, as that is not viable in the RPC-CMSSM.

The plot on the upper right in Fig. 12 shows in thick solid black the same CheckMATE exclusion from the upper left plot, as well as the RPC exclusion from Fig. 11 as a solid dashed line. It furthermore shows which LHC analysis implemented in CheckMATE is most sensitive at a given parameter region using the same color code as in Fig. 11. When comparing with Fig. 10, we see that most of the parameter range is most sensitively covered by atlas_conf_2013_036, Ref. [56].

As a result of $\lambda_{122} \neq 0$, the neutralino decays will lead to four more charged 1st- or 2nd-generation leptons compared to the RPC case, in regions where the neutralino is the LSP, cf. Tab. III. Consequently, analyses looking for four or more leptons, Ref. [56], are very sensitive to this scenario and yield a stronger limit than in the RPC case. Thus the solid black curve in the upper left plot is more restrictive than the dashed black curve. The search in Ref. [56] contains separate signal regions designed for both RPC and RPV signatures, respectively. It is interesting that, although their signal regions designed for the RPV signatures are the ones with the best exclusion power, the RPC signal region performs almost equally well.

When looking more closely at the CheckMATE output we see that it is a specific search region in Ref. [56], which is most sensitive to the $LL\bar{E}$ case we are considering here, namely the electroweak pair-production of neutralinos and charginos. This production channel is not very promising for RPC models in the CMSSM, as the largest electroweak cross-section is usually obtained by the production of a charged and a neutral wino. Within the CMSSM boundary conditions, both would decay to the bino by emitting a W and a Higgs/ Z -boson respectively. This comparably small electroweak signal rate is usually not enough for these final states to be detected over the background. Thus the RPC-CMSSM is most stringently constrained by gluino pair production. In contrast, in the $\Lambda_{\mathcal{R}_p}$ -CMSSM the neutralino decays via λ_{122} lead to a clean signal with many charged leptons.

Specifically, for $M_0 \gtrsim 500$ GeV, corresponding to regions with a neutralino LSP, we can exclude values of $M_{1/2} \lesssim 950$ GeV, which feature a bino of $m_{\tilde{\chi}_1^0} \simeq 400$ GeV and winos of $m_{\tilde{\chi}_2^0} \simeq m_{\tilde{\chi}_1^\pm} \simeq 800$ GeV, as well as gluinos over 2.1 TeV. Thus within the $\Lambda_{\mathcal{R}_p}$ -CMSSM, the indirect constraint on the gluino mass (via the universal gaugino mass) is much stricter than the RPC gluino search can reach.

These $\Lambda_{\mathcal{R}_p}$ -CMSSM bounds obtained using CheckMATE can, to some degree, be compared to the results from Ref. [110], where bounds on the pair-production of winos

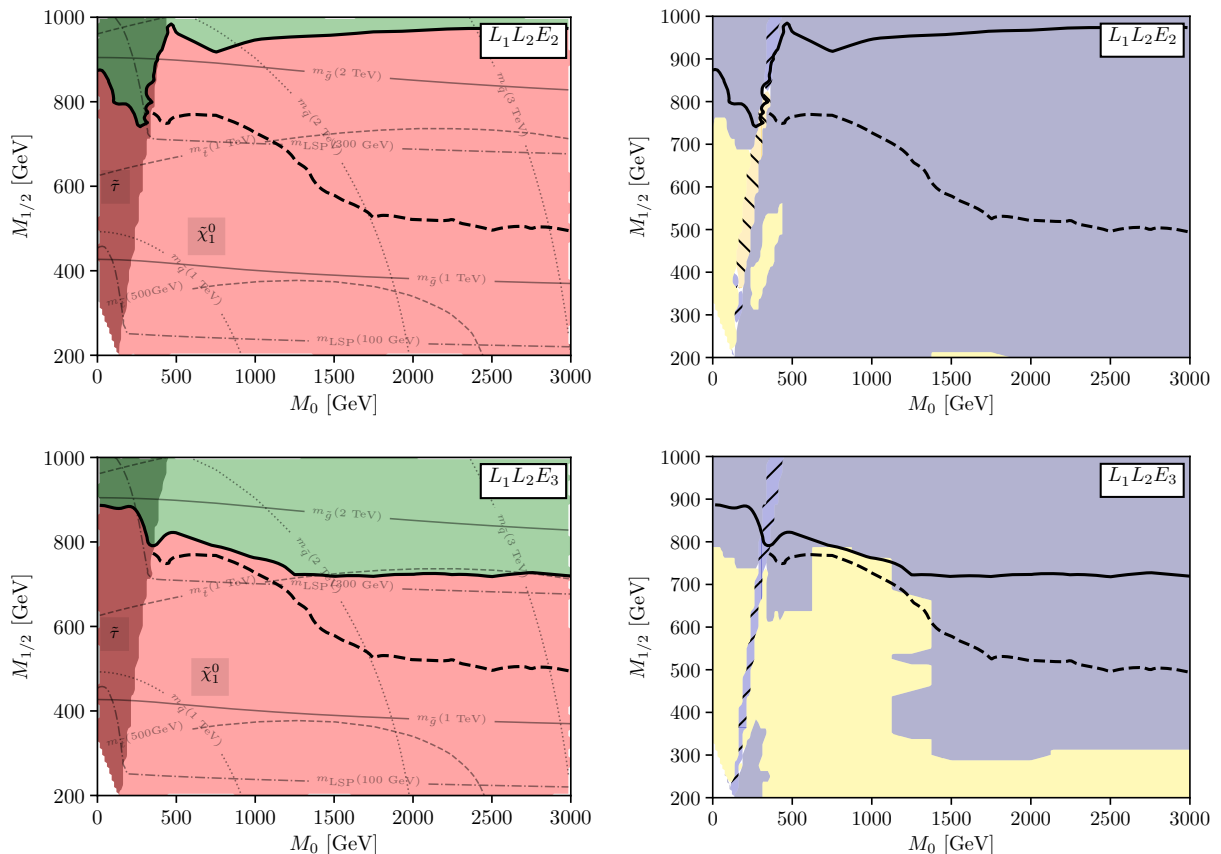


FIG. 12: Interpreting the LHC experimental searches as exclusion regions of the $LL\bar{E}$, Λ_{R_p} -CMSSM in the M_0 - $M_{1/2}$ -plane using **CheckMATE**, and focusing on the cases λ_{122} and λ_{123} . The other CMSSM parameters are as in Fig. 11. In the upper left hand plot, corresponding to a λ_{122} model, regions below the thick solid black line are excluded, and colored in red. Parameter regions above the thick black solid line are allowed by **CheckMATE** and colored in green. The dark red and dark green regions have a $\tilde{\tau}$ LSP, which is viable in the Λ_{R_p} -CMSSM. The light red and light green regions have a $\tilde{\chi}_1^0$ LSP. The light gray iso-mass curves are as in Fig. 11. The RPC-CMSSM exclusion line of Fig. 11 (thick solid black curve there) is shown here as a thick dashed black curve for comparison. It does not extend into the $\tilde{\tau}$ -LSP region, as that is not viable in the RPC-CMSSM. The figure on the upper right shows in thick solid black the **CheckMATE** exclusion from the upper left plot, as well as the RPC exclusion from Fig. 11. It furthermore shows which LHC analysis implemented in **CheckMATE** is most sensitive, at a given parameter region, using the color code of Fig. 10. The lower two plots are as the upper except for turning on λ_{123} instead of λ_{122} . The small white area at very low M_0 and $M_{1/2}$ is where the lightest stau becomes tachyonic.

decaying via $LL\bar{E}$ are set. This analysis excludes wino masses up to 900 GeV also for $\lambda_{122} \neq 0$, when assuming that the neutral wino is the LSP. In the case at hand we have a lighter bino to which the wino will decay. This change in kinematics (for instance, the final state leptons will be less energetic) with respect to the simplified model analysis in Ref. [110] explains the small differences observed in the bounds on the wino mass.

In the upper left plot of Fig. 12, the low M_0 region features a stau LSP and we observe that the exclusion power close to the LSP-boundary drops significantly. This occurs due to the produced neutralinos (charginos) decaying into $\tau\tilde{\tau}_1$ ($\nu\tilde{\tau}_1$) and $\tilde{\tau}_1$ decaying via the RGE-induced λ_{133} coupling. As a result the stau has equal branching ratios into both $e\nu$ and $\tau\nu$ final states. Compared to the expected signatures of neutralino-LSP regions explained

above, several final-state 1st- and 2nd-generation leptons are now replaced by τ leptons. The expected event rates therefore drop by powers of the leptonic tau branching ratio and hence significantly affect the resulting bound from the same analysis.

As M_0 approaches 0, the mass of all sleptons and sneutrinos further decreases. This slowly opens further decays of the neutralino (chargino) into other $\ell_i\tilde{\ell}_i$ and $\nu_i\tilde{\nu}_i$ ($\nu_i\tilde{\ell}_i$ and $\ell_i\tilde{\nu}_i$) combinations, which for $i \neq 3$ lead to the same decay signatures via the λ_{122} as discussed before for the neutralino LSP region. Hence, the exclusion line approaches the earlier, stricter bound for $M_0 \rightarrow 0$.

Next, we consider the bottom row of Fig. 12 with a non-zero λ_{123} coupling. The labelling and the included curves are to be understood as for the upper two plots. In the lower right plot we see that again at-

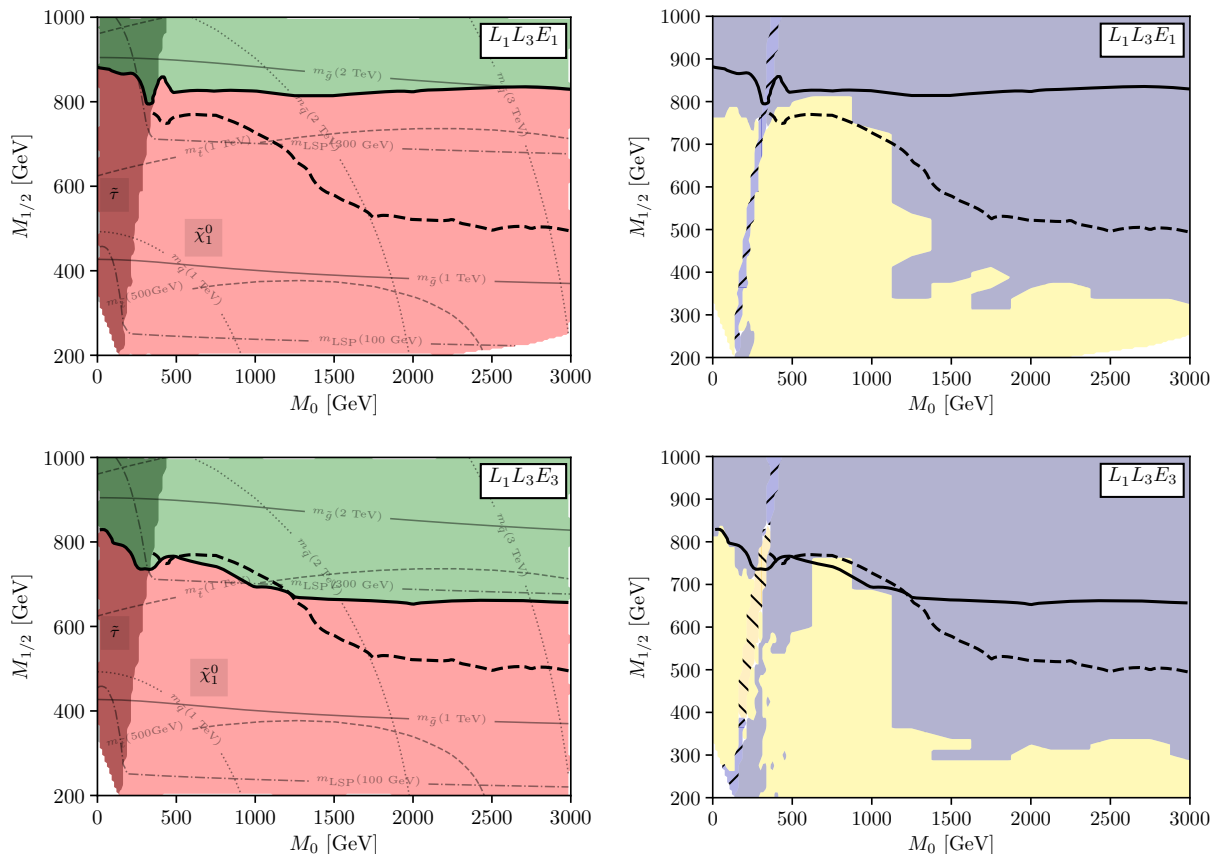


FIG. 13: Same as for Fig. 12, but considering the nonzero operators (in descending order) λ_{131} and λ_{133} .

las_conf_2013_036, Ref. [56], is most sensitive over most of the parameter region, however only if M_0 is large and the squarks are decoupled. For small M_0 , analyses which look for jets and like-sign charged leptons, for example Ref. [133] (denoted atlas_1404_2500 in Fig. 10), become more sensitive. In fact, these two analyses are similarly sensitive in this parameter region but the second gets contributions from light squark decays and thus starts dominating the exclusion line for small M_0 .¹¹ To the right in the lower left plot, the neutralino-LSP decay now always involves tau leptons, *cf.* Eq. (18). The resulting overall bound, the thick solid black curve, is weaker than in the λ_{122} case in the neutralino-LSP region, as the multilepton signal is diluted by these taus. However, it is still stricter than the RPC case, the thick black dashed curve. We furthermore observe in the lower left plot, that the considered analyses in the stau LSP region, *i.e.* for small M_0 , are *more* sensitive, than in the λ_{122} case. The search

is more sensitive, as the stau now decays via λ_{123} into a neutrino and a 1st- or 2nd-generation charged lepton, rather than a tau final state as in the λ_{122} case, *cf.* the second line in Eq. (31).

For completeness we in turn show the results for non-zero values of λ_{131} and λ_{133} in Fig. 13, respectively. The notation is as in Fig. 12. Again, the differences with respect to Fig. 12 can be explained by respectively considering the number of charged 1st- and 2nd-generation charged leptons versus the number of tau leptons in the relevant final states. For the λ_{131} coupling, the neutralino will decay with almost equal branching ratios into both $ee\nu$ and $e\tau\nu$ which is why the excluded region is larger than for λ_{123} but smaller than for λ_{122} . For the case of λ_{133} , the neutralino decays either into $\tau\tau\nu$ or $e\tau\nu$, which is why the LHC sensitivity is lower compared to all previous cases. Remarkably however, it is still more sensitive than the RPC case for most values of M_0 . Lastly, we note there are only minor differences between the exclusion lines if we were to exchange RPV couplings to (s)electrons by couplings to (s)muons which is due to the comparable identification efficiency between electrons and muons at both ATLAS and CMS. All other $LL\bar{E}$ couplings are obtained by exchanging flavor indices $1 \leftrightarrow 2$ and the respective bounds can therefore be inferred from

¹¹ Atlas_1404_2500 only becomes the most sensitive analysis if higher order cross sections are used for the strong production modes — at leading order the electroweak processes are dominant setting negligibly weaker bounds via analysis atlas_conf_2013_036.

the scenarios shown above.

For all of the $LL\bar{E}$ cases, we see that the 4ℓ +MET search of atlas_conf_2013_036, Ref. [56] and the jets+ $SS\ell$ search of atlas_1404_2500, Ref. [133], are the most sensitive in CheckMATE over most of the parameter range. The most important message from looking at the different $LL\bar{E}$ operators and comparing to the RPC case is, however, that within the CMSSM, as a complete supersymmetric model, the LHC is actually more sensitive to scenarios in which R -parity is violated via an $LL\bar{E}$ operator than if R -parity is conserved. This statement holds even if the signal regions designed for RPV in Ref. [56] are disregarded.

3. $LQ\bar{D}$, Λ_{Rp} -CMSSM

We now turn to the discussion of the $LQ\bar{D}$ operator. In general, when compared to the previous $LL\bar{E}$ case, it is clear that the LHC sensitivity is reduced, as we have to replace either a neutrino and a charged lepton or even two charged leptons by two quarks in the final RPV decay of a neutralino LSP, see Eq. (24) and Sec. III C. Stau LSPs, in turn, will mostly decay either into a pair of quarks or via a four-body decay into a tau, a charged lepton or neutrino, and two quarks, see Eq. (31) and Sec. IV.

Furthermore, we generally observe that the electroweak gaugino-pair-production is no longer relevant in the case of a decay via $LQ\bar{D}$. Due to the hadronic decay products of the neutralino- or stau-LSP the efficiency in the electroweak gaugino case is no longer significantly higher than in the strong production case. The latter then wins due to the significantly higher production cross section.

Let us discuss the results for the individual couplings. The first row in Fig. 14 shows the case of a nonzero λ'_{222} operator. As just mentioned, the overall exclusion sensitivity is significantly lower than in the $LL\bar{E}$ case, and is comparable to the RPC-CMSSM case, shown here as the thick black dashed line. In a small region around $M_0 = 750$ GeV, the RPC is even stricter. In the neutralino-LSP region with high M_0 , we find that analyses which look for jets and like-sign charged leptons, for example Ref. [133] (denoted atlas_1404_2500 in Fig. 10), are most sensitive. See the right-hand plot. In this region the first and second generation squarks are relatively heavy. Therefore gluino and stop pair-production are the most dominant production modes. These produce final states with many b -jets, lower quark generation jets, and leptons and hence populate the $3b$ signal region of a “2 same-sign ℓ or 3ℓ ” analysis (atlas_1404_2500), for which the Standard Model background is nearly zero. Here, the high final state multiplicity induced by the $LQ\bar{D}$ decay results in a slightly increased sensitivity when compared to the RPC case.

In regions with lower M_0 where gluino-squark associated production and squark pair production become relevant, generic squark-gluino searches like at-

las_conf_2013_062, Ref. [199], which look for jets, leptons and missing transverse momentum dominate. For these, the increased final state multiplicity via the additional $LQ\bar{D}$ -induced decays results in a worse bound than for the RPC case. This is due to the signal regions setting strong cuts on the required momentum of the final state objects and the missing transverse momentum of an event. These are necessary to sufficiently reduce the Standard Model background contribution, especially from multiboson production, which also produces final states with high jet and lepton multiplicity and some missing transverse momentum. Since the expected missing transverse momentum of the event is significantly larger in RPC models for which the LSP does not decay, breaking R -parity weakens the bounds in these regions, cf. Ref. [197, 198].

Within the stau LSP region, the wedge at low M_0 , the stau will undergo two-body decays due to the RGE-generated λ_{233} operator for large $\tan\beta$, see also Fig. 7. Therefore, this scenario mimics the results from the stau LSP region in the case where λ_{233} is already present at M_X , see our discussion of the phenomenologically almost identical λ_{133} operator, in Sec. VI B 2.

We continue with the discussion of λ'_{113} , with the only phenomenologically relevant difference that \bar{D}_2 is replaced by \bar{D}_3 . Hence, in the neutralino LSP case, the only phenomenological difference is that two b -jets replace two normal jets. (We found that the sensitivity in the λ'_{222} and λ'_{112} cases are almost identical, since the experimental efficiencies for muons and electrons are similar.) Due to the good b -jet tagging efficiency, this clearly improves the distinguishability with respect to the Standard Model background and results in an increase in sensitivity. This effect is most prominent for large values of M_0 . The same analysis as in the previous λ'_{222} case, see atlas_1404_2500, Ref. [133], provides the most stringent bounds as it contains special signal regions which tag additional b -jets. For smaller values of M_0 barely any change in sensitivity is visible in comparison to before.

In the $\tilde{\tau}$ -LSP region of the λ'_{113} case, the stau will almost always undergo a four-body decay, thereby decaying into both $\tau e b j$ and $\tau \nu b j$ at approximately equal rates. The increase in sensitivity with respect to the neutralino-LSP region comes from the additional tau leptons in the final state.

We continue with the cases λ'_{131} and λ'_{133} in the lower two rows in Fig. 14 and focus on the neutralino LSP region first. Here, the top quark in the decay products does not improve the sensitivity when compared to the λ'_{222} case. When comparing to the λ'_{113} case, we see the sensitivity also goes down. On the one side we no longer have the bottom quark jet in every decay and on the other hand the operator λ'_{13i} in principle allows for neutralino decays into both $t+\ell+j_i$ and $b+\nu+j_i$. However, the mass of the LSP is so low in the relevant parameter range, that the decay into the top quark is kinematically suppressed. Hence, most of the neutralinos will decay via the neutrino mode and as such do not produce the final state leptons

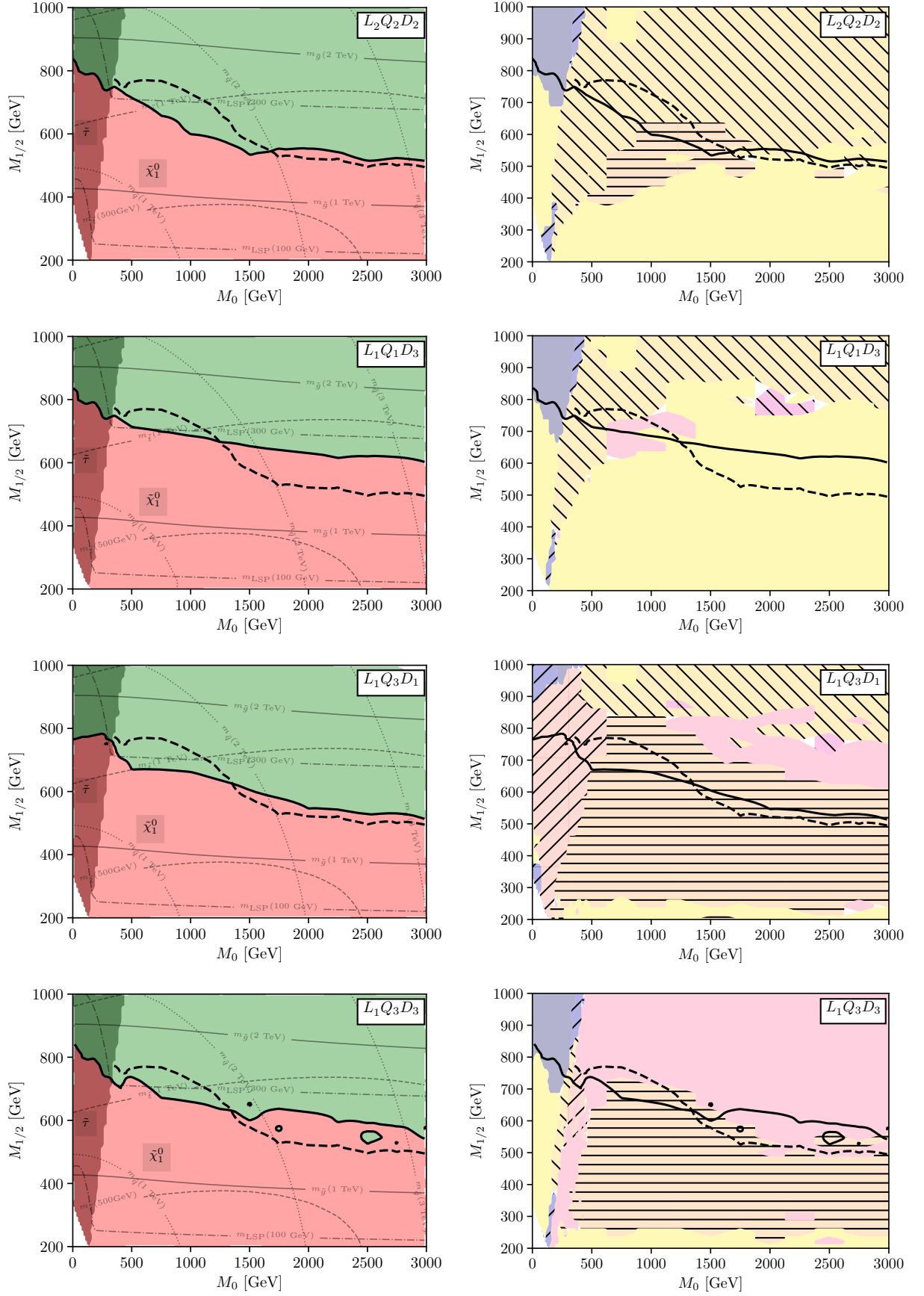


FIG. 14: Same as for Fig. 12, but considering the nonzero operators (in descending order) λ'_{222} , λ'_{113} , λ'_{131} and λ'_{133} .

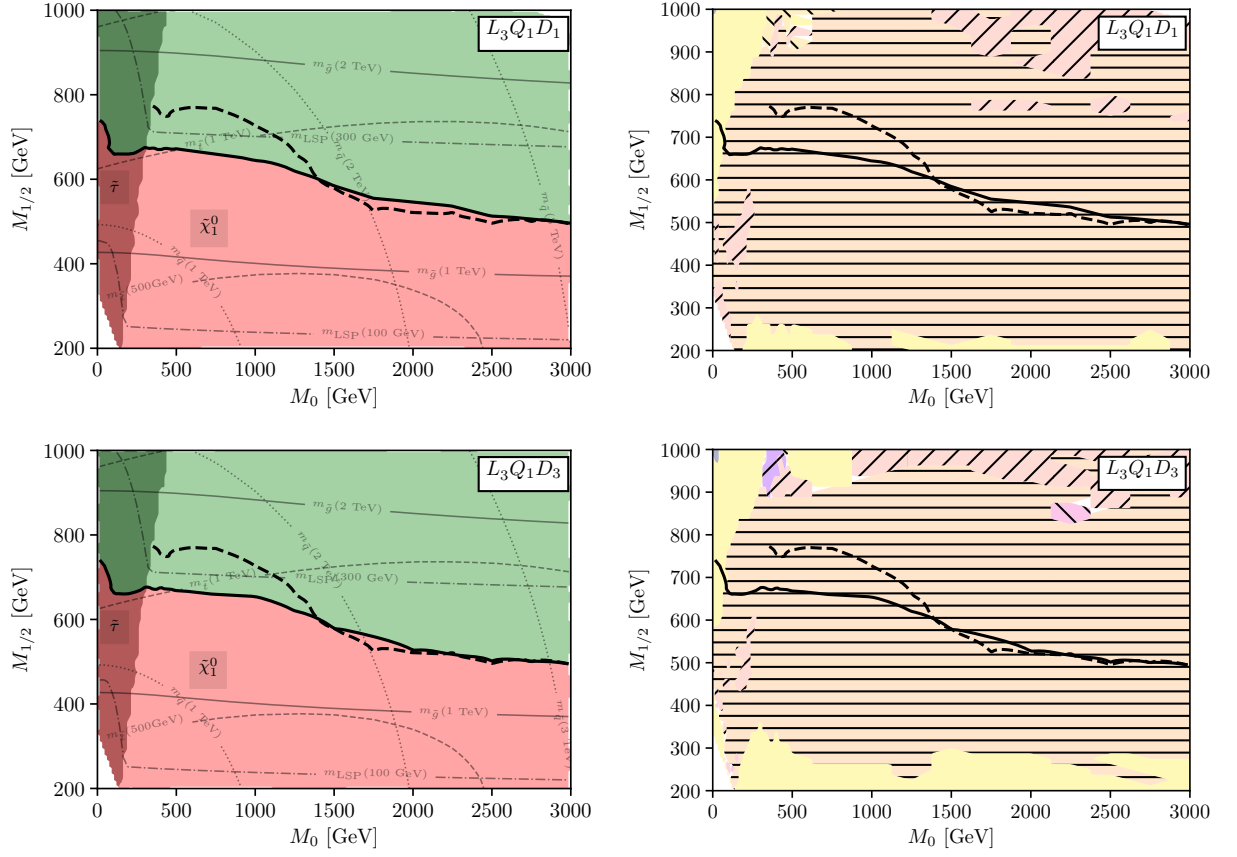


FIG. 15: Same as for Fig. 12, but considering the nonzero operators (in descending order) λ'_{311} and λ'_{313} , which all violate tau lepton number.

which are required for the aforementioned “2 same-sign ℓ or 3 ℓ ” analysis to be sensitive. Instead, the most relevant analysis in the large- M_0 region turns out to be a search looking for events with more than seven jets plus missing energy, see atlas_1308_1841, Ref. [128]. The high jet multiplicity for $\lambda'_{131,133}$ arises from hadronically decaying tops, produced from the standard $\tilde{g} \rightarrow t\bar{t}, \tilde{t} \rightarrow t\tilde{\chi}_1^0$ decay chains in this parameter region, as well as jets from the final neutralino decay $\tilde{\chi}_1^0 \rightarrow jj \cancel{E}_T$.

Comparing λ'_{133} to λ'_{131} , the two additional b -jets in the final state result in a slightly improved exclusion power via the multi- b analysis in atlas_conf_2013_061, Ref. [196].

In the $\tilde{\tau}$ -LSP region, the case λ'_{133} is analogous to the λ'_{222} case in that the RGE-generated λ_{133} operator determines the $\tilde{\tau}$ decay, leading to similar bounds. In the λ'_{131} case, the situation is similar to $\lambda'_{113} \neq 0$ in that the four-body decay dominates. However, as the final state including the top quark, $\tilde{\tau} \rightarrow \tau etj$, is kinematically suppressed, the stau almost exclusively decays into $\tau \nu bj$. This scenario therefore exhibits the worst LHC measurement prospects of all the $\lambda'_{aij} \neq 0$, $a = 1, 2$, $\tilde{\tau}$ -LSP scenarios.

Turning to the λ'_{311} scenario shown in the top row of Fig. 15, all differences with respect to the former λ'_{222} case can be explained by the exchange of muons by taus in the final state, which reduces the overall final state identification efficiency. As a result, the searches looking for leptons lose sensitivity and, similar to the above λ'_{i3i} cases, the best constraints are instead provided by the high jet multiplicity analysis described in atlas_1308_1841, Ref. [128]. Whilst in the λ'_{222} scenario the lower M_0 region was most constrained by the squark-gluino searches in atlas_conf_2013_062, Ref. [199], here this region is again covered by the high multiplicity jet analyses. A closer look at the event rates however reveals that these two analyses are almost equally sensitive and hence the resulting bounds are nearly the same.

In the λ'_{311} scenario, the LHC sensitivity does not change significantly when traversing from the neutralino- into the stau-LSP region since the stau itself decays directly into light quark jets. Hence, only the kinematics change when the LSP crossover occurs, while the final state signatures stay the same. This is why we see exactly the same behavior for the other $i = 3$ cases λ'_{313} , λ'_{331} , $\lambda'_{333} \neq 0$, the former of which we show in the second row of Fig. 15. Consequently, the additional b -tagging in these scenarios does not noticeably improve the exclusion power of atlas_1308_1841, Ref. [128].

Here we have considered all distinct types of nonzero $LQ\bar{D}$ operators, which in principle have differing LHC phenomenology. In the region where the neutralino is the LSP and $M_0 \lesssim 1.2$ TeV, the corresponding LHC bounds that we obtain using CheckMATE are slightly weaker compared to the R -parity-conserving CMSSM. This corresponds to the region where squark pair-production dominates and the additional decay of the neutralino LSP reduces the \cancel{E}_T . In the parameter region where gluino and

stop pair production dominates, *i.e.* for large M_0 , we instead find most $LQ\bar{D}$ scenarios are as constrained as the RPC-CMSSM because of the equally good performance of the multijet searches preferred by RPV and the multi- b searches sensitive to RPC. The special cases $L_i Q_j \bar{D}_3$ with $i, j \in \{1, 2\}$ are significantly more constrained in this region of the R -parity violating CMSSM, due to the additional extra leptons and b -jets in the final state. In all cases, regions with stau LSP are well covered by either multilepton or combined lepton+jet searches and yield comparable bounds as in parameter regions with a neutralino LSP.

4. $\bar{U}\bar{D}\bar{D}$

Here we discuss the $\bar{U}\bar{D}\bar{D}$ operator for which one typically expects the weakest LHC bounds as there is no striking missing energy signal nor any additional leptons, see for example Ref. [169, 200, 201].

In Fig. 16, we show the results in analogy with the previous subsections. We first consider the case of λ'_{121} , the top row, where the neutralino LSP decays into three light jets. Therefore multi-jet searches should yield the most stringent limits for such scenarios. Indeed, as can be seen in the top right plot of Fig. 16, the analysis in atlas_1308_1841, Ref. [128] provides the best exclusion power for the entire neutralino-LSP region. Interestingly, the bounds on the parameter space which we obtain are almost as strong as the bounds on the RPC scenario, the thick black dashed line, *cf.* Fig. 11. This can be regarded as an impressive success for the experimental groups, since multi-jet analyses belong to the most challenging signatures at a hadron collider.

In the large M_0 region where the exclusion lines from RPC and RPV are very similar, gluino pair production has the highest cross section. The gluinos then decay down to a top quark and a stop which itself decays to a top and a neutralino. The dominant $\tilde{g} \rightarrow t\bar{t}$ decay occurs because of the large stop mixing in this region which significantly reduces the \tilde{t}_1 mass with respect to the other squark masses. The neutralino then eventually undergoes a three-body decay into three light jets. As a result, the signal region looking for ≥ 10 jets and missing energy (denoted “10j50” in Ref. [128]) provides the best constraints. This is somewhat surprising as the analysis vetoes against isolated leptons while requiring missing energy. Naively, one would have expected searches for b -jets, missing energy and leptons to dominate. However, we find that only the next-best analysis looks for that, Ref. [202], with the best applicable signal region “SR-1 ℓ -6j-C” looking for one lepton, more than six jets and missing energy. Furthermore note that also in Ref. [128], a RPV interpretation has been performed, assuming gluino pair-production, which decay into $t\bar{t}$, with $\tilde{t} \rightarrow bs$, obtaining bounds of $m_{\tilde{g}} \gtrsim 1$ TeV. Translating the bounds we obtain for the CMSSM-like scenario to gluino mass bounds, we obtain even stricter mass limits, which is due

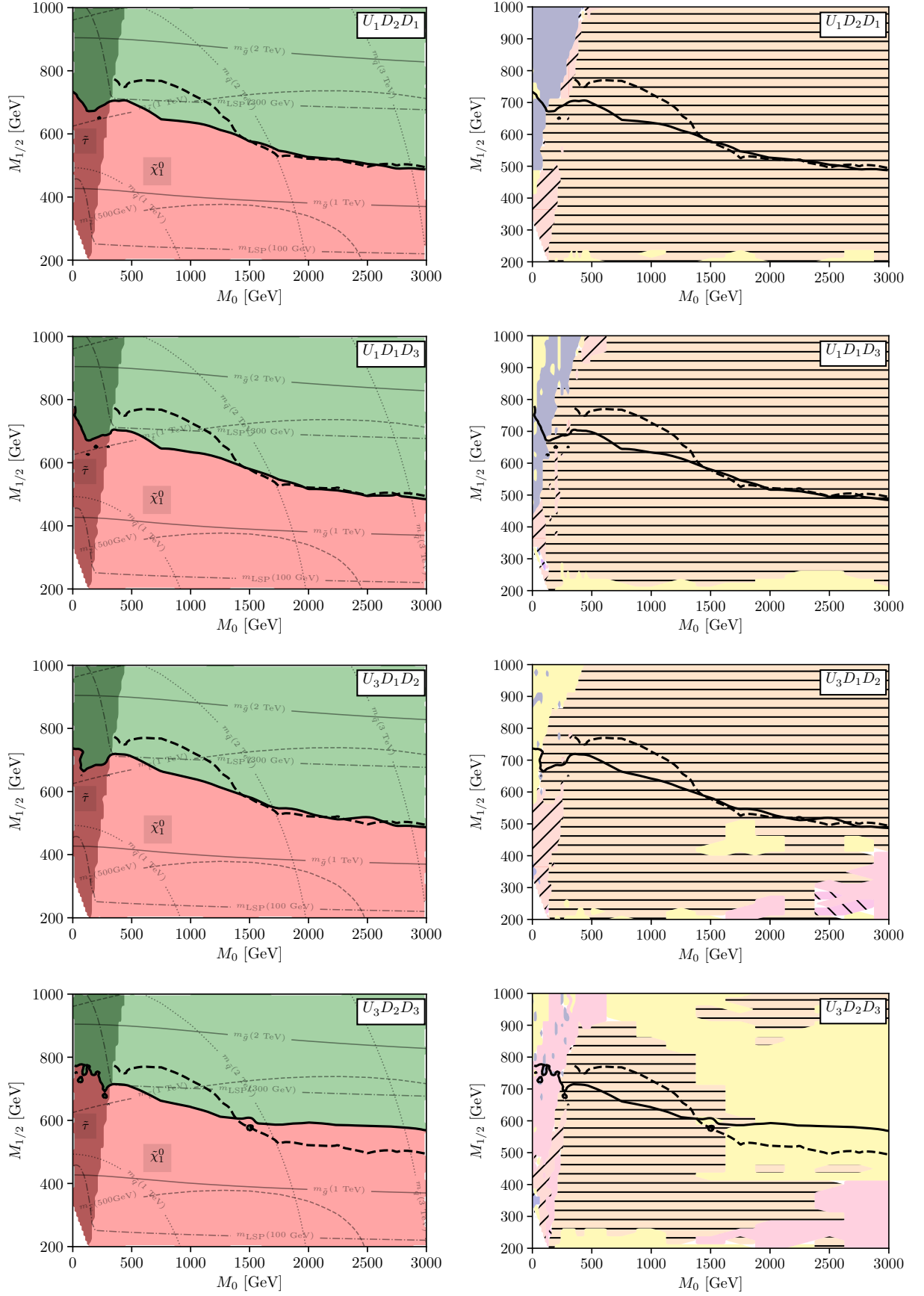


FIG. 16: Same as for Fig. 12, but considering the nonzero operators (in descending order) λ''_{121} , λ''_{131} , λ''_{312} and λ''_{323} .

to the higher jet multiplicity in the final state from including the intermediate neutralino in the decay chain.

In the lower M_0 regions where the exclusion in RPC parameter space is stricter, squark-gluino associated production is dominant. Therefore, while the RPC–CMSSM provides a large missing energy signal and is therefore probed by analyses like atlas_1405_7875, Ref. [129], the RPV counterpart is still best covered by the 10-jet signal region of [128].

We once more want to emphasize that the bounds we obtain on the parameter space rely on the boundary conditions which we impose at the high scale and the corresponding (s)particle spectrum. In particular, as seen in the large M_0 region, the presence of top quarks in the decay is of major importance. In Ref. [203], a re-interpretation of LHC results in a natural SUSY context and $\lambda''_{12} \neq 0$ has been performed. In their scenario the stop and gluino masses are varied independently and a Higgsino LSP decaying into three light jets is assumed. The results show that in this case, gluino and stop masses are generically less constrained when compared to the RPC analogue.

In the stau LSP region, at low M_0 , the decay into one tau lepton and three light jets dominates for λ''_{121} and into one tau, one b -jet and two light jets for λ''_{113} . Interestingly, most of this area is best covered by the 4-lepton analysis atlas_conf_2013_036 [56], which requires, in case of a τ -tag, at least three additional light leptons. This means that the other three τ -leptons can only be identified through their leptonic decay, reducing the overall acceptance by a factor $[\text{BR}(\tau \rightarrow \ell \nu \nu)]^3 \simeq 0.044$. In addition, we find that wino pair-production is important in this part of parameter space and that the charged wino state decays into $e/\mu + \tilde{\nu}$ in up to 30% of the cases, further contributing a charged lepton in the final state.

Turning to the cases where third-generation quarks are among the LSP decays, namely the bottom three rows in Fig. 16, we see that the bounds in the low M_0 region are similar to the λ''_{121} case, and that again the multi-jet search is most sensitive. In the high M_0 region, where gluino and stop pair-production becomes relevant, searches for same-sign leptons, atlas_1404_2500 [133], become effective for λ''_{3ij} . This is due to leptonically decaying top quarks in the final state and has already been analysed in detail in Ref. [204]. Note that in comparison to the $LQ\bar{D}$ operator λ''_{i3j} , where the top in the final state was phase-space suppressed and as such the alternative neutrino decay mode was favored, there is no other comparable decay mode for the neutralino in the case of $\bar{U}\bar{D}\bar{D}$. As such, it will always decay into a top quark whenever kinematically accessible, which is the case for $M_{1/2} \gtrsim 400$ GeV. Therefore, both gluino and stop pair production can lead to same-sign leptons from the leptonic top decay modes, rendering this scenario slightly more constrained than the λ''_{aij} , $a = 1, 2$, cases. Interestingly, we find that in addition electroweak gaugino production is even more important for the limit setting in the large- M_0 area than stop pair-production.

For the λ''_{323} case, the additional possibility of tagging more b -jets further improves sensitivity, such that the large- M_0 region is considerably more constrained than the RPC analogue.

For λ''_{312} , in regions with the stau being the LSP, the kinematical suppression of final states with top quarks results in the most abundant decay chains going via off-shell charginos into a neutrino, a bottom quark and two light-flavor jets, *cf.* Eq. (34). Therefore, searches for missing energy and several jets, *e.g.* atlas_1308_1841 and atlas_1405_7875, Refs. [128, 129], provide a good coverage. At very low M_0 , where the mass difference $m_{\tilde{\chi}_1^0} - m_{\tilde{\tau}_1}$ is largest, even the search for same-sign leptons, atlas_1404_2500 [133], which is sensitive to the leptonically decaying taus from $\tilde{\chi}^0 \rightarrow \tilde{\tau}\tau$, becomes effective enough to exclude the area below $M_{1/2} \lesssim 730$ GeV. However, the sensitivity of this analysis to the scenario at hand quickly drops off with decreasing $m_{\tilde{\chi}_1^0} - m_{\tilde{\tau}_1}$, as can be seen in the λ''_{312} case of Fig. 16. For $\lambda''_{323} \neq 0$, which features at least four b -jets in the final state, the search for large missing transverse momentum and at least three b -jets, atlas_conf_2013_061 [196], is furthermore able to exclude the rest of the $\tilde{\tau}$ -LSP parameter space below around $M_{1/2} \simeq 760$ GeV.

Summarizing, $\bar{U}\bar{D}\bar{D}$ couplings within the CMSSM are almost as well covered by LHC analyses as the RPC counterpart. Similarly to the $LQ\bar{D}$ case, regions with low M_0 are harder to detect at the LHC than the RPC scenario. For large M_0 the searches for many jets and missing energy are very sensitive, leading to bounds as strong as in the RPC–CMSSM, while in the case of a λ''_{3ij} coupling the bounds are even stricter. We stress again that these results are, in particular in the large M_0 region, specific to the CMSSM boundary conditions. For instance, if the stops were heavier than the gluinos, the bounds which one could set on the corresponding scenario would be considerably weaker [203]. In the stau LSP region, searches for several leptons provide the best constraints whereas for λ''_{323} , multi- b -jet analyses are even more sensitive.

Finally, a comment is in order. Much of the considered parameter space can be excluded or detected in the near future due to the decay products of intermediate top quarks in the final state. This is a consequence of the CMSSM boundary conditions where the stops often appear in either the production or decay channels. At the LHC, there are two methods to identify top quarks. The first method involves reconstructing the individual decay products of the top quark. The second, referred to as top-tagging, involves reconstructing the top-quark decay products inside a single fat-jet. This is possible by analysing the jet substructure if the top is boosted enough, and tagging is in principle already possible if $p_{T,t} \gtrsim 150$ GeV [205]. While top quarks can be produced directly from squark or gluino decays in $LQ\bar{D}$ and $\bar{U}\bar{D}\bar{D}$ scenarios, this does not happen in the considered scenarios because of the small couplings and the lighter neutralinos to which each coloured sparticle will decay first. Moreover, the lightest neutralino decays to a top

final states in λ''_{3ij} scenarios, but boosted tops would require much heavier neutralinos than what is accessible in the near future (in a CMSSM context). Hence the only possibility for boosted tops is through the stop decays into $\tilde{\chi}_1^0 t$ which happens for \tilde{t}_R mainly (while \tilde{t}_L would decay to the wino first). A naive estimate shows that $p_{T,t}$ of $\mathcal{O}(150 \text{ GeV})$ is possible in all the remaining parameter space which has not yet been excluded in the figures above. Requiring, however, a significant boost of $\mathcal{O}(400 \text{ GeV})$ for which the tagging efficiency is greatly improved [206], then this occurs only in the upper part of the $M_0 - M_{1/2}$ plane, as this requires a significant mass splitting between the stop, the top and the neutralino. The associated region is not yet accessible with stop pair production, in particular not at the 8 TeV LHC, since it requires stop masses beyond a TeV, featuring a production cross section of sub-fb. This region will, however, be accessible with more accumulated data at the 13 TeV LHC.

VII. LARGE $\Lambda_{\mathcal{R}_p}$: OTHER LSP SCENARIOS

Here, we briefly comment on scenarios with a large $\Lambda_{\mathcal{R}_p}$ coupling, as discussed in Sec. V. In this case, the mass spectrum changes with respect to the RPC-CMSSM so that a direct comparison is no longer meaningful. However, qualitative changes only occur if not only the spectrum but also the relative hierarchy of particle masses is altered. This can lead to (i) changes in the final state signature and/or (ii) changes in the kinematic distributions.

A drastic example of case (i) is the squark LSP scenario, which we envisage for large $\tilde{U}\tilde{D}\tilde{D}$ couplings, *cf.* Tab. II. Then, as discussed in Sec. V, squark LSPs will be pair-produced and decay directly into pairs of dijet resonances via the (large) λ'' coupling. Even though we operate within CMSSM boundary conditions here, the possible squark LSP scenarios correspond quite closely to the simplified models employed in the experimental analyses searching for this exact scenario, as the pair-production of the comparably light squarks will dominate over all other production modes. We therefore refer to the analyses summarized in Sec. V for the respective bounds on the squark masses.

We cannot perform a recast of the bounds on the squark LSP scenarios with the current version of **CheckMATE** since the respective analyses containing 4-jet final states of which two combine to a dijet resonance are not yet handled by this tool. We leave the inclusion of these results for future work.

In the case of a slepton or sneutrino LSP, the change in the final-state signature is milder as the pair-production of the LSP is suppressed with respect to squark/gluino and also wino production. There will therefore at most be changes in the intermediate cascade decays as well as the kinematics of the final state particles; we do not expect drastic changes.

It is nevertheless instructive to check this statement with our tools at hand. In Fig. 17 we show an example of parameter space with either neutralino or sneutrino LSP, corresponding to the scenario shown earlier in Fig. 3. In the top plot on the left we have turned off the R -parity violating coupling, $\lambda'_{233} = 0$, and show only the $\tilde{\chi}_1^0$ -LSP region, as is appropriate in the RPC-CMSSM. This agrees with Fig. 11. On the right we see that the most sensitive signature in the exclusion region, the lower right-hand corner of the plot, is the $0\ell, 2-6j + \cancel{E}_T$ search of atlas_1405_7875 [129].

In the lower two plots in Fig. 17 we have $\lambda'_{233} = 0.08$ at M_X (corresponding to $\lambda'_{233} \simeq 0.19$ at the weak scale). Comparing the lower left plot to the upper left plot, we have now included the $\tilde{\tau}$ - and the $\tilde{\nu}$ -LSP regions (lower left and upper left regions in the plots in the lower row). We see that the $\tilde{\chi}_1^0$ -LSP region has slightly shrunk, compared to the RPC case in the upper left plot. This is the effect of the RPV coupling on the RGE running of the masses.

In the RPV case, we now want to compare the bounds on $M_{1/2}$ in the sneutrino-LSP and the neutralino-LSP region, respectively. In both cases, the production of stop squarks dominates the LHC supersymmetric production cross section. Despite the large λ'_{233} coupling invoked, the stop mainly decays into a top quark and a bino. In the region on the right-hand side of the figure, the bino-LSP has a dominant three-body decay. While in the left-hand region, the bino is *not* the LSP and it first decays into $\nu_\mu \tilde{\nu}_\mu$ or $\mu \tilde{\mu}$, with the nearly degenerate $\tilde{\nu}$ or $\tilde{\mu}$ on-shell. The latter then decay further via the λ' coupling. The dominant final state is therefore the same in the $\tilde{\chi}_1^0$ -LSP and the $\tilde{\nu}$ -LSP scenarios, and only the final state particles' kinematics differ. As expected, we thus observe that, except for a small dip in the cross-over region ($|m_{\tilde{\chi}_1^0} - m_{\tilde{\nu}_1}|$ is small) the bounds in the sneutrino-LSP and the neutralino-LSP region are comparable.

Interestingly, in some of the sneutrino-LSP region, the cross section of the pair-production of sneutrinos and smuons is even comparable to the stop pair-production. However, due to the additional top quark in the final state, the latter provides a better discrimination against Standard Model background and sneutrino/smuon pair-production does not provide any mentionable constraints on the parameter space by itself.

From this, we conclude that even though the mass hierarchies of the lightest supersymmetric particles may be affected for larger RPV couplings, the resulting bounds are hardly dependent on the details of this hierarchy, as long as both LSP and NLSP are only electroweakly interacting. Small, fine tuned parameter regions with degenerate LSP-NLSP masses form a mild exception as here the soft decay kinematics of the NLSP-to-LSP decay weaken the resulting bounds.

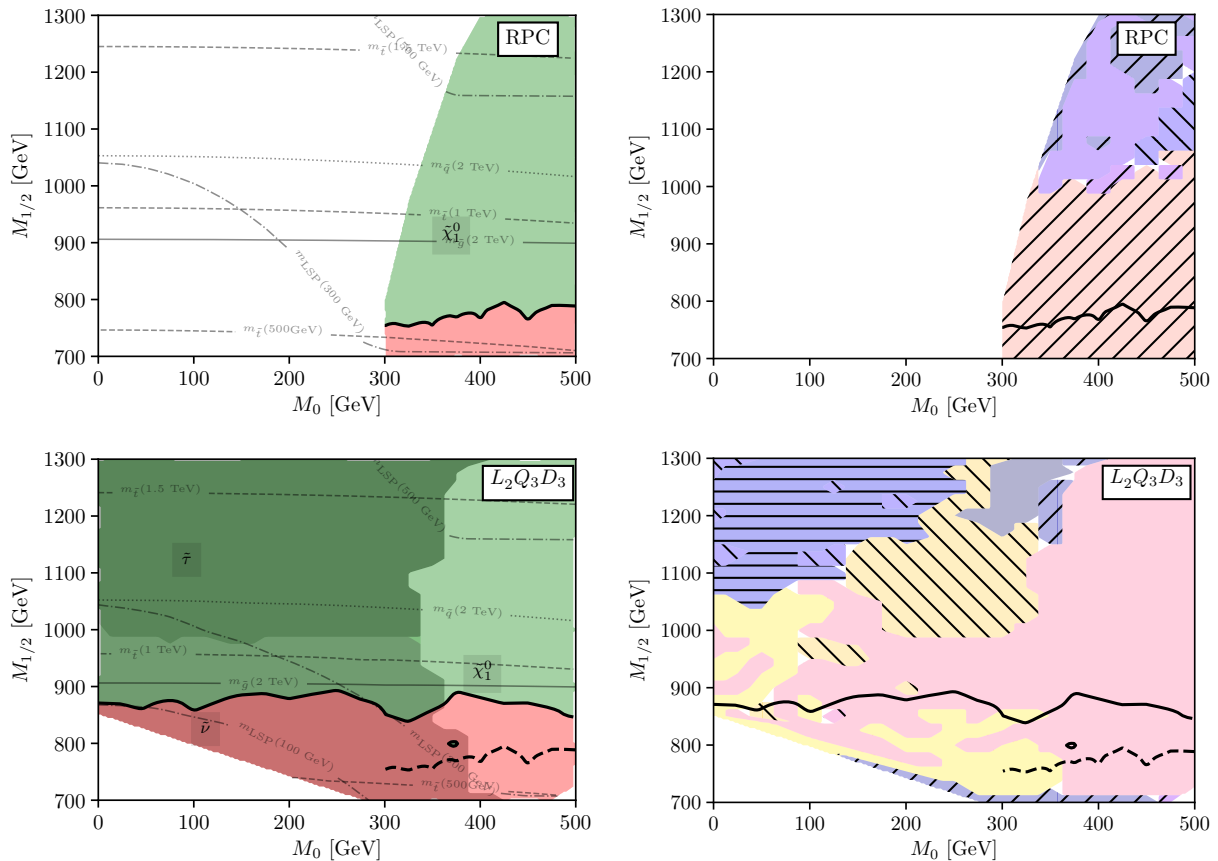


FIG. 17: Same as for Fig. 12, but this time using the parameter choices as in Fig. 3, *i.e.* with $A_0 = -2800$ GeV fixed, and $\lambda'_{233} = 0.08$. Note also the change in M_0 and $M_{1/2}$ parameter ranges compared to Figs. 11-16. This makes the $\tilde{\nu}$ -LSP region more readily visible. Contrarily to the previous figures, we also show the mass contours in the forbidden charged LSP region in the top left figure. This is however only for the purpose of improving the readability of the individual contour labels.

VIII. ABSOLUTE LOWER MASS BOUNDS ON RPV-CMSSM SCENARIOS

In this last section, we present a set of lower supersymmetric mass bounds within the CMSSM. These thus assume a complete supersymmetric model, with possibly involved cascade decay chains. This is unlike the experimental bounds in Tabs. IV, VI and VIII, which are based on simplified models.

The bounds here in Tab. XII are the result of the analyses of Sec. VI, which lead to the Figs. 11 - 16. For each case the allowed parameter range (green) is scanned and the lightest respective sparticle mass is determined. We list separately the bounds for the case of a neutralino LSP (left) and for a stau LSP (right). In both cases we give the lower mass bounds for: the gluino, the lightest stop, the first/second generation squarks, the lightest neutralino and the lightest chargino. These are the particles which are also directly produced. Bounds on other particles also exist, but are always indirect, and obtained only through the CMSSM boundary conditions. They inform us about the Λ_{RP} -CMSSM, not necessarily the

sensitivity of the LHC. For the stau LSP scenario we include the lower bound on the lightest stau, as this is an essential parameter of these models. We emphasize that all the bounds in the stau-LSP case are new, as such bounds do not yet exist in the literature.

Looking at the bounds more closely, for example in the upper left plot of Fig. 12 for $\lambda_{122} \neq 0$, we would expect the lightest allowed gluino mass in the $\tilde{\chi}_1^0$ -LSP case to correspond to the dip in the exclusion curve near $(M_0, M_{1/2}) \simeq (800 \text{ GeV}, 920 \text{ GeV})$. Looking at the light gray dot-dashed gluino mass iso-curve, we therefore expect a lower mass exclusion bound of just over 2000 GeV. In Tab. XII in the row for λ_{122} , we see the lower gluino mass bound is indeed 2070 GeV. Correspondingly in the lower left plot on the left in Fig. 12, for $\lambda_{123} \neq 0$, the exclusion curve is significantly lower, about three quarters of the way between the 1 TeV and 2 TeV gluino iso-mass curves. It also has no marked dip. The bound in Tab. XII is 1700 GeV. In these cases, the strong bounds on the gluino mass are caused by direct bounds on the electroweak gaugino sector through multi-lepton searches which translate into bounds on the gluino mass via the CMSSM boundary conditions. Since the cross section for

$\tilde{\chi}_1^0$ LSP region						$\tilde{\tau}_1$ LSP region					
Coupling	$m_{\tilde{g}}$	$m_{\tilde{t}_1}$	$m_{\tilde{q}_{1st/2nd}}$	$m_{\tilde{\chi}_1^0}$	$m_{\tilde{\chi}_1^\pm}$	$m_{\tilde{g}}$	$m_{\tilde{t}_1}$	$m_{\tilde{q}_{1st/2nd}}$	$m_{\tilde{\chi}_1^0}$	$m_{\tilde{\chi}_1^\pm}$	$m_{\tilde{\tau}_1}$
RPC	1280	710	1560	220	430	—	—	—	—	—	—
λ_{122}	2070	1320	1960	400	750	1690	1140	1520	320	600	230
λ_{123}	1700	980	1630	310	600	1790	1220	1620	340	640	260
λ_{131}	1850	1120	1700	350	670	1740	1180	1580	330	620	260
λ_{133}	1590	920	1540	290	560	1690	1140	1520	320	600	230
λ'_{111}	1220	700	1520	210	410	1690	1140	1520	320	600	230
λ'_{113}	1480	850	1530	260	510	1690	1140	1520	320	600	230
λ'_{131}	1310	750	1450	230	440	1690	1150	1520	320	600	220
λ'_{133}	1310	750	1470	220	440	1690	1140	1520	320	600	230
λ'_{311}	1250	750	1400	210	420	1530	1040	1360	280	530	190
λ'_{313}	1290	730	1410	220	440	1530	1040	1360	280	530	190
λ'_{323}	1280	720	1400	220	430	1530	1040	1370	280	540	200
λ'_{331}	1330	750	1440	230	450	1580	1080	1420	290	560	210
λ'_{333}	1350	770	1420	240	470	1620	1060	1460	310	600	240
λ''_{113}	1250	720	1350	210	420	1420	970	1270	260	490	180
λ''_{121}	1260	730	1350	210	420	1480	1010	1330	270	520	200
λ''_{312}	1250	730	1350	210	420	1430	960	1290	260	500	180
λ''_{323}	1400	780	1350	250	480	1530	1040	1360	280	530	190

TABLE XII: Lower mass bounds on the particle spectrum in GeV. The mass bounds for each RPV coupling are obtained from the the most conservative points that appear in the M_0 – $M_{1/2}$ planes of Figs. 11 - 16 from Sec. VI. In the RPC case there are no $\tilde{\tau}$ -LSP regions.

gluino production at such high masses is of order $\mathcal{O}(\text{ab})$, direct measurements of gluino-induced topologies cannot provide competitive bounds.

Turning to the case $\lambda'_{113} \neq 0$ shown in Fig. 14, we see the exclusion curve sloping downwards for large M_0 , thus the bound is obtained at the limit of our scan region, $M_0 = 3000$ GeV. This is similar to the extended simplified models considered in Ref. [112], where both the squarks and the gluinos were kinematically accessible. The lower mass bounds on the gluino/squarks shown in the second to last row of the gluino section and the last row of the squark section in Tab. VI strongly depend upon the chosen squark/gluino masses, *i.e.* the gluino mass bound depends upon the assumed or allowed squark masses and vice versa.

The remaining gluino mass bounds in the $\tilde{\chi}_1^0$ -LSP scenario for λ' and λ'' are all very similar, mainly around 1300 GeV. They are determined by the limit of the scanning region and rest on the production cross sections at $M_0 = 3000$ GeV. Contrarily to the above $LL\bar{E}$ discussion, the most sensitive signatures require the production of gluinos and hence set a comparably weaker bound. In all these cases a lighter gluino should be possible for completely decoupled squarks.

The lower mass bounds on the lightest top squark are typically significantly weaker, in the range of 700 to 800 GeV over all couplings in the $\tilde{\chi}_1^0$ -LSP scenario. This is similar to the RPC CMSSM bound of 710 GeV. The exception are the cases λ_{122} (λ_{131}) with $m_{\tilde{t}_1} > 1320$ GeV (1120 GeV). The reason is that, because of the employed relation $A_0 = -2M_0$, the stop mass splitting increases with increasing M_0 . Thus the lowest stop mass bounds come from the bounds at large M_0 . As is seen in Figs. 12 and 13, the cases $\lambda_{122,131}$ are the only ones where the lower bound on $M_{1/2}$ is as severe or even stricter for large M_0 as for lower M_0 . For the 1st/2nd generation squarks the lower mass bounds come from the low- M_0 region and are consistently around 1400-1600 GeV, as in the RPC case. They are only markedly stricter in the $LL\bar{E}$ scenarios.

For the stau LSP scenarios the lower gluino mass bound is typically obtained in the dip region along the neutralino-LSP–stau-LSP cross over or close by. For λ_{122} this is clearly significantly lower, for $\lambda_{123,131,133}$ it is comparable to the neutralino-LSP case and for $\lambda'_{111,113,131,133,311,313}$, $\lambda''_{121,113,312,323}$ the lower gluino mass bound in the stau-LSP case should be considerably stricter than in the neutralino LSP case. This is con-

firmed in Tab. XII. For the $LL\bar{E}$ cases these gluino mass lower bounds are due to electroweak gaugino production. For $LQ\bar{D}$ and $\bar{U}\bar{D}\bar{D}$ the production process leading to the most sensitive limits is gluino and/or squark production, possibly involving top squarks. The other mass bounds are then determined indirectly via the CMSSM boundary conditions. Thus the gluino and lightest neutralino mass bounds can be roughly understood as the mass ratio $M_1/M_3 \simeq 1/6$. The chargino mass bounds are also due to direct electroweak gaugino production for the $LL\bar{E}$ case but are otherwise also derived quantities in the RPV-CMSSM. The stop and lightest generation squark bounds are a mixture, sometimes derived, but sometimes also obtained via direct production. The stau mass bounds in the stau-LSP scenarios are all derived quantities. Overall the stau-LSP parameter range is very narrow and thus the lower mass bounds are very similar across all couplings.

To emphasize these bounds are the result of using CheckMATE and therefore contain all the same deficiencies as discussed in Sec. VIA 2. Also, experimental bounds are typically interpreted within simplified models whereas CMSSM-based scenarios like ours have various potentially interesting decay signatures which appear simultaneously. Lacking a statistical combination of the numerous search channels then leads to a significant dilution of the bounds that can be derived compared to a single simplified model.

Despite being conservative our RPV-CMSSM gluino mass bounds are stricter in the $LL\bar{E}$ $\tilde{\chi}_1^0$ -LSP case than in Tab. IV. This is because they are in fact due to electroweak gaugino production, which can be reinterpreted within the Λ_{R_p} -CMSSM. In the $LQ\bar{D}$ case the bounds are largely similar, except for those from Ref. [118, 119] which are based on $\sqrt{s} = 13$ TeV data. In the $\bar{U}\bar{D}\bar{D}$ case the bounds are also similar.

IX. SUMMARY

We have performed a systematic appraisal of the LHC coverage of R -parity violating supersymmetric models. We have mainly focused on the Λ_{R_p} -CMSSM, with only a single non-zero RPV coupling at the unification scale. We have obtained the following results

(1) In Sec. II, starting from the small set of Λ_{R_p} -CMSSM parameters at M_X in Eq. (5), we have dynamically determined the possible LSPs at the weak scale, taking in particular the Higgs mass constraint into account. This is an update of Ref. [62]. The results are presented in Tab. II. We find an extensive parameter range with either a neutralino or a stau LSP. For special large RPV couplings we can also have one of $\{\tilde{e}_R, \tilde{\mu}_R, \tilde{\nu}_{e,\mu}, \tilde{s}_R, \tilde{d}_R, \tilde{b}_1, \tilde{t}_1\}$ as the LSP.

(2a) In Sec. III, we focussed first on the $\tilde{\chi}_1^0$ -LSP scenarios. For the various possible dominant operators, we have compiled tables detailing all possible LHC signatures: Tabs. III ($LL\bar{E}$), V ($LQ\bar{D}$), and VII ($\bar{U}\bar{D}\bar{D}$). We have

then compiled *all* relevant LHC analyses by ATLAS and CMS, and have presented the resulting bounds on the simplified supersymmetric mass spectra in Tabs. IV ($LL\bar{E}$), VI ($LQ\bar{D}$), and VIII ($\bar{U}\bar{D}\bar{D}$), again depending on the nature of the dominant RPV operator. These bounds are independent of the assumption of CMSSM-like boundary constraints and can thus be applied to all RPV models, provided the appropriate branching ratios are implemented. Comparing the two sets of tables we can thus determine the coverage of these models at the LHC. We have observed the following:

- $\tilde{\chi}_1^0$ -LSP, $LL\bar{E}$: These scenarios are very well covered via LHC analyses looking for 4 leptons (including a number of taus) plus missing transverse energy, *cf.* Ref. [107]. We also note that electroweak gaugino production can play an important role due to the large number of additional leptons in the final states, significantly boosting the efficiencies.
- $\tilde{\chi}_1^0$ -LSP, $LQ\bar{D}$: The typical signatures containing charged leptons with a number of jets, b -tagged or otherwise, are well covered. However, final states lacking charged leptons and instead containing hadronically decaying taus and or missing transverse energy are not completely covered, *cf.* cases IIg-k in Tab. V. Most existing analyses focus on high jet multiplicity plus missing transverse energy which provide some sensitivity to the above scenarios. Note the recent analysis in Ref. [119] tags an isolated electron or muon, further requiring high jet multiplicity with no veto on missing transverse energy. This search is sensitive to many of the RPV scenarios beyond just the $LQ\bar{D}$ operators.
- $\tilde{\chi}_1^0$ -LSP, $\bar{U}\bar{D}\bar{D}$: Many scenarios are well covered, especially in the case that top quarks are produced in the cascade decay chain, yielding leptons in the final states. Searches for only jets with and without b -jets are in principle sensitive to all possible final states. However in Ref. [57] all $\bar{U}\bar{D}\bar{D}$ couplings were simultaneously switched on. This makes it very difficult to reinterpret the particular analysis in comparison to single operator dominance. Finally based on the simplified analyses with single operator dominance, λ_{312}'' coverage is lacking.

(2b) In Sec. IV, we next considered the stau-LSP scenarios in detail. The list of LHC signatures has been presented in Ref. [96]. However, these models, irrespective of the dominant RPV coupling, are not explicitly searched for at the LHC. The only exception is a CMSSM model with non-zero λ_{121} [106]. This analysis only uses $\sqrt{s} = 7$ TeV data and makes a number of assumptions about the four-body decay channels, completely ignoring two-body decay channels, which become relevant for large $\tan\beta$. We thus do not present a list of lower mass bounds on the supersymmetric particles in these scenarios. We are however encouraged by the recent search for multiple leptons with up to two hadronic tau candidates, motivated by electroweak gaugino production in

R -parity conserving models [147]. These signatures are also highly relevant for many stau-LSP scenarios. We further encourage experimentalists to perform dedicated analyses looking for final states with high tau, charged lepton and jet multiplicities, *cf.* Tab. IX.

(2c) In Sec. V we summarize the experimental LHC bounds on the non-standard LSP scenarios, *i.e.* those listed in Tab. II, which are obtained for large RPV couplings. The results are summarized in Tabs. X and XI. There are typically no direct searches for these scenarios at the LHC, except in the \tilde{t}_1 -LSP scenario. However in most cases the $\tilde{\chi}_1^0$ is the NLSP and for example the gluino cascade decay proceeds through the same chain as in the corresponding RPV $\tilde{\chi}_1^0$ -LSP case. The only difference is that the neutralino decay is now two-body instead of three-body. Thus the final state kinematic distributions should be slightly different. We expect this to only moderately affect the search sensitivities. In special cases entire decay modes can be kinematically blocked due to the heavy top quark for example, which in turn can affect bounds more significantly.

We have also collected a set of related searches which involve non-neutralino/stau LSPs, which do not arise in the Λ_{R_p} -CMSSM, but for which there are experimental searches. Here we have a sneutrino LSP, a squark LSP, and a gluino LSP. These are compiled in Tab. XI. Here we have also included reinterpreted leptoquark searches.

(3) In Sec. VI we performed collider studies using the program **CheckMATE** to assess the coverage at the LHC of RPV models in comparison to the CMSSM with R -parity conserved. We consistently only use analyses implemented in **CheckMATE** for the $\sqrt{s} = 8$ TeV data. We also only considered all supersymmetric production cross sections at leading order for both the R -parity violating and the R -parity conserving case, multiplied with K -factors determined by **NLLFast** for strongly produced final states. We found that the LHC constraints on RPV models are, for most regions of parameter space, at least comparable to the RPC case, while for the $LL\bar{E}$ operator the constraints are significantly stronger (*cf.* Fig. 12). The main caveats are $\bar{U}DD$ and $LQ\bar{D}$ operators with M_0 in the range 300 to 1000 GeV, *cf.* Figs. 14 to 16.

In the RPC case, the most sensitive analyses in these regions are searches looking for high- p_T jets plus missing transverse momentum. Including these RPV operators decreases sensitivity through both the reduction of the missing transverse energy and the distribution of the jet p_T over many jets. Therefore searches for many jets and a moderate amount of missing energy are usually most sensitive here, but not competitive to the RPC sensitivity. One should note that the analysis in Ref. [119] is not currently available in **CheckMATE**. We expect this search to be far more sensitive in these parameter regions, especially as it does not trigger on missing transverse energy.

The increased sensitivity outside of this M_0 range occurs as many RPV operators can lead to the production of particles in the final state which are not only

easier to detect experimentally but can also lead to greatly reduced SM background contamination. For example $\bar{U}DD$ operators which involve couplings to the top squarks, λ''_{3ij} , can lead to final states with jets (including b -jets) and two like-sign leptons or even three or more leptons, which is what analyses like Ref. [133] have been designed for. Because of these rather special lepton signatures, these final states can be better discriminated against the SM background compared to the typical signatures arising from the RPC-CMSSM in the large- M_0 region, which are one lepton, b -jets and missing transverse momentum.

We stress that we have used all available 8 TeV analyses implemented in **CheckMATE**, however, this does not yet include a large number of ATLAS and CMS analyses optimized for RPV models. We find that many of these missing analyses are essential when one considers RPV couplings which are large enough to directly affect the mass spectrum of the model. Since **CheckMATE** is currently restricted to cut-and-count based analyses, no resonance searches could be considered which might also be relevant for certain RPV scenarios, as discussed in the main text.

(4) In Sec. VIII we have collected the resulting mass bounds of the RPV-CMSSM **CheckMATE** analysis of Sec. VI. We present explicit lower mass bounds for the gluino, the first/second generation squarks, the lightest stop, the lightest neutralino and the lightest chargino. We present these separately for the case of a $\tilde{\chi}_1^0$ -LSP and for a $\tilde{\tau}$ -LSP. We compare the bounds with the corresponding RPC-bounds obtained also with **CheckMATE**, as well as with the experimental bounds collected here in Sec. III. The lower mass bounds in the stau-LSP case are all new, as both ATLAS and CMS have not yet determined any lower mass bounds in this case.

Overall R -parity violating models have been searched for, but we strongly encourage the experimental collaborations to increase the effort to systematically cover all possible models.

Acknowledgments

We thank Santiago Folgueras for interesting discussions about multi-lepton searches at CMS, as well as Florian Staub for technical support with **SARAH**. One of us, H.K.D. thanks the organizers of the conference ‘Is SUSY Alive and Well?’ held at the IFT UA Madrid in Sept. 2016, which partially stimulated this work. We also thank Howie Haber, Steve Martin and Tim Stefaniak for discussions. D.D. acknowledges the support of the Collaborative Research Center SFB 676 ‘Particles, Strings and the Early Universe’ of the DFG. M.E.K. thanks the DFG for financial support through the Research Unit 2239 ‘New Physics at the LHC’ and the IFIC Valencia for hospitality while part of this work was completed. T.O. is supported by the SFB-Transregio TR33 ‘The Dark Uni-

verse". A.R. thanks the Cusanuswerk for funding, and Tel Aviv University and the Weizmann Institute for hospitality while part of this work was completed. H.K.D. thanks Nikhef and MITP Mainz for hospitality while part of this work was completed.

Appendix A: RpV Bounds

Here we summarize the current status of the bounds on the R -parity violating trilinear Yukawa couplings. In

Tab. XIII we present the constraints on single couplings. These results are adopted from [105] and are based on indirect decays and perturbativity.

-
- [1] Yu. A. Golfand and E. P. Likhtman, JETP Lett. **13**, 323 (1971), [Pisma Zh. Eksp. Teor. Fiz.13,452(1971)].
 - [2] D. V. Volkov and V. P. Akulov, Phys. Lett. **B46**, 109 (1973).
 - [3] J. Wess and B. Zumino, Phys. Lett. **B49**, 52 (1974).
 - [4] J. Wess and B. Zumino, Nucl. Phys. **B70**, 39 (1974).
 - [5] S. R. Coleman and J. Mandula, Phys. Rev. **159**, 1251 (1967).
 - [6] R. Haag, J. T. Lopuszanski, and M. Sohnius, Nucl. Phys. **B88**, 257 (1975).
 - [7] P. Ramond (2016), URL <https://workshops.ift.uam-csic.es/files/205/Ramond.pdf>.
 - [8] E. Gildener, Phys. Rev. **D14**, 1667 (1976).
 - [9] M. J. G. Veltman, Acta Phys. Polon. **B12**, 437 (1981).
 - [10] W. Adam (2016), URL <https://indico.cern.ch/event/432527/contributions/2223633/attachments/1321984/1982992/SusyICHEP2016.pdf>.
 - [11] M. Drees and J. S. Kim, Phys. Rev. **D93**, 095005 (2016), 1511.04461.
 - [12] S. S. AbdusSalam et al., Eur. Phys. J. **C71**, 1835 (2011), 1109.3859.
 - [13] S. Dimopoulos and H. Georgi, Nucl. Phys. **B193**, 150 (1981).
 - [14] H. P. Nilles, Phys. Lett. **B115**, 193 (1982).
 - [15] R. Barbieri, S. Ferrara, and C. A. Savoy, Phys. Lett. **B119**, 343 (1982).
 - [16] A. H. Chamseddine, R. L. Arnowitt, and P. Nath, Phys. Rev. Lett. **49**, 970 (1982).
 - [17] G. L. Kane, C. F. Kolda, L. Roszkowski, and J. D. Wells, Phys.Rev. **D49**, 6173 (1994), hep-ph/9312272.
 - [18] S. Cassel, D. M. Ghilencea, S. Kraml, A. Lessa, and G. G. Ross, JHEP **05**, 120 (2011), 1101.4664.
 - [19] P. Bechtle et al., JHEP **06**, 098 (2012), 1204.4199.
 - [20] O. Buchmueller et al., Eur. Phys. J. **C74**, 2922 (2014), 1312.5250.
 - [21] P. Bechtle et al., PoS **EPS-HEP2013**, 313 (2013), 1310.3045.
 - [22] P. Bechtle et al., Eur. Phys. J. **C76**, 96 (2016), 1508.05951.
 - [23] A. Djouadi et al. (MSSM Working Group) (1998), hep-ph/9901246.
 - [24] C. F. Berger, J. S. Gainer, J. L. Hewett, and T. G. Rizzo, JHEP **02**, 023 (2009), 0812.0980.
 - [25] J. A. Conley, J. S. Gainer, J. L. Hewett, M. P. Le, and T. G. Rizzo, Eur. Phys. J. **C71**, 1697 (2011), 1009.2539.
 - [26] K. J. de Vries et al., Eur. Phys. J. **C75**, 422 (2015), 1504.03260.
 - [27] G. Bertone, F. Calore, S. Caron, R. Ruiz, J. S. Kim, R. Trotta, and C. Weniger, JCAP **1604**, 037 (2016), 1507.07008.
 - [28] H. K. Dreiner (1997), [Adv. Ser. Direct. High Energy Phys.21,565(2010)], hep-ph/9707435.
 - [29] R. Barbier et al., Phys. Rept. **420**, 1 (2005), hep-ph/0406039.
 - [30] N. Escudero, D. E. Lopez-Fogliani, C. Munoz, and R. Ruiz de Austri, JHEP **12**, 099 (2008), 0810.1507.
 - [31] S. Weinberg, Phys. Rev. **D26**, 287 (1982).
 - [32] L. J. Hall and M. Suzuki, Nucl. Phys. **B231**, 419 (1984).
 - [33] H. K. Dreiner and M. Thormeier, Phys. Rev. **D69**, 053002 (2004), hep-ph/0305270.
 - [34] B. C. Allanach, A. Dedes, and H. K. Dreiner, Phys. Rev. **D69**, 115002 (2004), [Erratum: Phys. Rev.D72,079902(2005)], hep-ph/0309196.
 - [35] R. M. Godbole, P. Roy, and X. Tata, Nucl. Phys. **B401**, 67 (1993), hep-ph/9209251.
 - [36] J. L. Goity and M. Sher, Phys. Lett. **B346**, 69 (1995), [Erratum: Phys. Lett.B385,500(1996)], hep-ph/9412208.
 - [37] L. E. Ibanez and G. G. Ross, Phys. Lett. **B260**, 291 (1991).
 - [38] T. Banks and M. Dine, Phys. Rev. **D45**, 1424 (1992), hep-th/9109045.
 - [39] H. K. Dreiner, C. Luhn, and M. Thormeier, Phys. Rev. **D73**, 075007 (2006), hep-ph/0512163.
 - [40] H. K. Dreiner, C. Luhn, H. Murayama, and M. Thormeier, Nucl. Phys. **B774**, 127 (2007), hep-ph/0610026.
 - [41] H. K. Dreiner, M. Hahnussek, J.-S. Kim, and C. H. Kom, Phys. Rev. **D84**, 113005 (2011), 1106.4338.
 - [42] H. K. Dreiner, M. Hahnussek, and C. Luhn, Phys. Rev. **D86**, 055012 (2012), 1206.6305.
 - [43] P. Fileviez Perez, Int. J. Mod. Phys. **A28**, 1330024 (2013), 1305.6935.
 - [44] H. K. Dreiner, H. Murayama, and M. Thormeier, Nucl. Phys. **B729**, 278 (2005), hep-ph/0312012.
 - [45] C. Csaki, Y. Grossman, and B. Heidenreich, Phys. Rev. **D85**, 095009 (2012), 1111.1239.
 - [46] S. Davidson and M. Losada, JHEP **05**, 021 (2000), hep-ph/0005080.
 - [47] D. E. Lopez-Fogliani and C. Munoz, Phys. Rev. Lett. **97**, 041801 (2006), hep-ph/0508297.
 - [48] H.-B. Kim and J. E. Kim, Phys. Lett. **B527**, 18 (2002), hep-ph/0108101.
 - [49] E. J. Chun and H. B. Kim, Phys. Rev. **D60**, 095006

ijk	$\lambda_{ijk}(M_W)$	$\lambda'_{ijk}(M_W)$	$\lambda''_{ijk}(M_W)$
111	-	$5.2 \times 10^{-4} \times \left(\frac{m_{\tilde{e}}}{100 \text{ GeV}}\right)^2 \times \sqrt{\frac{m_{\tilde{\chi}^0}}{100 \text{ GeV}}}$	-
112	-	$0.021 \times \frac{m_{\tilde{s}_R}}{100 \text{ GeV}}$	$10^{-15} \times \left(\frac{m_{\tilde{q}}}{\tilde{\Lambda} \text{ GeV}}\right)^{5/2}$
113	-	$0.021 \times \frac{m_{\tilde{b}_R}}{100 \text{ GeV}}$	10^{-4}
121	$0.049 \times \frac{m_{\tilde{e}_R}}{100 \text{ GeV}}$	$0.043 \times \frac{m_{\tilde{d}_R}}{100 \text{ GeV}}$	$10^{-15} \times \left(\frac{m_{\tilde{q}}}{\tilde{\Lambda} \text{ GeV}}\right)^{5/2}$
122	$0.049 \times \frac{m_{\tilde{\mu}_R}}{100 \text{ GeV}}$	$0.043 \times \frac{m_{\tilde{s}_R}}{100 \text{ GeV}}$	-
123	$0.049 \times \frac{m_{\tilde{\tau}_R}}{100 \text{ GeV}}$	$0.043 \times \frac{m_{\tilde{b}_R}}{100 \text{ GeV}}$	(1.23)
131 ^a	$0.062 \times \frac{m_{\tilde{e}_R}}{100 \text{ GeV}}$	$0.019 \times \frac{m_{\tilde{t}_L}}{100 \text{ GeV}}$	10^{-4}
132	$0.062 \times \frac{m_{\tilde{\mu}_R}}{100 \text{ GeV}}$	$0.28 \times \frac{m_{\tilde{t}_L}}{100 \text{ GeV}} (1.04)$	(1.23)
133	$0.0060 \times \sqrt{\frac{m_{\tilde{\tau}_R}}{100 \text{ GeV}}}$	$0.0014 \times \sqrt{\frac{m_{\tilde{b}_R}}{100 \text{ GeV}}}$	-
211	$0.049 \times \frac{m_{\tilde{e}_R}}{100 \text{ GeV}}$	$0.059 \times \frac{m_{\tilde{d}_R}}{100 \text{ GeV}}$	-
212	$0.049 \times \frac{m_{\tilde{\mu}_R}}{100 \text{ GeV}}$	$0.059 \times \frac{m_{\tilde{s}_R}}{100 \text{ GeV}}$	(1.23)
213	$0.049 \times \frac{m_{\tilde{\tau}_R}}{100 \text{ GeV}}$	$0.059 \times \frac{m_{\tilde{b}_R}}{100 \text{ GeV}}$	(1.23)
221	-	$0.18 \times \frac{m_{\tilde{s}_R}}{100 \text{ GeV}} (1.12)$	(1.23)
222	-	$0.21 \times \frac{m_{\tilde{s}_R}}{100 \text{ GeV}} (1.12)$	-
223	-	$0.21 \times \frac{m_{\tilde{b}_R}}{100 \text{ GeV}} (1.12)$	(1.23)
231	$0.070 \times \frac{m_{\tilde{e}_R}}{100 \text{ GeV}}$	$0.18 \times \frac{m_{\tilde{b}_L}}{100 \text{ GeV}}$	(1.23)
232	$0.070 \times \frac{m_{\tilde{\mu}_R}}{100 \text{ GeV}}$	$0.56 (1.04)$	(1.23)
233	$0.070 \times \frac{m_{\tilde{\tau}_R}}{100 \text{ GeV}}$	$0.15 \times \sqrt{\frac{m_{\tilde{b}_R}}{100 \text{ GeV}}}$	-
311	$0.062 \times \frac{m_{\tilde{e}_R}}{100 \text{ GeV}}$	$0.11 \times \frac{m_{\tilde{d}_R}}{100 \text{ GeV}} (1.12)$	-
312	$0.062 \times \frac{m_{\tilde{\mu}_R}}{100 \text{ GeV}}$	$0.11 \times \frac{m_{\tilde{s}_R}}{100 \text{ GeV}} (1.12)$	0.50 (1.00)
313	$0.0060 \times \sqrt{\frac{m_{\tilde{\tau}_R}}{100 \text{ GeV}}}$	$0.11 \times \frac{m_{\tilde{b}_R}}{100 \text{ GeV}} (1.12)$	0.50 (1.00)
321	$0.070 \times \frac{m_{\tilde{e}_R}}{100 \text{ GeV}}$	$0.52 \times \frac{m_{\tilde{d}_R}}{100 \text{ GeV}} (1.12)$	0.50 (1.00)
322	$0.070 \times \frac{m_{\tilde{\mu}_R}}{100 \text{ GeV}}$	$0.52 \times \frac{m_{\tilde{s}_R}}{100 \text{ GeV}} (1.12)$	-
321	$0.070 \times \frac{m_{\tilde{\tau}_R}}{100 \text{ GeV}}$	$0.52 \times \frac{m_{\tilde{b}_R}}{100 \text{ GeV}} (1.12)$	0.50 (1.00)
331	-	0.45 (1.04)	0.50 (1.00)
332	-	0.45 (1.04)	0.50 (1.00)
333	-	0.45 (1.04)	-

^aThe constraint on λ'_{131} is at the 3σ level, since the data disagree with the standard model prediction.

TABLE XIII: Upper bounds on the magnitude of R -parity violating couplings at the 2σ confidence level, taken from [105]. The constraints arise from indirect decays. The concrete processes are described in detail in the original paper. Additionally the perturbativity constraints are shown in parentheses in case they are more stringent than for $m_{\tilde{q},\tilde{l}} = 1 \text{ TeV}$. The numbers where no mass-dependence is specified where derived assuming a degenerate mass spectrum of 100 GeV . The constraints on $\lambda''_{112,121}$ are derived from double nucleon decay and depend on a hadronic scale $\tilde{\Lambda}$ that can be varied from 0.003 to 1 .

- (1999), hep-ph/9906392.
- [50] E. J. Chun and H. B. Kim, JHEP **10**, 082 (2006), hep-ph/0607076.
 - [51] H. K. Dreiner, F. Staub, and L. Ubaldi, Phys. Rev. **D90**, 055016 (2014), 1402.5977.
 - [52] W. Buchmuller, L. Covi, K. Hamaguchi, A. Ibarra, and T. Yanagida, JHEP **03**, 037 (2007), hep-ph/0702184.
 - [53] G. Arcadi, L. Covi, and M. Nardecchia, Phys. Rev. **D92**, 115006 (2015), 1507.05584.
 - [54] P. A. R. Ade et al. (Planck), Astron. Astrophys. **571**, A16 (2014), 1303.5076.
 - [55] H. K. Dreiner, K. Nickel, and F. Staub, Phys. Lett. **B742**, 261 (2015), 1411.3731.
 - [56] ATLAS (2013), ATLAS-CONF-2013-036.
 - [57] Tech. Rep. ATLAS-CONF-2016-057, CERN, Geneva (2016), URL <https://cds.cern.ch/record/2206149>.
 - [58] R. Caminal Armadans, Nucl. Part. Phys. Proc. **273-275**, 618 (2016).
 - [59] B. C. Allanach, A. Dedes, and H. K. Dreiner, Phys. Rev. **D60**, 056002 (1999), [Erratum: Phys. Rev. **D86**, 039906(2012)], hep-ph/9902251.
 - [60] H. K. Dreiner and G. G. Ross, Nucl. Phys. **B365**, 597 (1991).
 - [61] H. K. Dreiner, F. Staub, A. Vicente, and W. Porod, Phys. Rev. **D86**, 035021 (2012), 1205.0557.
 - [62] H. K. Dreiner and S. Grab, Phys. Lett. **B679**, 45 (2009), 0811.0200.
 - [63] M. Drees, H. Dreiner, D. Schmeier, J. Tattersall, and J. S. Kim, Comput. Phys. Commun. **187**, 227 (2015), 1312.2591.
 - [64] J. S. Kim, D. Schmeier, J. Tattersall, and K. Rolbiecki, Comput. Phys. Commun. **196**, 535 (2015), 1503.01123.
 - [65] D. Dercks, N. Desai, J. S. Kim, K. Rolbiecki, J. Tattersall, and T. Weber (2016), 1611.09856.
 - [66] B. Brahmachari and P. Roy, Phys. Rev. **D50**, R39 (1994), [Phys. Rev. **D50**, no.1, R39(1994)], hep-ph/9403350.
 - [67] R. Hempfling, Nucl. Phys. **B478**, 3 (1996), hep-ph/9511288.
 - [68] V. D. Barger, M. S. Berger, R. J. N. Phillips, and T. Wohrmann, Phys. Rev. **D53**, 6407 (1996), hep-ph/9511473.
 - [69] B. de Carlos and P. L. White, Phys. Rev. **D54**, 3427 (1996), hep-ph/9602381.
 - [70] E. Nardi, Phys. Rev. **D55**, 5772 (1997), hep-ph/9610540.
 - [71] F. Staub (2008), 0806.0538.
 - [72] F. Staub, Comput. Phys. Commun. **181**, 1077 (2010), 0909.2863.
 - [73] F. Staub, Comput. Phys. Commun. **182**, 808 (2011), 1002.0840.
 - [74] F. Staub, Computer Physics Communications **184**, pp. 1792 (2013), 1207.0906.
 - [75] F. Staub, Comput. Phys. Commun. **185**, 1773 (2014), 1309.7223.
 - [76] F. Staub, Adv. High Energy Phys. **2015**, 840780 (2015), 1503.04200.
 - [77] W. Porod, Comput. Phys. Commun. **153**, 275 (2003), hep-ph/0301101.
 - [78] W. Porod and F. Staub, Comput. Phys. Commun. **183**, 2458 (2012), 1104.1573.
 - [79] G. Aad et al. (ATLAS, CMS), Phys. Rev. Lett. **114**, 191803 (2015), 1503.07589.
 - [80] P. Athron, J.-h. Park, T. Steudtner, D. Stüßjäger, and A. Voigt, JHEP **01**, 079 (2017), 1609.00371.
 - [81] J. M. Frere, D. R. T. Jones, and S. Raby, Nucl. Phys. **B222**, 11 (1983).
 - [82] J. A. Casas, A. Lleyda, and C. Munoz, Nucl. Phys. **B471**, 3 (1996), hep-ph/9507294.
 - [83] J. E. Camargo-Molina, B. O'Leary, W. Porod, and F. Staub, Eur. Phys. J. **C73**, 2588 (2013), 1307.1477.
 - [84] J. E. Camargo-Molina, B. O'Leary, W. Porod, and F. Staub, JHEP **12**, 103 (2013), 1309.7212.
 - [85] M. Davier, A. Hoecker, B. Malaescu, and Z. Zhang, Eur. Phys. J. **C71**, 1515 (2011), [Erratum: Eur. Phys. J. **C72**, 1874(2012)], 1010.4180.
 - [86] D. Stockinger, in SUSY 2007 Proceedings (2007), pp. 720–723, 0710.2429.
 - [87] F. Jegerlehner (2017), 1705.00263.
 - [88] A. Gould, B. T. Draine, R. W. Romani, and S. Nussinov, Phys. Lett. **B238**, 337 (1990).
 - [89] L. E. Ibanez and C. Lopez, Nucl. Phys. **B233**, 511 (1984).
 - [90] L. E. Ibanez, C. Lopez, and C. Munoz, Nucl. Phys. **B256**, 218 (1985).
 - [91] M. Drees and S. P. Martin (1995), hep-ph/9504324.
 - [92] S. P. Martin (1997), [Adv. Ser. Direct. High Energy Phys. **18**, 1(1998)], hep-ph/9709356.
 - [93] H. K. Dreiner, S. Grab, and M. K. Trenkel, Phys. Rev. **D79**, 016002 (2009), [Erratum: Phys. Rev. **79**, 019902(2009)], 0808.3079.
 - [94] B. de Carlos and P. L. White, Phys. Rev. **D55**, 4222 (1997), hep-ph/9609443.
 - [95] B. C. Allanach, M. A. Bernhardt, H. K. Dreiner, C. H. Kom, and P. Richardson, Phys. Rev. **D75**, 035002 (2007), hep-ph/0609263.
 - [96] K. Desch, S. Fleischmann, P. Wienemann, H. K. Dreiner, and S. Grab, Phys. Rev. **D83**, 015013 (2011), 1008.1580.
 - [97] D. Choudhury, H. K. Dreiner, P. Richardson, and S. Sarkar, Phys. Rev. **D61**, 095009 (2000), hep-ph/9911365.
 - [98] H. K. Dreiner, C. Hanhart, U. Langenfeld, and D. R. Phillips, Phys. Rev. **D68**, 055004 (2003), hep-ph/0304289.
 - [99] H. K. Dreiner, S. Heinemeyer, O. Kittel, U. Langenfeld, A. M. Weber, and G. Weiglein, Eur. Phys. J. **C62**, 547 (2009), 0901.3485.
 - [100] H. K. Dreiner, M. Hanussek, J. S. Kim, and S. Sarkar, Phys. Rev. **D85**, 065027 (2012), 1111.5715.
 - [101] C. Patrignani et al. (Particle Data Group), Chin. Phys. **C40**, 100001 (2016).
 - [102] S. Dawson, Nucl. Phys. **B261**, 297 (1985).
 - [103] H. K. Dreiner and P. Morawitz, Nucl. Phys. **B428**, 31 (1994), [Erratum: Nucl. Phys. **B574**, 874(2000)], hep-ph/9405253.
 - [104] K. Agashe and M. Graesser, Phys. Rev. **D54**, 4445 (1996), hep-ph/9510439.
 - [105] B. C. Allanach, A. Dedes, and H. K. Dreiner, Phys. Rev. **D60**, 075014 (1999), hep-ph/9906209.
 - [106] G. Aad et al. (ATLAS), JHEP **12**, 124 (2012), 1210.4457.
 - [107] G. Aad et al. (ATLAS), Phys. Rev. **D90**, 052001 (2014), 1405.5086.
 - [108] G. Aad et al. (ATLAS), JHEP **08**, 138 (2015), 1411.2921.
 - [109] CMS (2013), CMS-PAS-SUS-13-010.
 - [110] V. Khachatryan et al. (CMS), Phys. Rev. **D94**, 112009

- (2016), 1606.08076.
- [111] CMS (2016), CMS-PAS-SUS-16-022, URL <https://cds.cern.ch/record/2205165>.
- [112] CMS (2012), CMS-PAS-SUS-12-027, URL <http://cds.cern.ch/record/1494689>.
- [113] ATLAS (2016), ATLAS-CONF-2016-075.
- [114] S. Chatrchyan et al. (CMS), Phys. Rev. Lett. **111**, 221801 (2013), 1306.6643.
- [115] CMS (2013), CMS-PAS-SUS-13-010, URL <https://cds.cern.ch/record/1550552>.
- [116] Tech. Rep. ATLAS-CONF-2015-018, CERN, Geneva (2015), URL <https://cds.cern.ch/record/2017303>.
- [117] Tech. Rep. CMS-PAS-SUS-13-005, CERN, Geneva (2013), URL <https://cds.cern.ch/record/1547780>.
- [118] M. Aaboud et al. (ATLAS) (2017), 1706.03731.
- [119] M. Aaboud et al. (ATLAS) (2017), 1704.08493.
- [120] V. Khachatryan et al. (CMS), Phys. Lett. **B760**, 178 (2016), 1602.04334.
- [121] V. Khachatryan et al. (CMS), Phys. Lett. **B739**, 229 (2014), 1408.0806.
- [122] V. Khachatryan et al. (CMS), Phys. Rev. **D93**, 032004 (2016), 1509.03744.
- [123] H. K. Dreiner, P. Richardson, and M. H. Seymour, Phys. Rev. **D63**, 055008 (2001), hep-ph/0007228.
- [124] H. K. Dreiner, S. Grab, M. Kramer, and M. K. Trenkel, Phys. Rev. **D75**, 035003 (2007), hep-ph/0611195.
- [125] G. Aad et al. (ATLAS), JHEP **04**, 116 (2015), 1501.03555.
- [126] Tech. Rep. CMS-PAS-SUS-16-042, CERN, Geneva (2017), URL <http://cds.cern.ch/record/2257294>.
- [127] Tech. Rep. CMS-PAS-SUS-16-037, CERN, Geneva (2017), URL <http://cds.cern.ch/record/2256652>.
- [128] G. Aad et al. (ATLAS), JHEP **10**, 130 (2013), [Erratum: JHEP01,109(2014)], 1308.1841.
- [129] G. Aad et al. (ATLAS), JHEP **09**, 176 (2014), 1405.7875.
- [130] M. Aaboud et al. (ATLAS), Eur. Phys. J. **C76**, 392 (2016), 1605.03814.
- [131] A. M. Sirunyan et al. (CMS) (2017), 1704.07781.
- [132] Tech. Rep. CMS-PAS-SUS-16-036, CERN, Geneva (2017), URL <http://cds.cern.ch/record/2256872>.
- [133] G. Aad et al. (ATLAS), JHEP **06**, 035 (2014), 1404.2500.
- [134] G. Aad et al. (ATLAS), JHEP **12**, 086 (2012), 1210.4813.
- [135] G. Aad et al. (ATLAS), Phys. Rev. **D91**, 112016 (2015), [Erratum: Phys. Rev.D93,no.3,039901(2016)], 1502.05686.
- [136] G. Aad et al. (ATLAS), JHEP **06**, 067 (2016), 1601.07453.
- [137] ATLAS (2016), ATLAS-CONF-2016-022.
- [138] V. Khachatryan et al. (CMS), Submitted to: Phys. Lett. (2016), 1608.01224.
- [139] V. Khachatryan et al. (CMS), Phys. Lett. **B747**, 98 (2015), 1412.7706.
- [140] S. Chatrchyan et al. (CMS), Phys. Lett. **B730**, 193 (2014), 1311.1799.
- [141] S. Chatrchyan et al. (CMS), JHEP **01**, 163 (2014), [Erratum: JHEP01,014(2015)], 1311.6736.
- [142] ATLAS (2013), ATLAS-CONF-2013-091.
- [143] CMS (CMS Collaboration), Tech. Rep. CMS-PAS-SUS-16-013, CERN, Geneva (2016), URL <https://cds.cern.ch/record/2205147>.
- [144] ATLAS (2016), ATLAS-CONF-2016-094.
- [145] ATLAS (2017), ATLAS-CONF-2017-013.
- [146] F. de Campos, O. J. P. Eboli, M. B. Magro, W. Porod, D. Restrepo, M. Hirsch, and J. W. F. Valle, JHEP **05**, 048 (2008), 0712.2156.
- [147] CMS (2017), CMS-PAS-SUS-16-039.
- [148] Tech. Rep. ATLAS-CONF-2015-026, CERN, Geneva (2015), URL <http://cds.cern.ch/record/2037653>.
- [149] G. Aad et al. (ATLAS), Phys. Rev. Lett. **115**, 031801 (2015), 1503.04430.
- [150] V. Khachatryan et al. (CMS), Eur. Phys. J. **C76**, 317 (2016), 1604.05239.
- [151] A. Faessler, T. S. Kosmas, S. Kovalenko, and J. D. Vergados (1999), hep-ph/9904335.
- [152] W. H. Bertl et al. (SINDRUM II), Eur. Phys. J. **C47**, 337 (2006).
- [153] Tech. Rep. CMS-PAS-EXO-16-029, CERN, Geneva (2016), URL <https://cds.cern.ch/record/2231062>.
- [154] Tech. Rep. ATLAS-CONF-2016-084, CERN, Geneva (2016), URL <https://cds.cern.ch/record/2206277>.
- [155] J. A. Evans and Y. Kats, JHEP **04**, 028 (2013), 1209.0764.
- [156] Y. Bai, A. Katz, and B. Tweedie, JHEP **01**, 040 (2014), 1309.6631.
- [157] Tech. Rep. CMS-PAS-EXO-16-001, CERN, Geneva (2016), URL <https://cds.cern.ch/record/2149046>.
- [158] M. Aaboud et al. (ATLAS), Eur. Phys. J. **C76**, 541 (2016), 1607.08079.
- [159] G. Aad et al. (ATLAS), Eur. Phys. J. **C76**, 5 (2016), 1508.04735.
- [160] Tech. Rep. ATLAS-CONF-2015-015, CERN, Geneva (2015), URL <https://cds.cern.ch/record/2002885>.
- [161] V. Khachatryan et al. (CMS), JHEP **07**, 042 (2015), [Erratum: JHEP11,056(2016)], 1503.09049.
- [162] S. Dimopoulos, R. Esmailzadeh, L. J. Hall, and G. D. Starkman, Phys. Rev. **D41**, 2099 (1990).
- [163] J. L. Feng, J. F. Gunion, and T. Han, Phys. Rev. **D58**, 071701 (1998), hep-ph/9711414.
- [164] J. L. Hewett and T. G. Rizzo, in *High-energy physics. Proceedings, ICHEP'98* (1998), pp. 1698–1702, hep-ph/9809525.
- [165] H. K. Dreiner and T. Stefaniak, Phys. Rev. **D86**, 055010 (2012), 1201.5014.
- [166] G. Moreau, E. Perez, and G. Polesello, Nucl. Phys. **B604**, 3 (2001), hep-ph/0003012.
- [167] M. A. Bernhardt, S. P. Das, H. K. Dreiner, and S. Grab, Phys. Rev. **D79**, 035003 (2009), 0810.3423.
- [168] S. Chatrchyan et al. (CMS), JHEP **12**, 055 (2012), 1210.5627.
- [169] J. A. Evans and Y. Kats, PoS **EPS-HEP2013**, 287 (2013), 1311.0890.
- [170] E. J. Chun, S. Jung, H. M. Lee, and S. C. Park, Phys. Rev. **D90**, 115023 (2014), 1408.4508.
- [171] Z. Marshall, B. A. Ovrut, A. Purves, and S. Spinner, Phys. Lett. **B732**, 325 (2014), 1401.7989.
- [172] G. Aad et al. (ATLAS), JHEP **10**, 054 (2015), 1507.05525.
- [173] S. Chatrchyan et al. (CMS), Phys. Rev. **D90**, 112001 (2014), 1405.3961.
- [174] J. Alwall, R. Frederix, S. Frixione, V. Hirschi, F. Maltoni, O. Mattelaer, H. S. Shao, T. Stelzer, P. Torrielli, and M. Zaro, JHEP **07**, 079 (2014), 1405.0301.
- [175] T. Sjöstrand, S. Ask, J. R. Christiansen, R. Corke, N. Desai, P. Ilten, S. Mrenna, S. Prestel, C. O. Rasmussen, and P. Z. Skands, Comput. Phys. Commun.

- 191**, 159 (2015), 1410.3012.
- [176] J. de Favereau, C. Delaere, P. Demin, A. Giammanco, V. Lemaitre, A. Mertens, and M. Selvaggi (DELPHES 3), *JHEP* **02**, 057 (2014), 1307.6346.
 - [177] M. Cacciari, G. P. Salam, and G. Soyez, *Eur. Phys. J.* **C72**, 1896 (2012), 1111.6097.
 - [178] M. Cacciari and G. P. Salam, *Phys. Lett.* **B641**, 57 (2006), hep-ph/0512210.
 - [179] A. L. Read, *J. Phys.* **G28**, 2693 (2002).
 - [180] C. Degrande, C. Duhr, B. Fuks, D. Grellscheid, O. Mattelaer, and T. Reiter, *Comput. Phys. Commun.* **183**, 1201 (2012), 1108.2040.
 - [181] M. D. Goodsell, K. Nickel, and F. Staub, *Eur. Phys. J.* **C75**, 32 (2015), 1411.0675.
 - [182] M. Goodsell, K. Nickel, and F. Staub, *Eur. Phys. J.* **C75**, 290 (2015), 1503.03098.
 - [183] M. D. Goodsell and F. Staub, *Eur. Phys. J.* **C77**, 46 (2017), 1604.05335.
 - [184] H. K. Dreiner, M. Kramer, and J. Tattersall, *Europhys. Lett.* **99**, 61001 (2012), 1207.1613.
 - [185] W. Beenakker, R. Hopker, M. Spira, and P. Zerwas, *Nucl. Phys.* **B492**, 51 (1997), hep-ph/9610490.
 - [186] W. Beenakker, M. Kramer, T. Plehn, M. Spira, and P. M. Zerwas, *Nucl. Phys.* **B515**, 3 (1998), hep-ph/9710451.
 - [187] A. Kulesza and L. Motyka, *Phys. Rev. Lett.* **102**, 111802 (2009), 0807.2405.
 - [188] A. Kulesza and L. Motyka, *Phys. Rev.* **D80**, 095004 (2009), 0905.4749.
 - [189] W. Beenakker, S. Brensing, M. Kramer, A. Kulesza, E. Laenen, et al., *JHEP* **0912**, 041 (2009), 0909.4418.
 - [190] W. Beenakker, S. Brensing, M. Kramer, A. Kulesza, E. Laenen, and I. Niessen, *JHEP* **08**, 098 (2010), 1006.4771.
 - [191] W. Beenakker, S. Brensing, M. Kramer, A. Kulesza, E. Laenen, et al., *Int. J. Mod. Phys.* **A26**, 2637 (2011), 1105.1110.
 - [192] W. Beenakker, R. Hopker, and M. Spira (1996), hep-ph/9611232.
 - [193] S. Belkner, Master's Thesis (2017).
 - [194] S. P. Martin and J. D. Wells, *Phys. Rev.* **D64**, 035003 (2001), hep-ph/0103067.
 - [195] K. Kohri and T. Takahashi, *Phys. Lett.* **B682**, 337 (2010), 0909.4610.
 - [196] Tech. Rep. ATLAS-CONF-2013-061, CERN, Geneva (2013), URL <http://cds.cern.ch/record/1557778>.
 - [197] H. K. Dreiner, S. Grab, and T. Stefaniak, *Phys. Rev.* **D84**, 035023 (2011), 1102.3189.
 - [198] M. Hanussek and J. S. Kim, *Phys. Rev.* **D85**, 115021 (2012), 1205.0019.
 - [199] Tech. Rep. ATLAS-CONF-2013-062, CERN, Geneva (2013), URL <http://cds.cern.ch/record/1557779>.
 - [200] B. C. Allanach, A. J. Barr, L. Drage, C. G. Lester, D. Morgan, M. A. Parker, B. R. Webber, and P. Richardson, *JHEP* **03**, 048 (2001), hep-ph/0102173.
 - [201] B. C. Allanach, A. J. Barr, M. A. Parker, P. Richardson, and B. R. Webber, *JHEP* **09**, 021 (2001), hep-ph/0106304.
 - [202] G. Aad et al. (ATLAS), *JHEP* **10**, 024 (2014), 1407.0600.
 - [203] M. R. Buckley, D. Feld, S. Macaluso, A. Monteux, and D. Shih (2016), 1610.08059.
 - [204] D. Bardhan, A. Chakraborty, D. Choudhury, D. K. Ghosh, and M. Maity (2016), 1611.03846.
 - [205] C. Anders, C. Bernaciak, G. Kasieczka, T. Plehn, and T. Schell, *Phys. Rev.* **D89**, 074047 (2014), 1312.1504.
 - [206] A. Abdesselam et al., *Eur. Phys. J.* **C71**, 1661 (2011), 1012.5412.